UNIVERSITY OF CAPE TOWN
IYUNIVESITHI YASEKAPA • UNIVERSITEIT VAN KAAPSTAD

Mechanical Engineering

A test-cell installation of a gas turbine engine to investigate the performance advantages of low aromatic fuel

Author:
Nigel Bester

Supervisor:
ADJ. Prof. Andy Yates

November 19, 2008

Declaration

1. I know the meaning of plagiarism and declare that all the work in the document, save for that which I have properly acknowledged, is my own.

2. I have used the IEEE convention for citation and referencing. Each significant contribution to, and quotation in this project from the work of other people has been attributed, and has been cited and referenced.

3. I have not allowed, and will not allow anyone to copy my work with the intention of passing it off as his or her own work.

Signature _____

Acknowledgments

The writer wishes to thank the following people for their time, input and support during this research project:

ADJ. Prof. Andy Yates - Project Supervisor

Mr Len Watkins - Manufacturing

Mr Glen Newins - Manufacturing

Mr Gavin Tomlinson - SAFL Lab Technician

Mr Johan Myburgh - Sasol Technology Fuels Research Lab Technician

Mr Paul Schaberg - Sasol Technology Fuels Research

To my friends and family, as well as my colleagues at the Sasol Advanced Fuels Laboratory, thanks very much for the encouragement and support throughout, it was much appreciated.

The writer also owes a debt of gratitude to Sasol Technology Fuels Research, who initiated and sponsored this research project.

Executive Summary

Background

The foreseeable opportunity for LTFT jet fuel has spurred an initiative for Sasol Technology Fuels Research to increase the level of gas turbine expertise within the mechanical group. This included gaining an intimate familiarity with the jet fuel business, and all relevant aspects of gas turbine technology and jet fuel combustion performance. This project formed a component of the research activity.

Objectives

The primary focus of the project was to ascertain the extent to which reducing aromatic content would affect the performance of a gas turbine. However, since no facilities existed at the Sasol Advanced Fuels Laboratory (SAFL) for jet fuels research, the first objective was to establish a working test cell with which to complete the research. Once operational, the engine was instrumented to study the thermal loading on the combustor, and a database of soot emissions measurements was populated while operating on a matrix of fuels.

Experimental Setup

A T63-A-700, Model 250-C18 B gas turbine was installed in a test cell at the Sasol Advanced Fuels Laboratory. The engine was instrumented to determine the performance implications of jet fuels with varying aromatic contents. Synthetic Paraffinic Kerosene (SPK) containing zero aromatics, and a petroleum–derived Jet A-1 fuel containing 19.0 % aromatics were the two test fuels incorporated to determine the effect of aromatics on engine performance.

Liner temperature measurements were attained via an instrumented combustor liner, as well as exhaust gas sampling employed to determine engine soot emissions.

Discussion of Results

The results showed a mean improvement in engine efficiency of 1.17% when operating at cruise conditions on SPK versus petroleum–dervied Jet A-1. The efficiency was attained via four means; an improvement in the thermodynamic properties of the combustion products, an increase in combustion efficiency, a reduction in the viscosity of the combustion products and a reduction in the liner pressure loss, also linked to viscous effects.

There was an 86.8% reduction in soot emissions at cruise conditions, and a 95.3% reduction in soot emissions at idle conditions with operation on SPK versus petroleum–derived Jet A-1. The reduction in soot was attributed to the reduction in aromatic content of the fuel.

There was a consistent reduction in liner operating temperature at cruise conditions measured with operation on SPK. The liner temperature reduced by $\approx 20°C$ in the vicinity of the primary combustion zone, and about $5°C$ at the turbine end of the combustor liner. The reduction in operating temperature was primarily attributed to the reduction in soot, and the resultant reduction in thermal radiation heat transfer.

Conclusions

The soot formation tendency of aromatics were seen during experimentation, with an 86.8% and 95.3% reduction in soot formation measured during operation on aromatic free SPK versus a petroleum–derived Jet A-1. The reduction in soot within the combustor resulted in a large reduction in the thermal radiation heat transfer to the combustor liner, and caused a lower combustor liner operating temperature to result.

The greater H/C ratio of SPK with respect to petroleum–derived Jet A-1 caused the thermodynamic properties of the combustion products to change directionally toward improving energy extraction via a turbine. The H/C ratio effect was due to the reduction of aromatic molecules in the fuel, and the inclusion of more paraffinic molecule with a greater H/C ratio.

Contents

1 Introduction **1**

1.1 Background 1

1.2 Project Aim 3

1.3 Plan of Development 3

2 Literature Review **4**

2.1 Combustor Liner Heat Transfer 4

2.2 Particulate Formation 9

2.3 Sasol Fully Synthetic Jet Fuel (FSJF) vs. Petroleum–Derived Jet Fuel 12

2.4 Emissions Characteristics of a Fischer–Tropsch Jet Fuel 14

3 Test Engine **26**

3.1 Specifications 26

3.2 Fuel Control System 27

3.3 Mounting 28

3.4 Operation Monitoring 29

3.5 Research Instrumentation 32

4 Test Cell Installation **36**

4.1 Load Control 36

4.2 Drive Shaft and Couplings 37

4.3 Fluid Supply Systems 38

5 Heat Transfer Theory **43**

5.1 Liner Analysis 43

5.2 Fuel Effects on the Modes of Liner Heat Transfer 45

6 Theory **46**

6.1 Adiabatic Flame Temperature 46

6.2 Hydrogen/Carbon Ratio Effects on Fuel Properties 50

6.3 Idealised Gas Cycle Model 53

6.4 Applying Theory to Analyse the Experimental Data 60

7 Measurement Accuracy and Results **62**

7.1 Power 62

7.2 Fuel Flowrate 63

7.3 Soot Emissions 65

7.4 NO_x Emissions 66

7.5 Gas Temperature 67

7.6 Engine Pressure 67

7.7 Liner Temperature 68

8 Discussion of Results **72**

8.1 Overall Engine Efficiency 72
8.2 Fuel Flowrate 75
8.3 Engine Soot Emissions 76
8.4 NO_x Emissions 77
8.5 Combustor Liner Temperature 77

9 Conclusions **81**
9.1 Test Cell Setup and Instrumentation 81
9.2 Performance Advantages 81
9.3 Soot Formation and Emission 82
9.4 Liner Temperature 83

10 Recommendations **84**
10.1 Test Cell Setup and Experimentation 84
10.2 Theoretical Confirmation through Experimentation 85

References **86**

A T63 Fuel Control Systems and Operation **A-1**
A.1 Introduction A-2
A.2 Gas Producer Fuel Control A-2
A.3 Power Turbine Fuel Governor A-5
A.4 Fuel System Response A-6

B Engine Mounting and Drive Shaft Design **B-1**

B.1 Engine Mounting B-2

B.2 Drive Train Design and Components B-9

C Test Cell Systems **C-1**

C.1 Fuel Supply System C-2

C.2 Oil System C-12

C.3 Water System C-18

C.4 Electrical System C-23

C.5 Ventilation System C-28

C.6 Load Control C-33

D Operational Procedures **D-1**

D.1 Pre-startup Checks D-2

D.2 System Activation D-2

D.3 Light-off D-7

D.4 Engine Operation and Shut-down D-8

D.5 Engine Operating Limits D-9

E Heat Transfer Theory **E-1**

E.1 Introduction E-2

E.2 Method of Liner Analysis E-2

E.3 Combustor Liner Heat Transfer Equations E-5

E.4 Radiation Sensor E-9

F Drawings **F-1**

F.1 Engine Mounting F-2

F.2 Air Separation Unit F-3

F.3 Radiation Sensor F-4

F.4 Drive Shaft and Couplings F-5

List of Figures

2.1 Comparison of measured and predicted values of wall temperature for a GE F101 combustor [1]. 7

2.2 Summary of time scales in a typical gas turbine combustor [2]. 10

2.3 Fuel effects on T700 combustor liner temperatures at maximum continuous power [3]. 13

2.4 Reductions in PN emissions from a T63 engine as a function of synjet in the blend [4]. 18

2.5 Effects of synjet fuel on T63 engine particle size distribution at idle [4]. 19

2.6 Reductions in PM mass emissions from a T63 engine as a function of synjet fuel in the blend [4]. 20

2.7 Swirl-stabilized combustor particle number as a function of equivalence ratio for several synjet/JP-8 blends [4]. 21

2.8 Effects of synjet fuel on particle size distribution in a swirl-stabilized combustor for $\Phi = 1.10$ [4]. 22

2.9 SO_2 emissions in a swirl-stabilized combustor as a function of synjet concentration in JP-8/synjet blends [4]. 23

2.10 PAH species in soot samples as a function of synjet concentration for $\Phi = 1.10$ [4]. 24

2.11 Comparison of synjet fuel effects on PM emissions for a swirl-stabilized research combustor and T63 engine [4]. 25

3.1 T63 test cell mounting configuration. 29

3.2 Instrumented T63 combustor liner. 33

3.3 Instrumented T63 combustor case. 34

4.1 Complete drive shaft and couplings. 37

4.2 Fuel supply system schematic. 39

4.3 Oil supply system schematic. 41

5.1 Modes of heat transfer to a combustor liner. 45

6.1 Adiabatic flame temperature for petroleum–derived Jet A-1 and SPK. 48

6.2 Combustion products temperature after combustion and dilution. 49

6.3 Overall engine equivalence ratio for a given power output. . . 54

6.4 Overall A/F ratio for a given power output. 55

6.5 Overall values of Gamma for the final products of combustion. 56

6.6 Overall values of R for the final products of combustion. . . . 57

6.7 Idealised overall engine efficiency. 58

6.8 Turbine inlet temperature. 59

6.9 Engine gravimetric fuel flowrate. 60

7.1 Fuel flowrate measurements of a T63 at cruise conditions. . . . 64

7.2 Soot emissions vs. %SPK for idle, 125 kW and 145 kW. 65

7.3 Engine NO_X emissions during operation at cruise conditions. . 66

7.4 Pressure drop across the combustor liner during operation at cruise power. 68

7.5 Thermocouple placement on an instrumented T63 liner. 69

7.6 T63 gas turbine combustor liner wall temperatures at cruise conditions. 71

8.1 Overall engine efficiency of a T63 at cruise conditions. 72

8.2 Percentage Allocation of the Measured Efficiency Gain. 73

A.1 Engine fuel control system schematic. A-3

A.2 Engine fuel system. A-5

B.1 X, Y and Z co-ordinate orientation. B-3

B.2 T63 gas turbine engine mounted in a helicopter. B-4

B.3 T63 mounting configuration. B-5

B.4 Lower strut forces and moments. B-6

B.5 Gas turbine drive shafts (a), (b). B-10

B.6 Complete drive shaft and couplings. B-13

B.7 Drive train analogy (a), (b), (c), (d). B-16

B.8 Solid shaft drive train resonance analogy (a), (b), (c). B-17

C.1 Fuel supply system schematic. C-4

C.2 Oil supply system schematic. C-14

C.3 Water supply system schematic. C-20

C.4 Electrical system schematic. C-25

C.5 Eddy-current dynos - type W3S 480 and W3S 700. . . . . C-34

E.1 T63 combustor liner. E-4

E.2 Radiation shape factor for concentric cylinders [5]. E-9

E.3 Radiation sensor design figures (a), (b). E-10

E.4 Radiation shape factor for parallel disks. E-12

F.1 Lower engine mounting assembly drawing. F-2

F.2 Right side engine support assembly drawing. F-2

F.3 Fuel/Air separation unit. F-3

F.4 Radiation sensor assembly drawing. F-4

F.5 Sensor manufacturing drawing. F-4

F.6 Drive shaft and couplings assembly drawing. F-6

F.7 Dyno–shaft adapter plate manufacturing drawing. F-7

F.8 Drive shaft manufacturing drawing. F-8

F.9 Shaft–coupling adapter plate manufacturing drawing. F-9

F.10 Coupling–Engine adapter plate manufacturing drawing. F-10

List of Tables

2.1 Summary of GC/MS Results for the Synthetic Fuel and an Average JP-8 [4] 16

2.2 ASTM Fuel Specification Test Results for JP-8, Synthetic Jet Fuel and Blends [4] 17

2.3 Effects of Synthetic Jet Fuel on T63 Engine Smoke Number [4] 19

2.4 Swirl-Stabilized Combustor and T63 Operating Parameters [4] 25

6.1 ASTM Fuel Specification Test Results for Jet A-1, SPK and Blends [6] 51

6.2 Combustion Products Properties 57

7.1 Fuel Flowrate Measurement Accuracy and Repeatability . . . 63

7.2 Effects of Aromatic Content on T63 Smoke Emissions at Idle and Cruise 66

B.1 Bohler V155 Properties, Hardened and Tempered B-12

B.2 Jurid Coupling: Type GD 80 Properties B-14

C.1 Summary of the Fuel System Components C-6

Chapter 1

Introduction

1.1 Background

Semi-synthetic jet fuel was approved for commercial use by all airlines flying from South Africa, after its incorporation into the UK Ministry of Defence's DEFSTAN 91-91, Issue 3, in 1999. The approval made provisions for 50% (vol) of jet fuel, adhering to the Jet A-1 specification, to consist of Coal-to-Liquid (CTL) synthetic jet fuel (synjet), attained from the Sasol Secunda HTFT plant. Semi-synthetic jet fuel (SSJF) has been in commercial used at OR Tambo Airport (Johannesburg) since July 1999 and no problems or incidents, linked to the use of the product, have been reported during this period. Fully synthetic jet fuel was approved for use in April 2008, allowing aircraft to operate on 100% CTL derived High Temperature Fischer-Tropsch (HTFT) synjet from Secunda.

The foreseeable opportunity for synthetic Low Temperature Fischer-Tropsch (LTFT) jet fuel has spurred an initiative for Sasol Technology Fuels Research to increase the level of gas turbine expertise within the mechanical group. This included gaining an intimate familiarity with the jet fuel business and all relevant aspects of gas turbine technology and jet fuel combustion performance. This project formed a component of the research activity.

Unless special interventions were included in the production plant, LTFT kerosene would be expected to differ from typical petroleum–derived Jet A-1 in the following aspects:

1. Ultra-lower sulfur content (<5 ppm)
2. Slightly lower volumetric energy content, but higher gravimetric energy content
3. Negligible aromatic content (<1%)
4. Potentially adjustable normal/iso-paraffin ratio

The zero sulfur content is not regarded as a problem, provided the lubricity of the fuel is not impaired (an associated property). A reduction in the sulfur content would imply an emissions benefit by reducing SO_2 emissions.

The energy content variations are regarded as a point of debate. If aromatics were blended into the kerosene from an LTFT plant, the density would change directionally towards meeting the current Jet A-1 specification. This would, however, have a number of foreseeable implications:

- Aromatic molecules are one of the classes of components that permeate into elastomeric materials causing swelling and softening. The O-ring seals used in gas turbine engines are designed to accommodate for this phenomenon, and a reduction in aromatic content could potentially cause shrinkage, resulting in leaks in age–hardened seals.
- Aromatics promote soot formation in the combustion chamber. Soot particles cause erosion of turbine blades and the particulate emissions are an identified atmospheric pollutant. Negligible aromatics would thus improve turbine life and reduce emissions, making negligible aromatics beneficial in this regard.
- Aromatic combustion has a strong infra-red radiant emission signature. A fuel without aromatics would be likely to impose a reduced radiant thermal loading on the combustor liner and fuel nozzle. Low aromatic fuel is generally regarded as a positive feature, provided that an abnormal thermal loading profile of the combustor liner does not result.

The normal/iso-paraffin ratio could have a significant influence on the fuel's auto-ignition characteristics. The current Jet A-1 specification does not include an auto-ignition specification, although the freezing point specification does place an indirect limitation on the normal paraffin content. The auto-ignition characteristics could conceivably influence the flame location within the combustion chamber (and hence localised thermal loading), the flame stability as well as the high-altitude re-light capability.

1.2 Project Aim

The primary focus of the project was to ascertain the extent to which reducing aromatic content would affect the performance of a gas turbine. However, since no facilities existed at the Sasol Advanced Fuels Laboratory (SAFL) for jet fuels research, the first objective was to establish a working test cell. Once the test cell was operational, and to analyze the fuel effect on engine performance, the engine had to be instrumented and finally a database of performance and soot emissions measurements had to be gathered while operating on a matrix of fuels.

The effect of aromatics to produce soot is well documented, resulting in higher particulate emissions, increased thermal loading and reduced turbine life. To quantify the aromatic effect on thermal loading, liner temperature measurements were sought, while exhaust gas sampling was employed to measure particulate emissions. Throughout operation pertinent performance data (i.e. fuel consumption, spool speeds, TOT etc.) was captured to allow a full comparison.

1.3 Plan of Development

This report begins with a literature review of heat transfer theory, factors affecting particulate formation and existing literature regarding low aromatic fuels. The engine selection and specifications are discussed, followed by the test cell setup. The necessary research instrumentation is described, along with the associated safety concerns.

The report then focuses on theory necessary to analyse and interpret data captured during experimentation. The results attained during experimentation are presented, then discussed in full. Conclusions are drawn on the basis of these findings, and finally recommendations are made based on these conclusions as well as what was learned throughout the research.

Chapter 2

Literature Review

This chapter reviews research regarding synthetic FT derived jet fuel and the related test cell setup, testing procedures and emissions measurements. The modes of heat transfer to the combustion liner within a gas turbine, as well as heat transfer modelling, are reviewed to gain an understanding of the mechanisms involved in thermal loading of the combustion liner. Testing of various FT fuel blends is reviewed as varying the FT blend ratio is effectively the same as varying the aromatic content of the fuel.

2.1 Combustor Liner Heat Transfer

Combustor liners form an integral part of a gas turbine engine, providing the means to sustain combustion. In so doing they experience mechanical stress, due to a pressure differential, and extreme thermal stresses in the form of high temperatures and thermal gradients. If the liner wall temperature exceeds ~1100 K the useful life dramatically reduces due to increased oxidation and dramatically reduced mechanical strength. The temperature of the flame encompassed by the combustor liner is ~2500 K, making the cooling of the combustor liner essential for sustained operation. The traditional method of cooling has been to provide a thin film of cool air along the inside surface of the combustor liner to shield the liner from combustion gases.

The modes of heat transfer to the combustor liner are forced convection from the combustion gases that are significantly hotter than the liner

wall, and radiation from both luminous (soot) and non-luminous (combustion gases) sources. The quantity of heat transferred by each mechanism varies according to combustor design, the fuel used and operational conditions, however, all modes are significant.

Forced convection can only occur where the cooling film has been breached and physical contact between combustion gases and the liner has resulted. Where the cooling film is intact, the only mechanism for heat transfer to the liner wall is thermal radiation.

Modern gas turbines are operating at increasing pressure ratios, resulting in an increase in the heat transfer to the liner walls by radiation. A secondary effect of higher pressure ratios is the increase in compressor discharge temperature which limits the ability of the annulus air to cool the liner via convection. This has resulted in up to one-third of the total combustor airflow being used to film cool the liner [7].

2.1.1 Gas Radiation

Radiation heat transfer to the combustor liner occurs from both the luminous and non-luminous gases within the combustion chamber. The non-luminous radiation emanates from gases that are heteropolar such as CO_2 and H_2O, while luminous radiation is that emitted by small solid particles, essentially soot. Both luminous and non-luminous radiation must be initially considered when calculating the overall heat transfer to the combustion liner to avoid large underestimates.

The quantity of heat transferred from the non-luminous gases can be calculated knowing the chemical composition, pressure and temperature of the combustion gases as well as size and shape of the gas volume. Since the chemical composition and temperature and of the gases are continually changing within a combustion chamber, Lefebvre [7] has provided a manner to calculated non-luminous radiation heat transfer knowing the bulk or average conditions of temperature, pressure and chemical composition.

Radiation from luminous gases essentially refers to radiation from soot particles, and moreover the fraction of the thermal radiation emitted in the infrared and visible spectrum. At atmospheric pressure soot particles are small in size and few in number but, at higher pressures, such as those encountered in modern gas turbines soot particles grow in size and number [8].

Under these conditions soot particles can attain a high enough concentration and sufficient size to radiate as blackbodies in the infrared region, greatly increasing the heat transferred to the liner walls.

2.1.2 Convection and Radiation

The above section lists the manners by which the liner wall receive energy, however, at equilibrium conditions the liner must loose energy in the form of heat as fast as it is gained. This is achieved by radiation heat transfer to the surrounding combustor case and convection to the cooler air in contact with the wall. Convective cooling occurs inwards to the film cooling air in the primary combustion zone where the film is unbroken, as well as outward to the surrounding air.

2.1.3 Particulate Properties Affecting Heat Transfer

Soot particulates take the form of spheres, long carbon polymetric chains and agglomerated chunks with no discernible shape [9]. If soot particles attain sufficient size and a high enough concentration, as they do in modern gas turbines, they radiate as black bodies [7]. Radiation then becomes the main mechanism by which heat transfer occurs.

The radiation emitted by particulates is affected by their size, shape, mass concentration and optical properties such as reflectance and emittance. Before the above characteristics can come into play, the creation of the soot is necessary. Soot formation is governed by combustion pressure and temperature, as well as the flame type (i.e. Diffusion vs. Premixed). Fuel composition in term of H/C ratio and aromatic content is known to have a pronounced effect on the sooting tendencies of a flame [4].

An increase in soot number density or mass concentration inside the combustion chamber increases the magnitude of radiation heat transfer. Soot optical properties are dependent upon the composition of the soot particulate, specifically the form of carbon comprising the soot particulate. Lee and Tien [10] concluded that the optical constants, reflectance and emittance, are relatively independent of H/C ratio, and Autio and Scala [11] showed that the emissivity of carbon was relatively constant at elevated temperatures. A variation in fuel aromatic content would effect a change in H/C ratio, and

from the research mentioned above this would not significantly effect the optical qualities of the soot produced, and hence the soot emissivity could be assumed roughly constant.

2.1.4 Fuel Hydrogen Content Effect

The hydrogen content of fuel has been shown by Lefebvre [1] to affect the liner wall temperature. Figure 2.1 shows the liner wall temperature at various operating conditions compared to fuel hydrogen content for a GE F101 combustor.

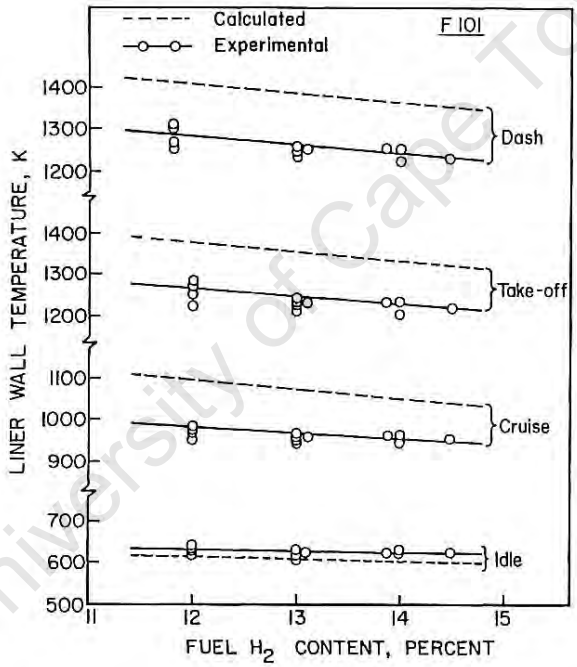

Figure 2.1: Comparison of measured and predicted values of wall temperature for a GE F101 combustor [1].

Reduction in fuel hydrogen content was shown to increase liner temperatures at all operating conditions, with increased load showing a larger temperature differential for the same hydrogen content variation.

The hydrogen content of aromatic–free Synthetic Paraffinic Kerosene (SPK) is higher than standard petroleum–derived kerosene, and as such similar results to those described in Figure 2.1 would be expected. Table 2.2 shows

that the hydrogen content of the fuel would be expected to increase by approximately 1.75% (mass), when changing from a petrolemu–derived jet fuel ($\approx$ 20% (vol) aromatics) to aromatic–free SPK. Figure 2.1 shows the liner wall temperature would be expected to reduce by $\approx$ 50 K at takeoff power, and $\approx$ 10 K at idle, with a 1.75% increase in fuel hydrogen content.

It has been shown that there is a strong link between the hydrogen to carbon ratio of a fuel and soot formation, with a higher H/C ratio resulting in less soot [12, 13]. FT fuel has a higher H/C ratio than JP-8 due to its higher composition of paraffins, reducing the number of carbon-carbon bonds within the fuel.

2.1.5 Cold-Side Convection and Radiation

Cold-side convection refers to the heat lost via the outer or cool side of the combustor liner. The magnitude of heat lost through cold-side convection is proportional to the annulus gas velocity and the liner-gas temperature differential. Low annulus velocities result through operation with a centrifugal compressors and radial air delivery to the combustor liner in the T63, leading to minimal cold-side convection [7].

Convective cold-side heat transfer from the cool side area of the liner can be increased via the incorporation of fins or ribs, increasing available heat transfer area. Fins or ribs are generally attached longitudinally although circumferential fins have also been incorporated at the expense of an increased pressure loss (engine efficiency). Evans and Noble [14] showed an average threefold increase in backside convective heat transfer when compared with similar geometries without the attached round wires welded to the surface.

Cold-side radiation refers to heat lost via radiation heat transfer of the combustor liner with the combustor case. The quantity of heat lost in this manner is generally small with respect to the cold-side convection [15].

2.2 Particulate Formation

Particulates are a continual problem in gas turbine engines, forming during the combustion process and growing in size in the combustor, turbine and exhaust. They can cause erosion of the turbine blades, clogging of injection nozzles, and aid in the creation of aircraft condensation trails. Particulates also increase the radiative heat transfer to the combustor liner, increasing film-cooling air requirements and specific fuel consumption. Particulates have also recently been linked to a number of health and environmental problems, affecting primarily the respiratory system.

2.2.1 Soot Nucleation and Growth

The basic soot formation process can be broken down into four steps [9]:

1. nuclei formation
2. primary particulate formation
3. growth by heterogeneous condensation of chemical reaction products
4. growth by turbulent coagulation

Soot is generally formed in the fuel-rich region in the primary combustion zone, adjacent to the fuel spray. In the primary combustion zone a large quantity of the burned products are recirculated upstream, to sustain combustion, and in so doing local pockets of fuel vapour become enveloped in oxygen-deficient zones at high temperature. Much of the soot formed here is subsequently oxidized as it is exposed to lean regions with excess oxygen and hence, the final quantity of soot emitted is the initially produced quantity minus the oxidized portion.

The mechanism of soot formation was explained by Glassman [16] as the pyrolysis of a hydrocarbon fuel leading to the formation of soot nuclei. As burned fuel is recirculated into the unburned zone to auto-ignite incoming fuel, the fuel is heated, and in the absence of oxygen the fuel does not oxidize but rather decomposes to form smaller hydrocarbons, specifically acetylene. The species that are formed by pyrolysis chemically react to form aromatic species which grow by the addition of adjacent aromatic species and small

alkyl species to form polycyclic aromatic hydrocarbons (PAH). Continued growth of the polycyclic aromatic hydrocarbons leads to the formation of soot nuclei with a diameter ∼1 nm.

Ballal and DeWitt [9] conducted a literature review of a number of different studies into the formation of soot with respect to the influence of aromatics and the process described above on the formation process. They found the following agreement between the papers reviewed:

- Soot particulate nucleation was extremely rapid and a physical rather than a chemical process, see Figure 2.2 for the time scales as described by Ballal and Harrison [2].
- Soot precursors were liquid droplets that eventually underwent a graphitization process (e.g. pyrolysis) to form mature soot particles.
- The primary particles in the soot agglomerates were of similar size and collisions were sticky and perfectly coalescent resulting in agglomerates being part soot and part liquid polynuclear aromatic compounds.
- The soot growth species was acetylene, indicating that the rate of pyrolysis of fuel to form acetylene dictates the growth rate of soot.

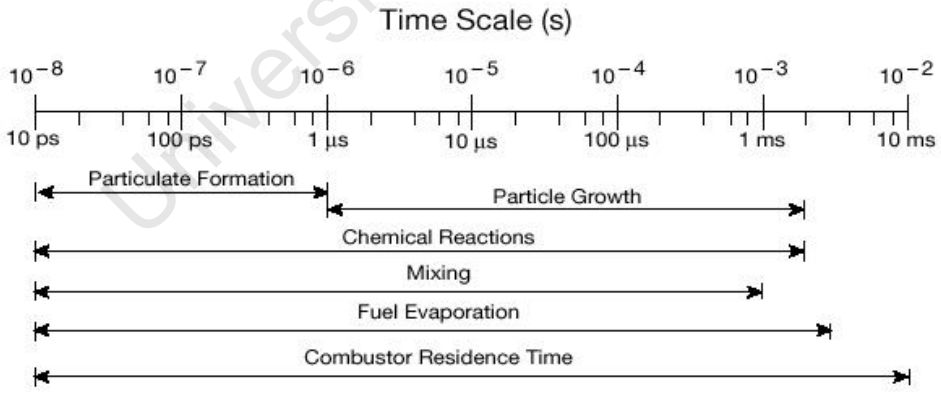

Figure 2.2: Summary of time scales in a typical gas turbine combustor [2].

The coherency found by Ballal and DeWitt [9] lead to the understanding that the instantaneous soot particulate production rate is controlled by the local acetylene concentration and, the particulate number density production

rate equals the nucleation rate minus the coagulation rate. El-Leathy et al. [17] showed a correlation to soot formation and the concentration of not only acetylene but also hydrogen-radicals. Soot formation was shown to begin where significant concentrations of both acetylene and hydrogen-radicals were present. Soot formation ends where acetylene concentration becomes low, even if hydrogen concentration remained high.

Frenklach et al. [18] described the mass concentration rate of soot as being equal to the mass created by nucleation plus the mass created by surface growth, again due to acetylene concentration on active sites.

2.2.2 Soot Oxidation

El-Leathy et al. [17] have shown experimentally in diffusion flames that the OH mechanism is primarily responsible for the oxidation of soot. The OH mechanism with a collision efficiency of 0.10 described soot oxidation rates reasonably well. The authors found no significant effect of fuel type on soot oxidation rates. It was shown that direct soot surface oxidation by '0' molecules, based on work done by Nagle and Strickland-Constable [19], is small compared to soot surface oxidation from OH radicals.

2.2.3 Health Implications of Particulate Size

Studies on gas turbine engines have shown that synthetic Fischer-Tropsch fuels have a tendency to reduce the particulate mass emissions. Synfuels have also showed a tendency to reduce the particulate number emissions, with a number of health implications [4].

A number of epidemiological investigations have shown a link between the health affects and ambient suspended particulate matter [20]. A specific finding has suggested that adverse health effects may be associated with ultrafine (<100 nm) particle fraction, after lung responses to particles in the 50 nm size range were greater than when the same material was introduced as 250 nm particulates. Particulates emitted from T63 gas turbines have been shown to be almost entirely smaller than 100 nm [4]. A reduction in the particulate number emissions in this range would thus provide a significant improvement in ambient air quality.

2.3 Sasol Fully Synthetic Jet Fuel (FSJF) vs. Petroleum–Derived Jet Fuel

2.3.1 Exhaust Emissions

The emissions characteristics of Sasol FSJF were evaluated by Pratt & Whitney prior to the approval of Sasol FSJF in April 2008. The evaluation of the exhaust emissions of CO, Unburned hydrocarbons (UHC), NO_x and smoke emissions was undertaken at the United Technologies Research Center Jet Burner Test Stand using an 80°, four-nozzle arc sector of a commercial combustor [21]. The synthetic fuel contained 10.9% aromatics and the test results were compared to those attained during operation on a petroleum–derived Jet A, whose aromatic content was not quoted in the source literature but could be assumed to be about 18% [22].

The CO emissions for the FSJF were lower than those for the conventional Jet A at all power settings, specifically at idle conditions. In the Landing and takeoff (LTO) test cycle CO emissions were seen to decrease by 19% with FSJF versus petroleum–derived Jet A. This was attributed to the lower viscosity of FSJF and the resultant improved atomization of the FSJF.

The Sasol FSJF was seen to produce less NO_x than conventional Jet A at all power setting except idle, where the NO_x emissions were virtually unchanged. In the simulated LTO cycle the Sasol FSJF produced 4% less NO_x. No reason was supplied in the source literature for the reduction in the NO_x seen with operation on Sasol FSJF. Theoretically a fuel with a lower aromatic content, such as the Sasol FSJF, would have a higher H/C ratio than the petroleum–derived Jet A. This would theoretically result in the flame temperature of the Sasol FSJF being lower than conventional Jet A, and less NO_x produced via the thermal route.

The differences in CO_2 emissions and combustion efficiency were quoted as being negligible.

The Sasol FSJF produces less smoke than the conventional Jet A fuel, attributed to the greater hydrogen content of the FSJF, or rather the lower aromatic content.

There was a marginal difference in the magnitude of the unburned hydrocarbon at idle conditions, with Sasol FSJF producing less UHCs. The Sasol

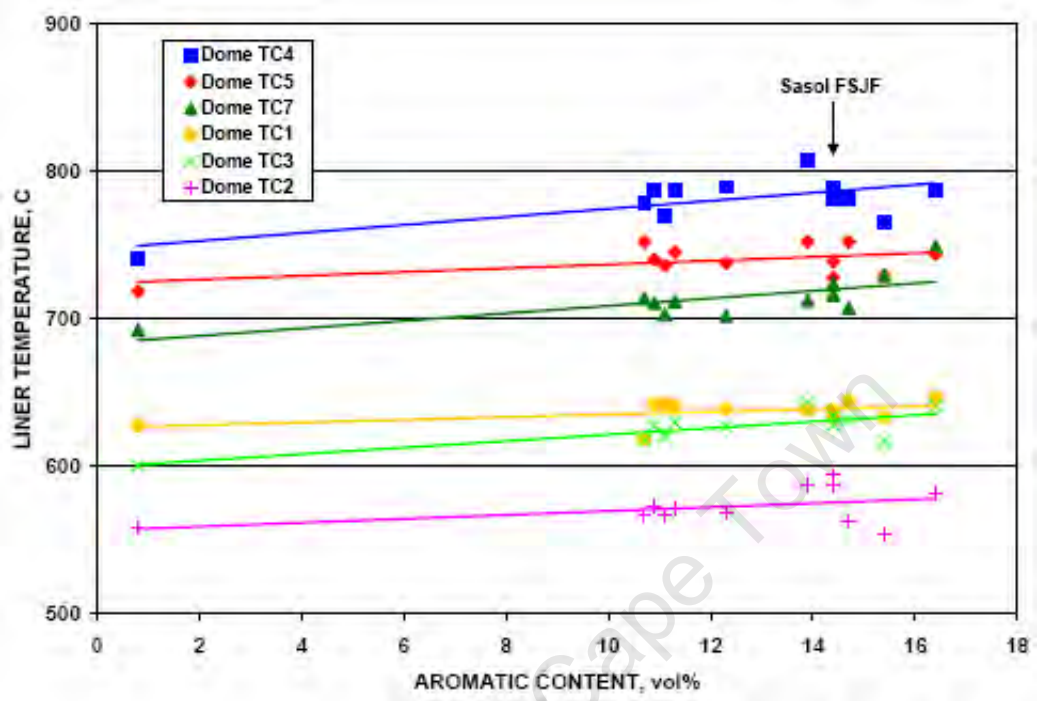

Figure 2.3: Fuel effects on T700 combustor liner temperatures at maximum continuous power [3].

FSJF was measured to produced 11.8 ppm of UHCs, while the conventional Jet A produced 16.0 ppm of UHCs. The difference in the UHC emissions at higher power setting were within the measurement limits of the equipment.

Smoke emissions were seen to decrease by between 10% and 60% with operation on Sasol FSJF, however, due to the excessive data scatter nothing concrete could be drawn other than the smoke emissions would be reduced with operation on Sasol FSJF.

2.3.2 Combustor Liner Thermal Loading

To determine the fuel effect on liner thermal loading a number of thermocouples were spot–welded to the surface of a General Electric T700-GE-701 gas turbine combustor liner at various axial locations [3]. The thermocouples were located from the primary combustion zone to the dilution zone. The combustor section used was the same as that used for the emissions data quoted in the previous section. Figure 2.3 shows the results of experimenta-

tion with fuel of varying aromatic content.

Liner thermal loading was shown to increase with the aromatic content of the fuel, show by the increase in temperature with a rise in the fuel aromatic content. The liner temperature was concluded to correlate with smoke point and fuel hydrogen content as well as fuel aromatic content.

2.4 Emissions Characteristics of a Fischer–Tropsch Jet Fuel

The following data was derived from a T63 gas turbine and an atmospheric combustion rig located at the Propulsion Directorate at the Wright-Patterson Air Force Base (WPAFB) [4]. The data attained from the testing was of great interest as it was performed on the same type of engine as that used at the SAFL, and the fuel blends tested contained varying aromatic contents. Standard JP-8 was used as the baseline fuel and was blended volumetrically with a synthetic FT jet fuel. The synthetic jet fuel that was tested was a natural-gas-derived jet fuel and was produced via the Low-Temperature Fischer-Tropsch process and, as such, would closely resemble the LTFT jet fuel produced by Sasol.

2.4.1 Experimental Setup and Procedure

The gas turbine used for testing was a RR-Allison T63-A-700 helicopter engine that was setup in a fully instrumented gas turbine test cell. The engine was initially run on JP-8 and then run on various blends of JP-8 and the FT fuel as well as neat FT fuel. Testing was done at two power settings, idle and cruise. Idle refers to ground idle, and cruise refers to 90 percent of maximum cruise for the engine. Ground idle is specified by 26 kW output shaft power and 399°C ± 55°C turbine-out-temperature (TOT) while 90 percent cruise is specified by 181 kW output shaft power and 663°C TOT for engine models 250-C18 [23]. During testing the engine power was kept constant by varying fuel flow rate and each test condition was maintained for about 30 minutes to allow for testing to occur at steady state, ensuring the highest repeatability.

To give the greatest run-to-run repeatability the TOT or engine shaft

power must be chosen to be kept constant. Depending on the inlet conditions the TOT will vary for a specific power setting. Although the changes will be slight the engine will be operating at a slightly different condition in terms of combustion pressure, temperature and engine efficiency.

2.4.2 Emissions Equipment

The test facility at the WPAFB is equipped with a number of emissions measurement hardware to facilitate both on-line and off-line measurements. The exhaust was probed with an oil-cooled probe with a heated sample line transporting the exhaust gases to the following sampling and instrumentation systems:

- Smoke Sampler
- Tapered Element Oscillating Microbalance (TEOM)
- Condensation Particulate Counter (CPC)
- Scanning Mobility Particulate Sizer (SMPS)
- Gaseous Emissions Analysis System

The Smoke Sampler, TEOM, CPC and SMPS were all used to measure various aspects of particulate matter (PM), while the Gaseous Emissions Analysis System was used to determine the NO_x, SO_x, HC, CO and CO_2 composition of the exhaust stream. The Smoke Sampler, an in-house design, was used as a general PM indicator providing a Smoke Number (SN) from 1 to 100 based on the reflectance of a piece of filter paper after a specific volume of exhaust gas had been drawn over the filter paper. The TEOM provided real-time measurement of the engine PM concentration while the CPC and SMPS provided particulate number per unit volume and particulate size distribution respectively. The purpose of the above equipment and resulting measurements was to fully classify the effects changes in fuel composition would have on emissions.

2.4.3 Fuel Composition and Properties

Jet A-1 primarily differs from JP-8 in that its specification ASTM D1655 does not mandate the requirement for the three additives that are specified and contained in JP-8; namely the Corrosion Inhibitor/Lubricity Enhancer ($\sim$ 20 ppm), the Fuel System Icing Inhibitor ($\sim$ 1000-1500 ppm), and the Static Dissipater Additive ($\sim$ 5 ppm). This implies that data attained through testing with JP-8 could be considered to apply to Jet A-1 as long as the area of evaluation is not directly effected by the additives contained by JP-8.

The composition of the two fuels as determined by gas chromatography (GC) and mass spectrometry (MS) for the FT fuel and the average values for JP-8 are reproduced in Table 2.1 [4, 24]. The GC/MS results show a significant difference in that the synthetic fuel had a much higher iso- to n-paraffin ratio as well as far fewer cyclic paraffins and alkyl benzenes.

Table 2.1: Summary of GC/MS Results for the Synthetic Fuel and an Average JP-8 [4]

Component	Synthetic Fuel	Average JP-8 (Jet A-1)
n-paraffins	18.0	18.0
iso-paraffins	82.0	41.0
monocycloparaffins	<1.0	10.8
dicycloparaffins	<1.0	8.9
tricycloparaffins	<1.0	<1.0
alkyl benzenes	<0.5	13.3
indans + tetralins	<0.5	4.7
naphthalene	<0.5	<0.2
substituted naphthalenes	<0.5	1.6

The variation in composition of the synthetic fuel is due to the production process of LTFT synthesis. The LTFT synthesis process used by the Syntrolem Corporation produces primarily linear paraffins, that are upgraded for use as jet fuel. The Syntroleum process produces very few cyclic paraffins and aromatic compounds. Depending on the specifications of the cracking unit the fraction of cyclic paraffins produced by the LTFT process may vary.

Shown in Table 2.2, synjet blended with petroleum–derived JP-8 meets all JP-8 specification with blending of up to 50%. Using higher than 50% synjet caused the specific gravity property of the final fuel to fall outsdide of the

Table 2.2: ASTM Fuel Specification Test Results for JP-8, Synthetic Jet Fuel and Blends [4]

ASTM test	standard	JP-8 (POSF 3773)	25% synjet	50% synjet	75% synjet	100% synjet (POSF 4737)
aromatics,% vol(D1319)	max.25.0	15.9	12.8	9.0	4.0	<0.1
hydrogen content,% by mass(D3343)	min.13.4	13.9	14.2	14.6	15.2	15.3
total sulfur,% mass(D4294)	max.30.0	0.06	0.05	0.04	0.02	<0.01
total acid number,mg KOH/g(D3242)	max.0.015	<0.001	<0.001	<0.001	<0.001	0.001
distillation-residue,%vol(D86)	max.1.5	1.3	1.2	1.3	1.4	1.4
distillation-ep,°C(D86)	max.300	256	265	268	271	271
freezing point,°C(D5972)	max.-47	-51	-52	-54	-56	-59
existent gum,mg/100mL(D381)	max.7.0	4.6	3.5	2.4	1.3	0.2
viscosity @ -20°C,cSt(D445)	max.8.0	4.1	4.6	4.3	4.6	4.6
specific gravity @ 15.5°C(D4052)	0.775-0.840	0.799	0.788	0.778	0.767	0.757
smoke point,mm(D1322)	min.19.0	25.0	29.0	37.5	46.0	>50
flash point,°C(D93)	min.38	48	48	48	48	49
heat of combustion,BTU/lb(D3338)	min.18400	18597	18707	18786	18878	18965

current specifications, with all other properties remaining within specification limits.

2.4.4 T63 Results and Conclusions

Throughout testing by Corporan et al. on the T63, no problems were encountered, and stable operation was maintained though testing on all fuel blends and throughout transitioning between fuel blends. Furthermore the authors claimed no significant change in engine performance and/or penalties for operation on the synthetic fuel or the blends. One would expect an increase in the volumetric fuel flowrate of $\approx 4\%$, and a decrease in the fuel mass flowrate of $\approx 2\%$, when switching from operation on petroleum–derived Jet A-1 to SPK. There should also theoretically be an improvement in efficiency with operation on SPK, explained in full in Chapter 6.

Particulate Number (PN) emissions from the T63 while operating on JP-8 averaged $6.0\text{x}10^7(\pm 5\%)$ particles/cm^3 at idle and $2.25\text{x}10^8(\pm 5\%)$ particles/cm^3 at cruise. The reduction in PN is shown in Figure 2.4, with the decrease claimed by the authors to be proportional to the concentration of FT fuel in the blend.

The reduction at idle is shown to be slightly greater than the reduction at cruise. Idle PN production is attributed to the production of smaller particles that are easier to oxidise, and the results with the inclusion on FT fuel further helping by the production of even smaller particulates. The reduction in

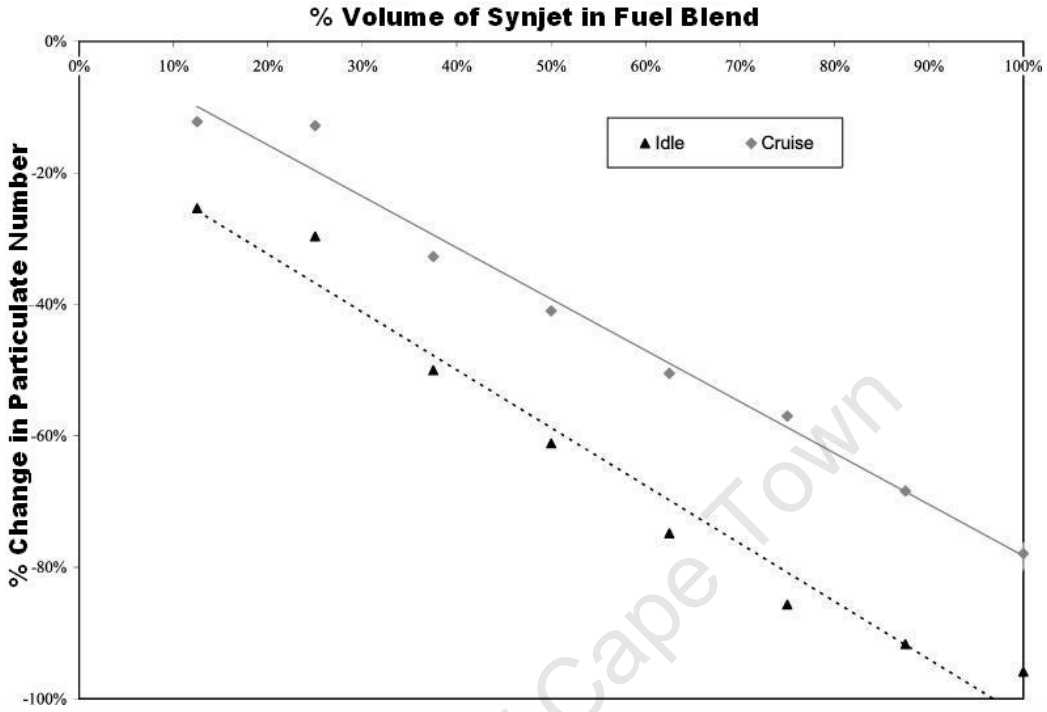

Figure 2.4: Reductions in PN emissions from a T63 engine as a function of synjet in the blend [4].

PM emissions with FT fuel for this study were primarily attributed to the reduction in aromatic components in the fuel blend.

The effects of FT fuel on the particulate size distribution (PSD) are displayed in Figure 2.5. As the content of FT fuel was increased the effect was to shift the peak left towards smaller diameter particles and to lower the peak due to a reduction in the concentration of particulates. A strong correlation was noted between the concentration of FT fuel and mean particulate diameter at both idle and cruise conditions. The particulate mean diameter was found to be 28 and 42 nm at idle and cruise respectively, while operating on JP-8. The mean diameter reduced linearly with FT fuel blends to 17 and 27 nm at idle and cruise respectively, for neat FT fuel. The reduction in particulate size is attributed again to the reduction in aromatics, reducing the number of soot nuclei and thus resulting in a reduction in particles available for coagulation and surface growth.

Variations in the PM emissions were measured with the TEOM and are shown in Figure 2.6. There was some variability in the results, ±15–25%

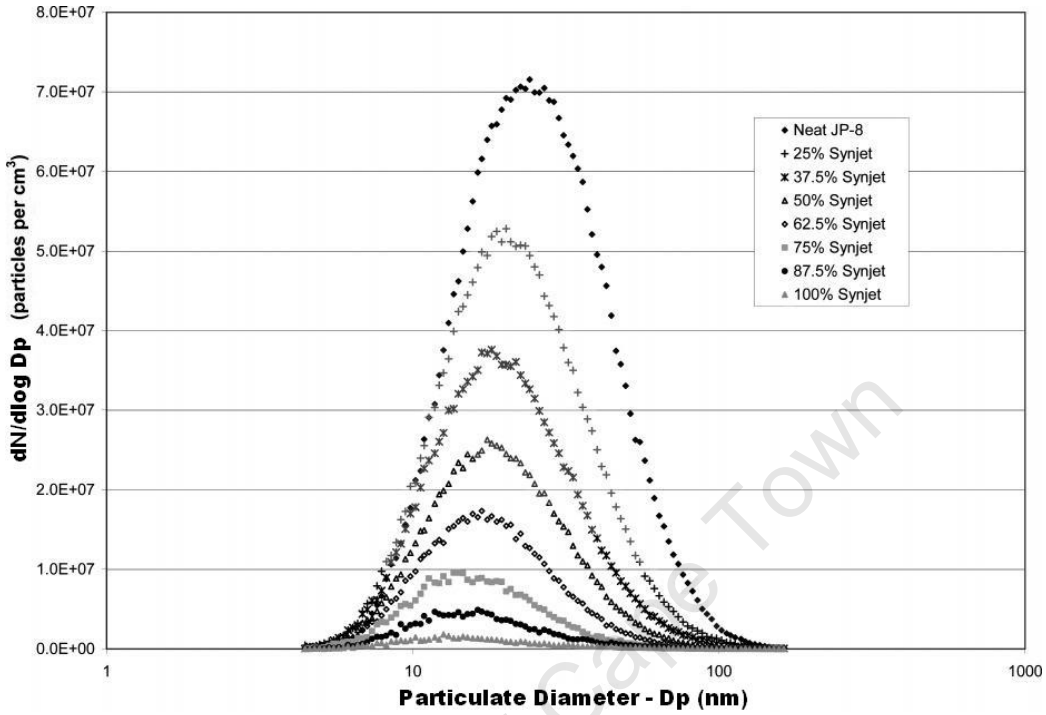

Figure 2.5: Effects of synjet fuel on T63 engine particle size distribution at idle [4].

at idle and ±10–20% at cruise conditions, but the trend showed a linear reduction in PM emissions with synfuel concentration in the fuel. A PM mass reduction of 95% at cruise with neat synjet and approximately 50% for a 50% FT/JP-8 blend at both engine operating conditions was seen.

Table 2.3: Effects of Synthetic Jet Fuel on T63 Engine Smoke Number [4]

	% synthetic fuel in fuel blend					
engine condition	0	12.5	25	37.5	75	100
idle	6.4	4.0	3.8	2.7	<1.0	<1.0
cruise	29.7	26.6	23.7	19.7	8.7	3.8

Engine smoke number (SN) was another measurement that was made while operating on the JP-8, FT fuel and various blends of the two. Three measurements were made for each condition resulting in uncertainty for SNs above 4.0 of ±10% or better, and less than ±20% for SNs between 2.0 and 4.0. The data collected from the SN test at various operating conditions and on various blends are displayed in Table 2.3. The data collected showed

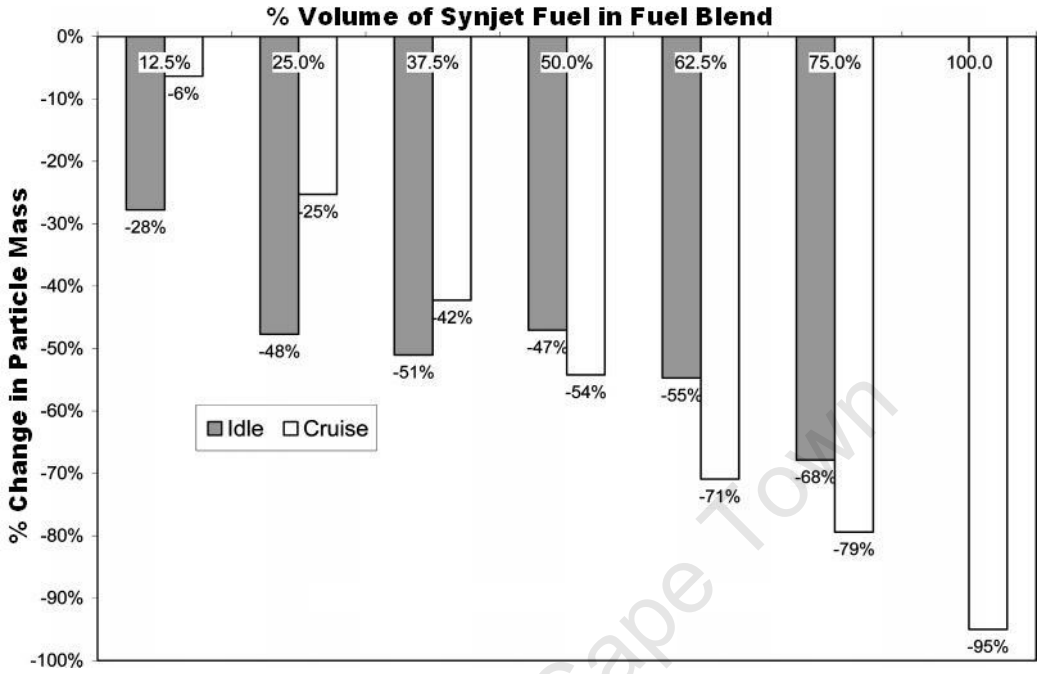

Figure 2.6: Reductions in PM mass emissions from a T63 engine as a function of synjet fuel in the blend [4].

a significant reduction in the SN, proportional to the concentration of FT fuel in the blend. Corporan et al. concluded from their results that although SNs are largely the result of large-diameter particles, the study demonstrated very good correlation between the smoke number, PN, and PM mass for the nanometer-size particles.

The primary gaseous emissions, CO, CO_2 and NO_X were negligibly affected by operation on the synfuel. SO_X emissions were the only emission observed to change, decreasing linearly as the concentration of synfuel in the blend was increased. This reduction was due to the synfuel being sulfur–free.

Unburned hydrocarbon (HC) emissions were slightly higher at the lower power conditions (∼800–1200 ppm) compared to cruise (<40 ppm).

2.4.5 Research Combustor Results and Conclusions

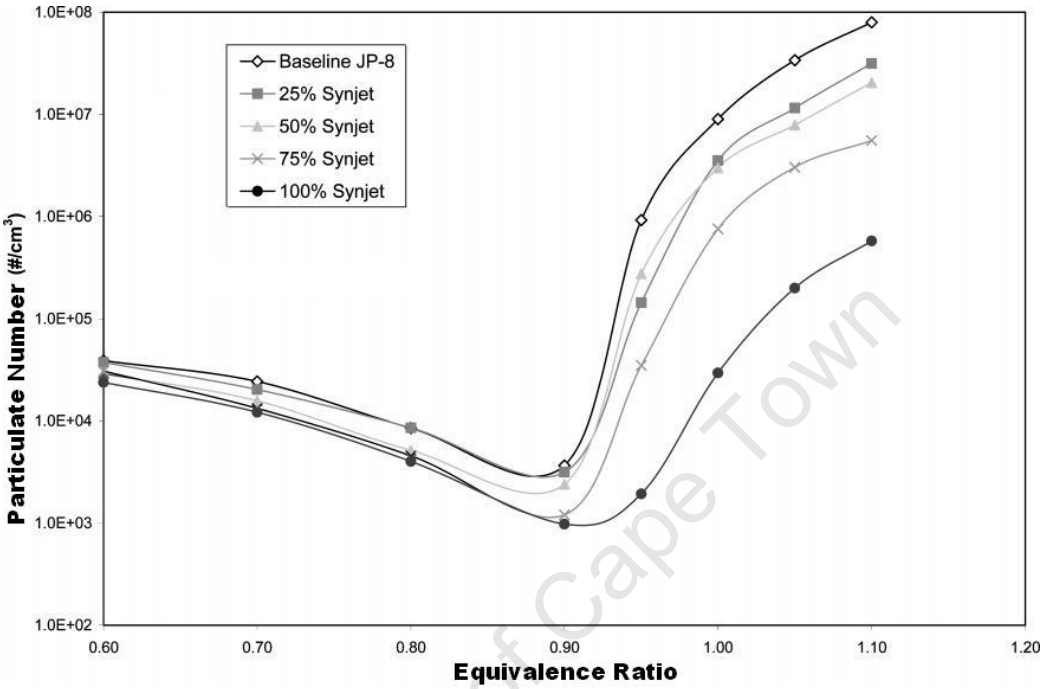

Figure 2.7: Swirl-stabilized combustor particle number as a function of equivalence ratio for several synjet/JP-8 blends [4].

As with the T63 engine, the swirl-stabilized research combustor, poorly described in the source literature, was operated on JP-8 as the baseline fuel, FT fuel and blends of the two. The research combustor provides the ability for one to determine the equivalence ratio effects of FT fuel against JP-8. The PN mass emissions for the combustor, between $3.6\text{x}10^3$ and $8.0\text{x}10^7$ particles/cm^3, were significantly lower than those observed in the T63 engine. The data attained is represented in Figure 2.7.

The data shows that fuel containing a higher concentration of FT fuel produces significantly fewer particulates. The effect of FT fuel was most noticeable at higher equivalence ratios, with a reduction of 2 orders of magnitude (>99%) observed for neat FT fuel for equivalence ratios between 0.95–1.10, compared to and average of 60% reduction between $\Phi = 0.60$–0.90.

The effects of synjet on PSD were evaluated at $\Phi = 1.10$ and are displayed in Figure 2.8. The results were consistent with those attained from the T63 and showed a reduction in particulate concentration and particulate size with

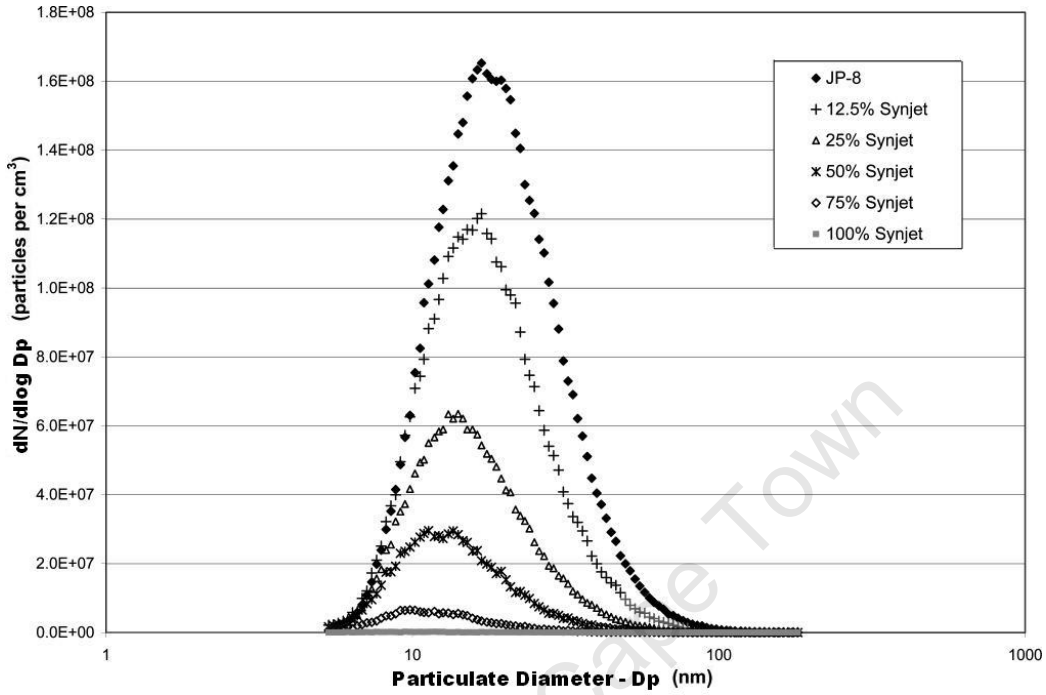

Figure 2.8: Effects of synjet fuel on particle size distribution in a swirl-stabilized combustor for $\Phi = 1.10$ [4].

increasing concentration of synjet. The mean particulate diameter ranged from 13 nm for neat synjet to 21 nm for neat JP-8, therefore the mean particulate size decreased with an increase in the concentration of synjet.

The effect of synjet on CO, CO_2 and NO_X emissions were reported as being minor. A 7% increase in water vapour was measured measured, due to the increased hydrogen to carbon ratio of synfuel. As predicted there was a linear decrease in SO_X emissions due to increasing concentration of sulfur–free synjet in the fuel, show in Figure 2.9.

A chemical analysis was performed for soot samples collected on quartz filters for the research combustor operated at $\Phi = 1.10$, using a thermal desorption technique with subsequent separation and analysis via GC/MS. The test results are depicted in Figure 2.10 and show very low yields of polycyclic aromatic hydrocarbons (PAH) species for products from the 25 and 50% synjet blends. PAH species were below detectable limits for blends with higher than 50% synjet.

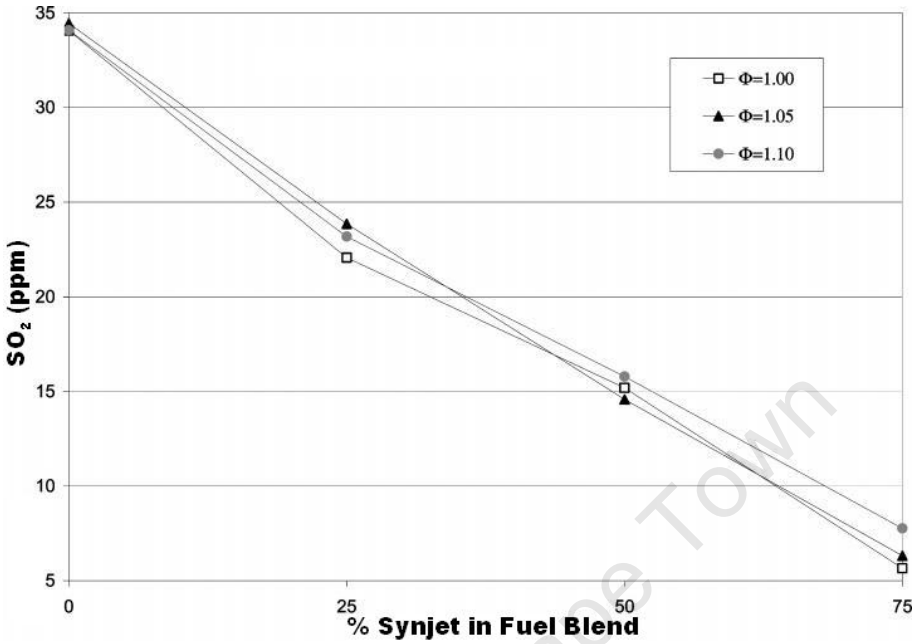

Figure 2.9: SO_2 emissions in a swirl-stabilized combustor as a function of synjet concentration in JP-8/synjet blends [4].

2.4.6 Comparison of T63 and Research Combustor Emissions Results

The T63 engine operates at a pressure 2.5 times higher at cruise than at idle. The increase in operating pressure also raises combustor inlet temperature by $\approx 140°C$. The operational parameter of the T63 engine and research combustor are displayed in Table 2.4. The reduction in both the T63 and combustor were related to the concentration of synfuel in the blend. Although the two combustion platforms are significantly different, the reduction in soot emissions from the research combustor is comparable in magnitude to those experienced by the T63 over the range of equivalence ratios considered. The relative reduction can be seen in Figure 2.11.

It was further concluded that a greater reduction in exhaust soot emissions may occur than those documented when using synfuel as opposed to standard JP-8. This was due to standard JP-8 containing a higher average aromatic content of 17.9% [22], compared to the 15.9% aromatic content of the fuel used to represent JP-8 is these experiments, refer to Table 2.2.

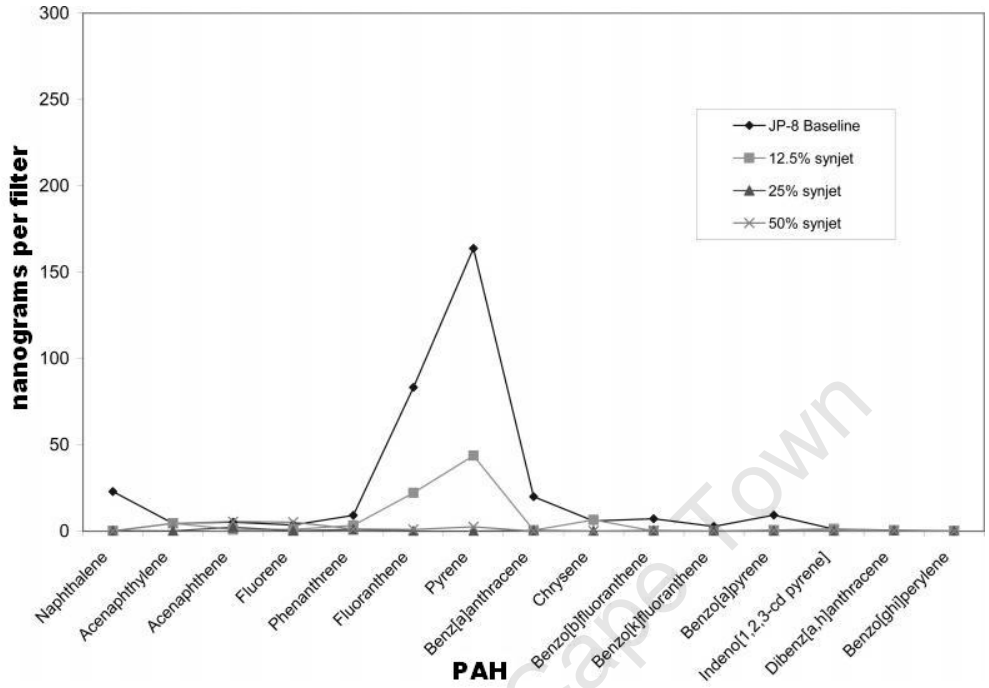

Figure 2.10: PAH species in soot samples as a function of synjet concentration for $\Phi = 1.10$ [4].

2.4.7 Conclusions

A reduction in PM, PN and smoke number was seen in the T63 with a similar reduction in PM prevalent in the research combustor. More than 90% reduction was seen with the PM and PN as well as a reduction in smoke number of more than 80% when operating on neat synjet fuel with resepct to operation on neat JP-8. The reduction was linear with the increase in synjet concentration and was more pronounced in the research combustor at higher equivalence ratios.

As the fraction of synjet was increased, a slight reduction in sulfur emissions was measured, as well as an increase in water vapor emissions in the research combustor. Apart from these emissions variations, other gaseous species emitted were seen to have negligible variations.

No measurable fuel flow rate penalties or detrimental fuel effects on engine operation were encountered with neat synthetic fuel operation or operation with the various blends. The reduction in particulate matter emissions were primarily attributed to the reduction in the aromatic content of the FT fuel.

Table 2.4: Swirl-Stabilized Combustor and T63 Operating Parameters [4]

parameter	T63 engine		research combustor
power	idle	cruise	N/A
combustor pressure(atm)	2.37	5.43	1.0
combustor inlet temp.(°C)	122	259	177
fuel flow(kg/min)	0.40	1.32	0.056-0.123
air flow(kg/min)	43.1	76.6	1.68
equivalence ratio(Φ)	0.135	0.255	0.60-1.10
particle number(particles per cm^3)	$5.0x10^7$	$1.5x10^8$	$3.6x10^3$ to $8.0x10^7$

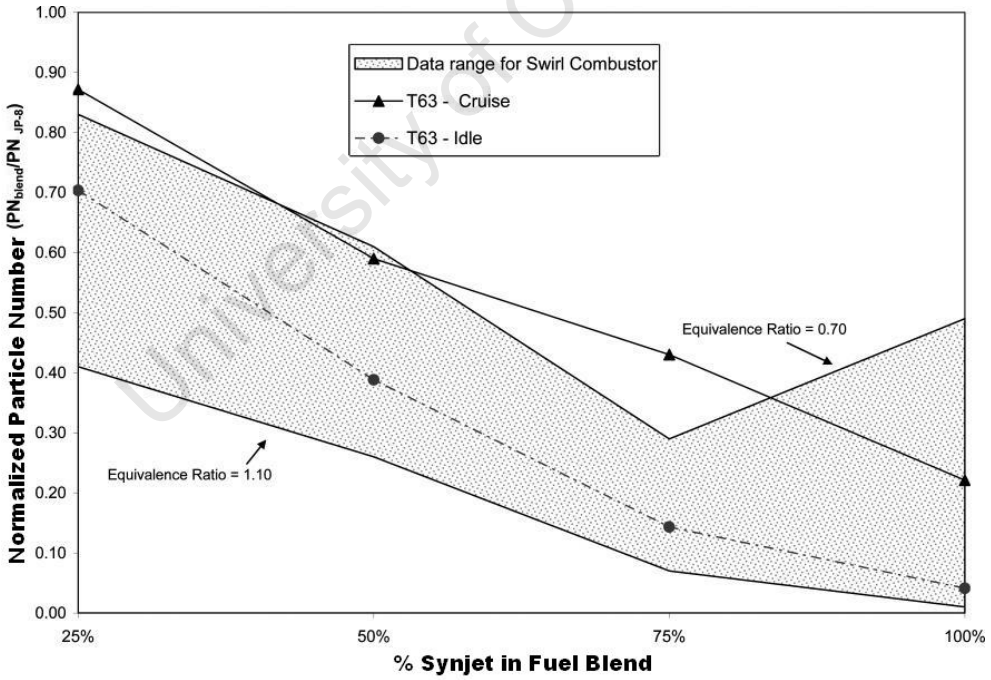

Figure 2.11: Comparison of synjet fuel effects on PM emissions for a swirl-stabilized research combustor and T63 engine [4].

Chapter 3

Test Engine

A RR-Allison T63-A-700 turboshaft gas turbine, model 250-C18 B, was selected for installation and testing at the Sasol Advanced Fuels Laboratory. The engine balances cost with pressure ratio and power output to provide a platform that allows test data to be compared to modern gas turbines. The combustion chamber in a modern gas turbine operates at 40 times the inlet pressure and more, with future engines targeting pressure ratios upwards of 60. The T63 used for experimentation operates at a pressure ratio of 6.18 at takeoff power, making this the lowest pressure ratio from which test data attained would be assumed comparable to commercial gas turbines.

3.1 Specifications

Design power output	317 shp (236 kW)
Design speeds:	
Gas producer (N_1)	100% (51,120 rpm)
Power turbine (N_2)	100% (35,000 rpm)
Power output shaft	100% (6,000 rpm)
Max. gas temp. (TOT)	1380°F (749°C)
Dimensions:	
Length	40.4 in (1026 mm)
Height	22.5 in (572 mm)
Width	19.0 in (483 mm)
Engine mass (dry)	141.2 lb (64.05 kg)

3.2 Fuel Control System

The fuel control system is the only control system on the T63 providing the necessary fuel flowrate to sustain combustion and engine power production. The fuel system is also responsible for protecting the engine N_1 spool by preventing overspeed operation, and the N_2 spool through sustained 100% N_2 speed operation. Engine damage may occur through exceeding the TOT or torque limits. It is the responsibility of the operator to prevent this damage as these sensor do not have direct feedback control of engine fueling. A full description of the fuel system operation is provided in Appendix A.

3.2.1 Operation

The fuel system consists of three main components: the N_1 and N_2 fuel governors and a high-pressure fuel pump. The interaction of the components is described in Figure A.2. Fuel is received via the fuel inlet on the fuel pump, pressurized and sent to the N_1 fuel control unit (FCU). The desired quantity of fuel is delivered to the nozzle, while excess fuel is bypassed back to the pump. The fuel circuit is thus completely contained within the pump and N_1 FCU, with the N_2 governor providing input to the N_1 FCU via the P_G (governor pressure) line. Figure A.1 in Appendix A shows schematically the functioning of the engine fuel control system.

3.2.2 Test Cell Implications

The recommended rotational inertia of a test–cell drive train is between 1.35 and 4.05 kg.m^2 to mimic that in a helicopter. The rotational inertia of the eddy-current dynamometer incorporated was 0.42 kg.m^2, well below the recommended range. Incorporation of a flywheel to raise the inertia to within limits was not desired, as 1 kg.m^2 rotating at 6,000 rpm corresponds to $\approx$ 200 kJ of additional energy.

To avoid the need to incorporate a flywheel, the fuel control system had to be adjusted to account for the low inertia drive train incorporated. Without an adjustment engine N_2 speed, driven by N_1 speed, was seen to oscillate about 6,000 rpm when load was adjusted. The fluctuations were induced by the engine fuel strategy design for response to a high inertia system.

The speed oscillations were minimized by incorporating a controlled bleed on the P_R pressure line, thereby reducing the magnitude of the P_R - P_G feedback with respect to speed (see Figure A.1).

3.3 Mounting

The T63 gearbox housing provides three separate mounting locations on its right, left and lower surface. Each mounting provides attachment for three 5/16 inch UNF (Unified National Fine) threaded members to fasten the engine to the mounting struts. The full mounting design and calculations are provided in appendix B.

3.3.1 Design

The engine was mounted via three separate struts. Each strut was individually adjustable, providing easy alignment of the engine and dyno. The mounting struts were attached via a single bolt to screw jacks, themselves mounted on horizontal trusses. The horizontal trusses were able to slide longitudinally along a sprung base. Figure 3.1 shows the T63 mounted in position on the test bed.

3.3.2 Stress Calculations

The dry mass of the engine, 64.05 kg, increases slightly during operation due to the addition of fuel and oil. The mass of the free-wheeling unit, and half the mass of the drive shaft and couplings were included in the design mass of the engine, conservatively estimated to be 80 kg. The mountings provide the reaction forces necessary to keep the engine motionless while producing torque. Engine spool acceleration is generally slow, thus the forces induced due to the acceleration of the rotating components were assumed negligible.

The CG of the engine is about 80 mm towards the combustor end of the mounting plane. This necessitates the mountings providing an axial force, and a moment to keep the engine stationary. The primary stresses present in the struts were calculated to be <2 MPa, significantly lower than the yield

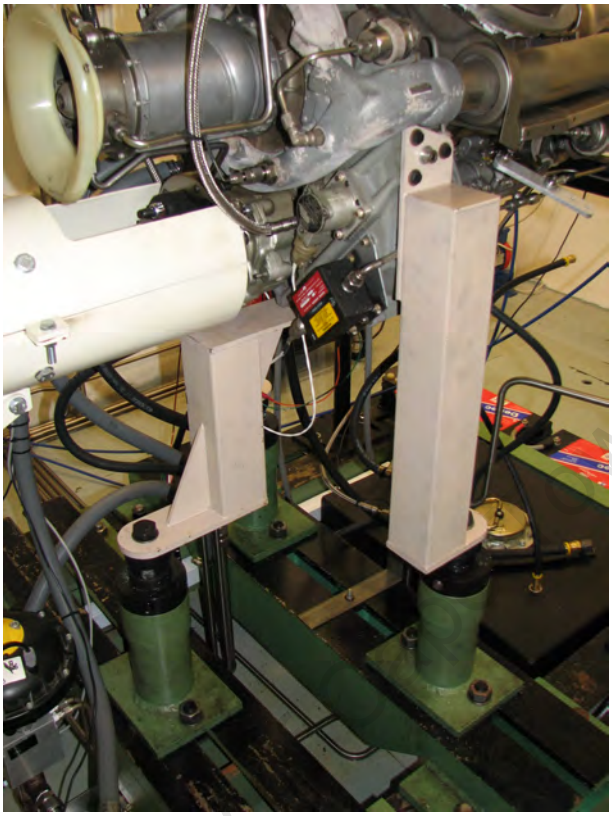

Figure 3.1: T63 test cell mounting configuration.

stress of mild steel $\approx$ 280 MPa [25]. The deflection of the struts under full load was negligible, as desired.

3.4 Operation Monitoring

To ensure safe operation of the engine, it was essential to monitor various systems operation. Engine TOT, N_1 and N_2 speeds, and oil pressure must be monitored and kept within limits to prevent permanent engine damage resulting. In the test cell there are a number of auxiliary systems whose operation must be monitored via temperature and pressure measurements. In addition to the engine and auxiliary systems monitoring, various sensors provide data for the respective research that must be monitored and/or captured.

3.4.1 Temperature

The necessary temperature measurements and limits were as follows:

Measurement	Upper Limit °C	Lower Limit °C
Engine Stabilised TOT	749	350
Mixed Exhaust Gas	200	None
Engine Oil-Out	107	0
PTO Oil-Out	107	0
Dyno Water-Out	60	1

Oil-out temperature was limited to prevent degradation of the oil, and to keep oil viscosity within the correct range. TOT limits exist to prevent irreversible damage to the combustor liner and turbine blades, while the exhaust gas mixed temperature was limited to prevent overheating of the test cell extraction fan.

3.4.2 Speed

100% speeds for both the N_1 and N_2 spools are stipulated in the specifications (section 3.1). At any operation above idle, the N_2 shaft must operate at 100 $\pm$ 2%.

The necessary speed measurements and limits were as follows:

Measurement	Upper Limit %	Lower Limit %
N_1	104	None
N_2 @ Idle	71	59
N_2 @ Normal Operation	102	98
N_2 @ Loss of Load	120	N/A

All engine speed limits are specified to protect drive train components from physical damage.

3.4.3 Pressure

Only engine oil and fuel supply pressure need monitoring to ensure proper engine functioning; however, ambient test cell pressure, water supply pressure and a number of others must also be monitored to ensure proper functioning of the dynamometer and ventilation system.

The necessary pressure measurements and limits were as follows:

Measurement	Upper Limit bar gauge	Lower Limit bar gauge
Engine Oil	8.96	6.21
PTO Oil	1	0.5
Engine Torque Sensor	6.89	2.07
Fuel Supply	0.7	0.4

Engine oil pressure was specified by the manufacturer and was crucial to proper engine functioning. Engine torque sensor pressure limits denote the operational range of the pressure–power correlation. Fuel supply pressure was also specified by the engine manufacturer to ensure proper engine functioning.

3.4.4 Torque

To determine power development it was necessary to capture the engine speed and torque. The dynamometer provided an accurate indication of engine output shaft speed and torque, comparable with the engine torque sensor power. To determine engine torque and power during flight, the engine produces a specific torque oil pressure reading, proportional to engine torque.

The necessary torque measurements and limits were as follows:

Measurement		Upper Limit Nm	bar gauge	kW
Torque	Continuous	337	5.86	212
	30 min limit	397	6.89	250
	10 sec limit	434	7.52	273

The torque and speed reading was available from the dynamometer, from which the power was calculated, while the pressure reading refers to that supplied by the engine torque sensor pressure.

3.5 Research Instrumentation

The T63 has a unique design in terms of the combustion chamber location. The combustion chamber is located on the aft end of the engine, allowing for easy maintenance of the combustion chamber and adjacent components. The location of the combustor reduced the complexity of temperature and pressure measurements within the combustion chamber, and was thus favourable for experimentation. The T63 was instrumented with several thermocouples on the combustor liner, as well as a thermal radiations sensor attached to the wall of the combustor case.

3.5.1 Combustor Liner

For the purpose of this research, it was necessary to attain several liner temperature measurements, as well as the liner and outer case pressure loss. A spare combustion liner was fitted with several 3 mm diameter, K-Type thermocouples, visible in Figure 3.2. The thermocouples contain a mineral-insulation sheath and are capable of sustained operation at temperatures up to 1100°C, above the maximum operating temperature of the combustor liner.

The thermocouples were shaped to lie flush with the surface of the combustor liner, and the outer 316 Stainless Steel casing removed to expose the internal chromel/alumel K-type thermocouple wires. The thermocouples were held in place by brackets, made to secure the thermocouple and present a large enough area to be spot welded. The brackets were spot welded to the surface of the combustor liner to provide a strong, durable connection. The intricate shape of the thermocouples provided additional length for attachment to the liner, and prevented the electrical interface between the thermocouple wires and surface being lost. The elongated tails of the thermocouples were included to ease assembly.

The thermocouples were attached to the surface at two different circum-

Figure 3.2: Instrumented T63 combustor liner.

ferential positions, and spaced evenly along the length of the liner. This supplied liner temperature measurements for a number of separate locations, providing insight into the different heat transfer mechanisms associated with the specific locations on the combustor liner.

There was also a 4 mm hole drilled into the liner to allow a hollow tube to enter during operation, and measure the internal pressure. The hole was placed on the same diameter as the spark igniter, but on the opposite side of the liner. A 3 mm hollow tube was inserted during assembly, and secured via a fitting welded to the surface of the case, providing real time measurement of the pressure inside the liner. The pressure after compression was measured, as well as the intermediate liner pressure, allowing calculation of the pressure drop across the outer case and combustor liner.

During light-off, the temperature of the combustor liner increases from room temperature to several hundred degrees C in several seconds. To avoid the added components breaking loose or cracking, the combustor liner was

heat treated after welding. The liner was heated slowly to it's operating temperature, allowing time for weld stress to be relieved without cracking occurring, then cooled in still air.

3.5.2 Combustor Case

The combustor case was fitted with several Swagelok tube fittings that would allow the thermocouples to exit the engine, while ensuring the case remain sealed. The fittings were welded on the same outer diameter as the combustor liner, enabling easy extraction of the thermocouples during assembly. The fittings were welding onto the surface of the case, and a nut and ferrel arrangement used to both secure the thermocouples, and keep the combustion chamber sealed. Figure 3.3 shows the case with attached fittings for extraction of the thermocouples.

Figure 3.3: Instrumented T63 combustor case.

After welding with the approved rods, the combustor case was heat treated to stress relieve the welded regions, as recommended.

The insertion of the radiation sensor was planned for location downstream of the liner quench holes, where the sensor would gain line of sight of the primary combustion zone via the quench hole. These are the larges openings

in the liner, and the cold-side air flow is extremely low downstream of these holes, limiting the influence of the sensor on annulus air flow.

3.5.3 Implications and Effects of Instrumentation

Research by Evans and Noble [14], whereby round wires were welded to the surface of a combustor liner, showed an increase in the magnitude of heat lost through the cold-side. It is mentions that wires are usually connected longitudinally, although radially connected fins have also been incorporated, at the cost of a slightly increased pressure loss.

The thermocouples attached to the surface of the liner would act to increase the surface area of the liner, thereby increasing the cold–side cooling. The thermocouples are, however, not attached along their entire length. They are pressed to the surface of the liner by the brackets in a few locations. The incomplete contact between the thermocouple and the surface will result in only a small quantity of heat being conducted through the thermocouple wires.

The magnitude of cold–side convection in the T63 is generally low, hence the effect of incorporating the thermocouple wires will be a slight increase in cold–side convection. The secondary effect of an increased pressure loss would be slight noting the small area covered by the thermocouples, and the resulting small reduction in flow cross-sectional area.

The effect of placing a hole in the combustor liner, to measure pressure, would be to provide a new route for air to penetrate the liner. The hole was sized to be blocked by the pressure probe inserted into the combustor liner. This prevented an excessive quantity of air entering of the combustor liner and disrupting the primary recirculation zone.

The welding of various fittings to the surface of the case could possibly create a leak in the outer case. Structurally the case would be unaffected and a leak would be detectable via a reduction in engine power and efficiency.

The radiation sensor was so placed to avoid impacting the major combustor flow regime. An obstruction in the flow may cause the combustion within the combustor liner to become unstable, asymmetric or incomplete. The variations could result in excessive heating of the liner and turbine blades, causing either reduced life or component failure.

Chapter 4

Test Cell Installation

A test cell was equipped to suit the T63 gas turbine engine, selected for the fuels testing. All systems necessary to enable engine operation were identified, designed and implemented. Once the test cell was complete, engine operation was possible throughout the entire load range, as well as the ability to perform exhaust gas sampling and engine performance analysis. The detailed design of the various test cell systems is included in appendix C.

4.1 Load Control

Engine load control was enabled through the incorporation of a Schenck W3S 480 eddy-current dynamometer. Type W3S is a heavy-duty eddy-current dyno with three rotors, designed and built for the testing of racing engines. The dyno is capable of operation at speeds up to 13,000 rpm.

The engine output shaft operates at an essentially constant speed of 6,000 rpm. Takeoff power corresponds to the maximum engine power output of 236.4 kW, or 376.2 Nm of torque at 6,000 rpm. Figure C.5 shows the speed–power operational range of the dyno. The engine power range, 15 to 236.4 kW at idle and takeoff power respectively, could easily be matched by the W3S 480.

4.2 Drive Shaft and Couplings

To couple the engine and dynamometer a drive shaft and couplings were designed, manufactured and fitted. The shaft and couplings were designed to operate at 6,000 rpm with a torque load of 376 Nm, corresponding to the maximum engine power output. The complete calculations for the drive shaft and couplings are contained in appendix B.

The drive shaft in helicopters is generally extremely short, having a natural frequency of about 620 rpm when coupled with a high inertia rotor and engine. Considering the low natural frequency of a complete helicopter system, it was decided to mimic this arrangement to be sure that operation between 3,600 and 6,000 rpm would be safe. Although resonance is not as much a problem with gas turbines due to the smooth, constant nature of the torque production, for added safety the system natural frequency was determined and avoided.

Figure 4.1: Complete drive shaft and couplings.

Flexible couplings were included on both sides of the drive shaft to increase torsional flexibility, both reducing the torsional natural frequency and dampening torsional vibrations. Figure 4.1 is a representation of the drive shaft and various couplings used to attach the engine to the dyno. The right side is the dyno flange, while the left is the free-wheeling unit mounting flange.

The drive shaft was 600 mm long, allowing space between the engine and dyno to accommodate the various gas turbine components and systems. The natural frequencies of the system were determined to occur at 1,830 rpm and 50,000 rpm, both well outside the operational range of the engine. The whirling frequency of the shaft was calculated to be 13,537 rpm, well above the maximum operational speed of the output shaft.

The lowest torsional natural frequency of the drive train would be passed during light-off, and operation between 3,600 and 6,000 rpm would be sufficiently removed from any system resonant frequencies.

4.3 Fluid Supply Systems

To sustain engine operation, the engine must be supplied with various fluids at the correct temperature. Water is used to cool the dynamometer rotors and engine oil, with engine oil used to transport excess heat from the engine to the oil cooler. Fuel is supplied via a low pressure pump in the desired quantity. All systems were configured to operate as required.

4.3.1 Fuel

Fuel flow varies between 28 kg/h at idle, and 100 kg/h at takeoff power. Fuel was supplied at ≈ 0.5 bar as recommended, to ensure constant delivery and prevent cavitation within the high pressure fuel pump. The fuel supplied was filtered to remove all particulates, and through cyclonic separation all water was removed. Figure 4.2 shows the fuel system designed and installed to supply the gas turbine with fuel.

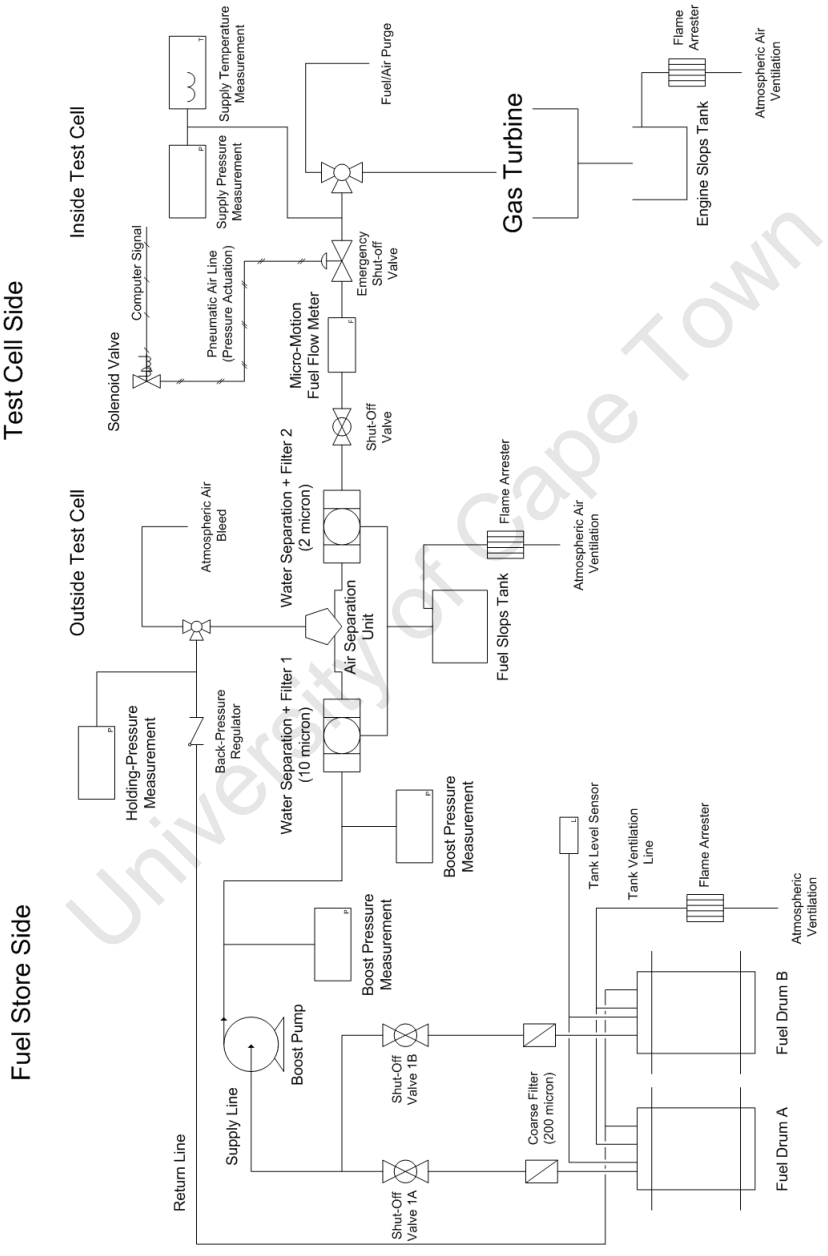

Figure 4.2: Fuel supply system schematic.

Fuel was sourced directly from an adjacent fuel store, limiting the quantity of fuel outside of the fuel store. Fuel was continually circulated, with the supply pressure maintained at 0.5 bar via a back–pressure regulator. An air separation unit was designed and incorporated to circulate the air entrained in the fuel system back to the source drum. This ensured consistent fuel flowrate readings from the micro-motion fuel flowrate sensor. Fuel was filtered at 2 microns to ensure the 5 micron fuel filter, incorporated by the gas turbine, did not require regular cleaning.

Various ball valves were included to allow for the purging of the fuel system, to change from one fuel to the next. Additional valves were incorporated for emergency isolation of the gas turbine engine from the fuel system. Since there was no return fuel line from the engine, fuel flow could be measured on the supply line to the engine. Fuel supply temperature was also measured to allow for conversion between volumetric and mass flowrate.

4.3.2 Oil

The oil supplied was used to lubricate various gears and bearings, and cool components in contact with combustion gases. The oil was gravity–fed to the engine, and cooled via a heat exchanger incorporated on the engine oil return line. This setup resembled that used in a helicopter, and made use of the high pressure – and scavenge gear type pumps. The two pumps supply the engine with oil, and returning oil to the storage tank. Figure 4.3 shows the oil system designed and installed to supply the gas turbine with oil.

The temperature of the oil leaving the engine was measured to ensure oil temperature limits were not exceeded, as well as various other temperatures monitored to ensure proper operation of the system. A separate PTO oil system was incorporated to provide the gas turbine output shaft spline and free–wheeling unit with lubrication.

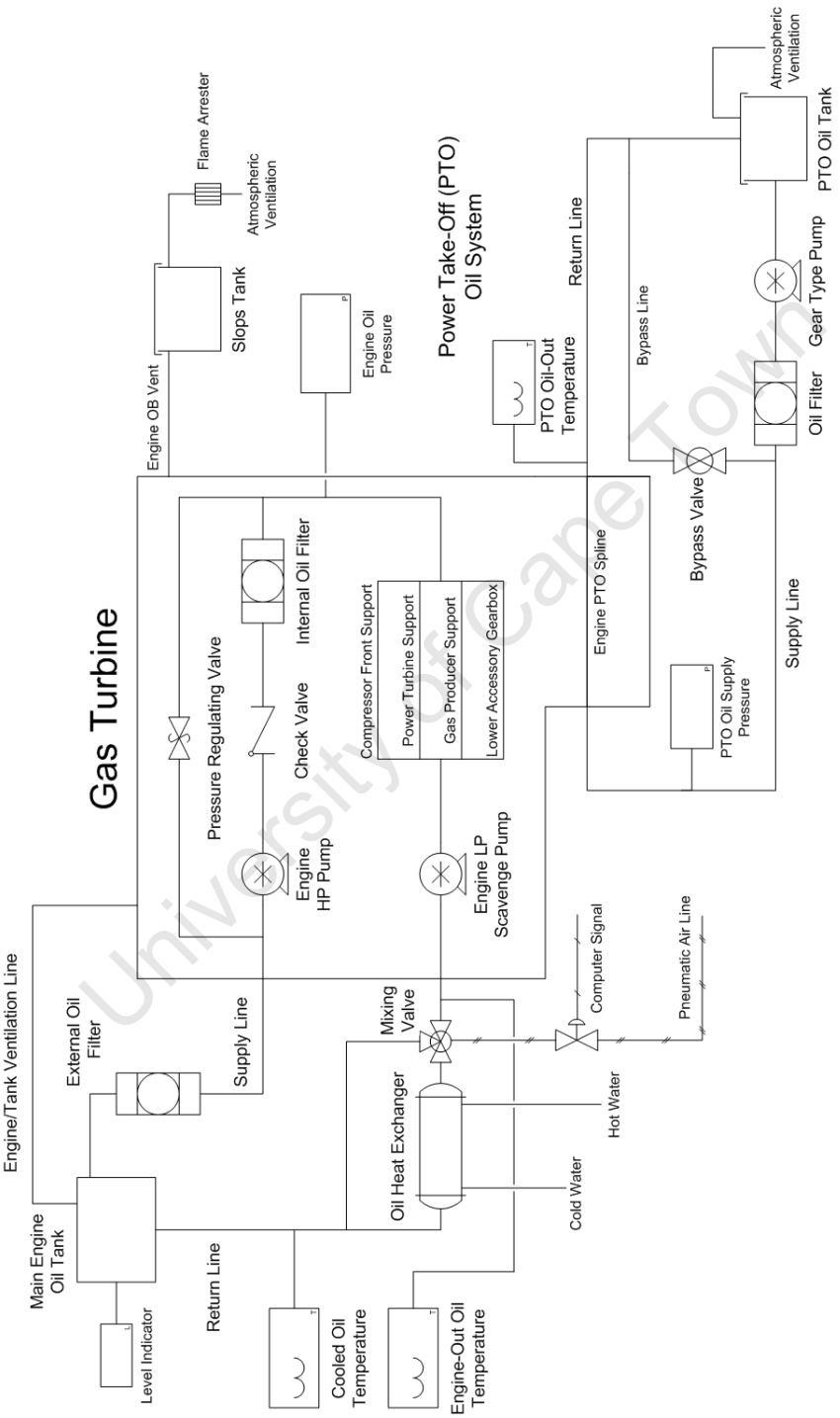

Figure 4.3: Oil supply system schematic.

4.3.3 Water

An existing water circulation and cooling system was incorporated in the gas turbine test cell. Water was used to remove the heat generated by the eddy-current dynamometer, 236.4 kW at takeoff power, as well as the heat removed from the engine via the oil system, $\approx$ 10 kW.

A plate heat exchanger was incorporated on the oil return line, and various valves to control the quantity of water flow to the individual components. The water supply pressure and dyno-out temperature were monitored to ensure proper operation of the system.

Chapter 5

Heat Transfer Theory

Wall cooling of the combustor liner is a continuing area of research by gas turbine OEMs. Combustion pressures continue to rise to aid efficiency, at the same time inlet air temperature associated with compression also increases. This limits the effectiveness of the film cooling air to cool the combustor liner, and raises the flame temperature which increases heat addition to the liner. The full details of the heat transfer analysis are provided in Appendix E.

5.1 Liner Analysis

The combustor liner gains heat via radiation and forced conduction from the hot combustion gases brought into contact with the liner wall. To prevent excessive heat addition the liner is protected via a cooling film projected along the inner surface of the liner wall. The film effectiveness reduces as combustion gases penetrate the flow through turbulent mixing, requiring periodic reinforcement along the length of the liner to sustain the film.

5.1.1 Radiative Heat Addition

Where the film is unbroken the only source of heat addition is radiation from the combustion gases. In these regions the liner looses heat via forced convection, both inwards and outwards, as well as radiating energy to the

surrounding case. The regions on the liner wall immediately downstream of film cooling jets may be approximated by the assumption of radiative heat addition only. In these regions a variation in the liner temperature will thus infer a variation in the quantity of radiative heat transfer from the combustion gases.

It should be noted that due to the cooling film, there is an axial temperature gradient, although the quantity of heat conducted axially along the liner is assumed negligible due to the liner wall being thin.

5.1.2 Convective and Radiative Heat Addition

In regions immediately upstream of cooling jet reinforcement, and in regions downstream of recirculation and dilution holes, it is an oversimplification to assume negligible convective heat addition. It was assumed, however, that the quantity of heat added through convection in these regions is approximately constant, irrespective of the jet fuel being used.

Assuming the above infers SPK, Jet A-1 and their blends have similar:

- Evaporative time scales
- Auto-ignition time scales
- Heat release rates
- Heat of combustion

The properties of petroleum–derived Jet A-1, SPK and various blends are provided in Table 6.1. The Table shows all blends and neat fuels to comply to the Jet A-1 specification, except density. Complying to the Jet A-1 specification implies that the specific fuel would perform as required, providing stable combustion throughout the necessary operational range.

If the flame position and structure, as well as the magnitude of the pressure perturbations within the combustor remain unchanged, combustion instability would be avoided. If these combustion characteristics remain unchanged, the heat transfer to the combustor line via convection would remain roughly constant at a specific operating condition.

5.2 Fuel Effects on the Modes of Liner Heat Transfer

To quantify the the effect a change in aromatic content would have on liner temperature, the combustor liner temperature was measured via thermocouples attached to the surface. Knowing the liner and cooling film temperatures, and calculating the convective heat transfer coefficients for the liner inner and outer surfaces, the magnitude of heat transfer via convection could be estimated. Knowing the outer case temperature, the radiative heat loss from the liner could be calculated.

Operating at steady state, heat addition must be equal to heat loss. Heat addition in regions that only attain radiative heat addition must be solely from thermal radiation. In regions where convection is present, heat is gained via forced convection and radiation, shown in Figure 5.1

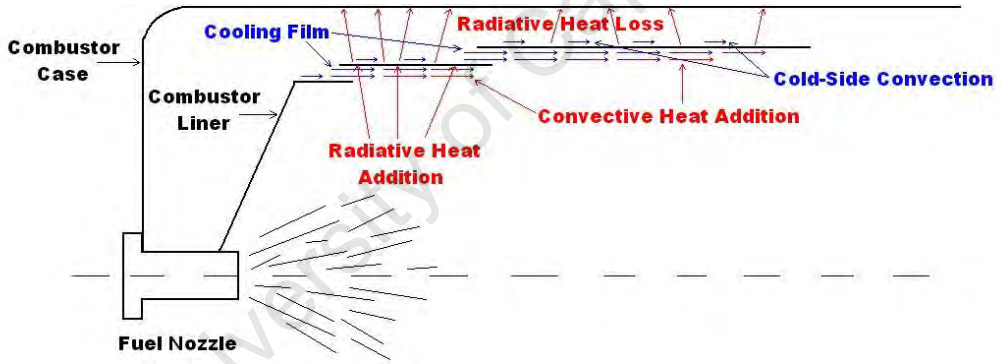

Figure 5.1: Modes of heat transfer to a combustor liner.

In both regions it is assumed variations in liner temperature are the result of variations in thermal radiation due to near constant convective heat addition at a specific operating condition. The equation used for the various calculation are described in full in Appendix E.

Chapter 6

Theory

This chapter contains the theory necessary to analyse and understand the data collected during experimentation on the T63 gas turbine. Incorporation of fuels with different aromatic contents implies a difference in Hydrogen to Carbon ratio, which has a number of implication on both the fuel reaction chemistry, specific energy, and the product properties is terms of the ratio C_p/C_v and R.

6.1 Adiabatic Flame Temperature

6.1.1 Assumptions and Theory

The adiabatic flame temperature (AFT) is an idealization of the temperature that the products of a combustion reaction would attain if no heat was lost (adiabatic) during the reaction. Only the initial reactant and final products are evaluated, without considering the intermediate reactions that occur in an actual combustion process.

The final products of a combustion reaction are well known, and although various paths are used to form the final products from the initial reactant, the total variation in enthalpy, or internal energy, can be evaluated and the total quantity of heat energy released during combustion calculated.

The AFT model used the specific chemical data for enthalpy, internal

energy and entropy from Chemkin ®. Dissociation reactions for CO_2 and the water-gas shift were incorporated to provide a more accurate estimate of the heat released, and the final temperatures attained during combustion. Nitrogen was assumed to not take part in the combustion reaction and passed through as diatomic nitrogen without reacting to form NO_X.

A blend of paraffinic and aromatic fuels were selected, and an equivalent hydrocarbon molecule formed to represent the various molecules within the actual fuel. Only the H/C ratio effects the final products chemistry in this combustion model, hence, model fuels with well known chemical values were incorporated to simulate the difference in H/C ratio between petroleum–derived Jet A-1 and SPK.

In modern lean burn combustors, combustion occurs just above the lean flammability limit, causing the AFT to be significantly lower than in rich burn combustors, thereby greatly reducing the quantity of NO_X formed during combustion. The T63 combustor is a rich burn combustor, and thus has a significantly higher local AFT, in the primary combustion zone, resulting in a significantly higher concentration of NO_X formed during combustion.

6.1.2 Representative Fuel Molecule

Toluene and n-Heptane were blended in order to generate a representative molecule with the appropriate H/C ratio. This allow for the theoretical determination of the fuel AFT and the composition of the combustion products so as to determine the effect of changing the fuel H/C ratio. Toluene and n-Heptane were selected as detailed thermodynamic data was freely available and trusted, and for the purposes of the model sufficient. The fuel modelled as conventional petroleum–derived Jet A-1 was assumed to take the form of a $C_{12}H_{23}$ molecule, and SPK was assumed to take the form of a $C_{12}H_{26}$ molecule. This allowed petroleum–derived Jet A-1 to be simulated via a blend of 25.86% (vol) Toluene and 74.14% (vol) n-Heptane, providing a representative molecule with the exact same H/C ratio as the idealise molecule, and a hydrogen mass content of 13.85%. SPK was simulated via a blend of 7.81% (vol) Toluene and 92.18% (vol) n-Heptane. This provided a representative molecule with the same H/C ratio as the idealised molecule, and a hydrogen mass content 15.38%.

Both of the above mentioned representative fuel molecules provided hydrogen mass fraction in very good correlation to measured values provided

in Table 2.2.

6.1.3 Calculated AFT

The AFT was calculated for reactants having an initial temperature, prior to combustion, of 230°C, and for the reaction to occur at 5 atmospheres absolute pressure. These are the typical conditions within the T63 during cruise power output, where test data was collected. The AFT was calculated using the above mentioned method for a range of equivalence ratios typically experienced in gas turbine combustors.

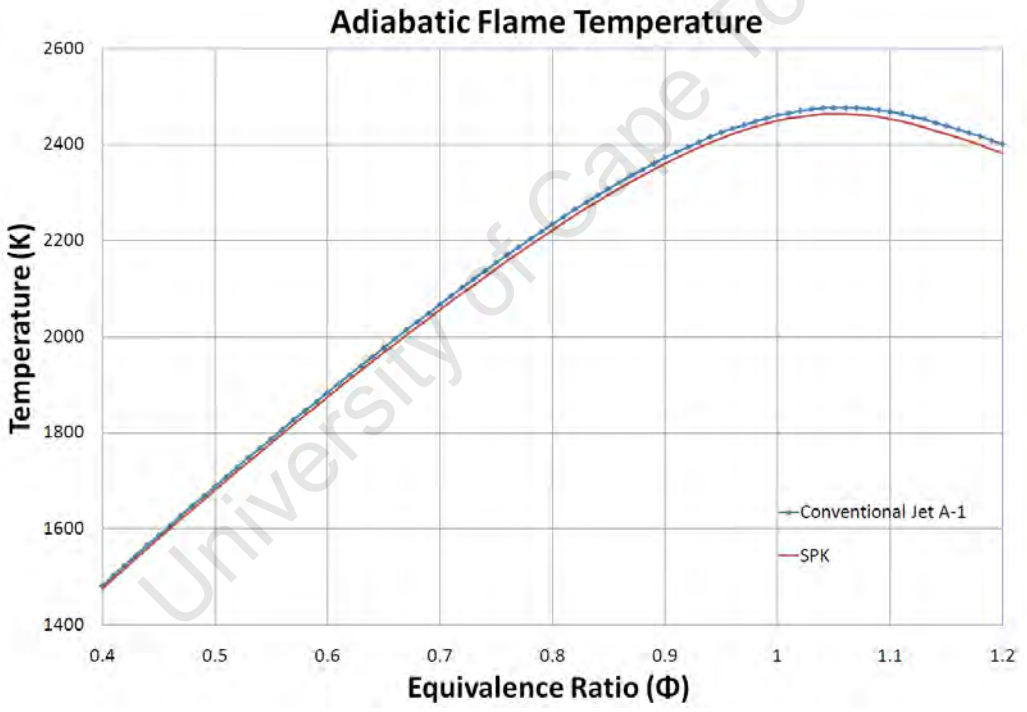

Figure 6.1: Adiabatic flame temperature for petroleum–derived Jet A-1 and SPK.

It can be seen that there is a significant difference in the AFT between combustion at an equivalence ratio of 1.1, slightly rich, as occurs in the T63 primary combustion zone, and combustion at $\phi = 0.5$ that occurs in modern learn burn, low NO_x combustors. At an equivalence ratio of 0.5 the AFT for petroleum–derived Jet A-1 and SPK was 1688.5.7 K and 1680.7 K respectively. At an equivalence ratio of 1.1 the AFT for petroleum–derived

Jet A-1 and SPK was 2468.1 K and 2452.9 K respectively.

The difference in AFT between petroleum–derived Jet A-1 and SPK at ϕ = 0.5 was 7.8 K, while the difference at ϕ = 1.1 was 15.2 K. This suggested that differences related to fuel AFT, forced convection heat transfer from combustion gases and thermal radiation from non-luminous sources, should be more noticeable with experimentation on the T63 than with modern lean burn combustors that operate close to ϕ = 0.5.

6.1.4 Final Gas Temperature

Using the same model as described above, the gas temperature after the secondary mixing zone can be estimated for the range of ϕ occurring during engine operation at cruise power. The AFT in Figure 6.2 represents the temperature of the final mixed products at cruise power prior to entrance into the turbines. This was calculated for both fuels and the following results obtained.

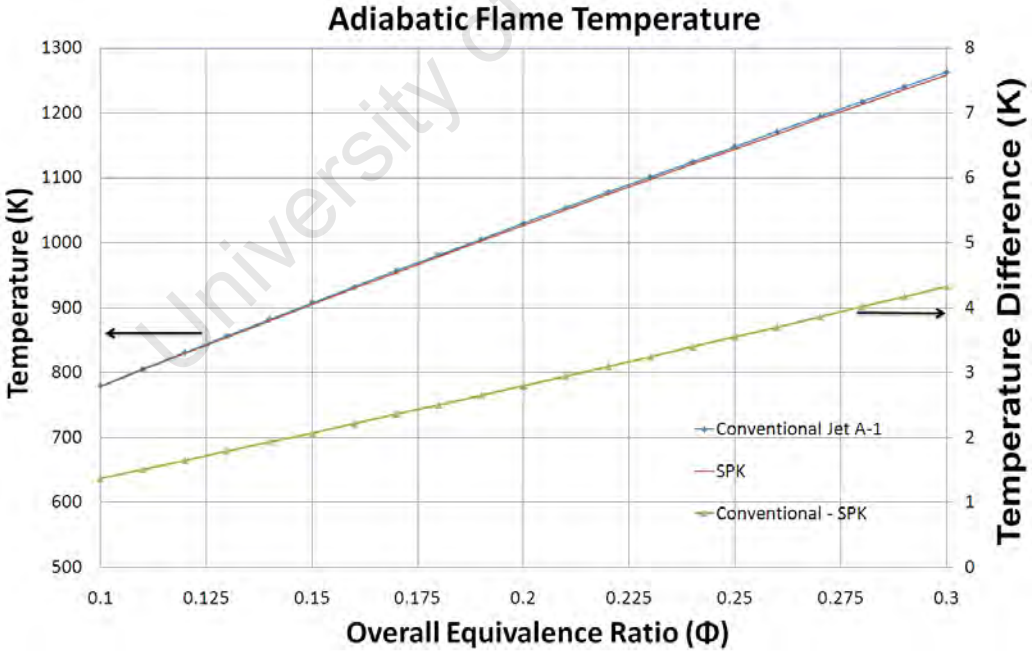

Figure 6.2: Combustion products temperature after combustion and dilution.

It can be seen that the difference in the final gas temperature is diminished from the initial larger variation due to the reduction in the fuel/air ratio. At

a value for $\phi = 0.22$, the difference in gas temperature was 3.1 K.

6.2 Hydrogen/Carbon Ratio Effects on Fuel Properties

The hydrogen to carbon (H/C) ratio of SPK is higher than petroleum–derived Jet A-1, and blending the two varies the H/C ratio of the final product. The H/C ratio amongst other properties influences the fuel energy content, density and C_p/C_v ratio of the final products.

6.2.1 Jet A-1 and SPK blend properties

The FT Synthetic Paraffinic Kerosene (SPK) consisted of highly branched paraffins with a relatively small n-paraffinic content, as well as a small fraction of cyclic paraffins. The SPK was derived from the Catalytic Polymerization (CatPoly) unit from an HTFT plant, and was completely aromatic free. The properties of SPK are compared to those of petroleum–derived Jet A-1 obtained exclusively from a MEROX^{TM} unit, and contained no other severely hydroprocessed or synthetic jet fuel components.

Properties of SPK and petroleum–derived Jet A-1 blends are presented in Table 6.1 [6]. The properties of the various fuels were examined prior to the addition of the static dissipating additive and lubricity improver, resulting in all properties being within specifications except conductivity. Blending SPK at greater than 50% by volume with petroleum–derived Jet A-1 results in density being outside of the ASTM specification.

6.2.2 Energy Density

With an increase in the H/C ratio of a fuel, the gravimetric energy density was seen to increase as shown in Table 6.1. This was in line with pure hydrogen having a lower heating value of 120,000 kJ/kg, 3.66 times greater than the heating value of 32,800 kJ/kg for pure carbon.

The fuel volumetric energy density was seen to decrease with an increase

Table 6.1: ASTM Fuel Specification Test Results for Jet A-1, SPK and Blends [6]

ASTM test	standard	Jet A-1	25% SPK	50% SPK	75% SPK	SPK
aromatics,% vol(D1319)	max.25.0	19.6		11.7		0.0
total sulfur,% mass(D4294)	max.30.0	0.14		0.07		0.0002
total acid number,mg KOH/g(D3242)	max.0.015	0.001		0.003		0.006
residue,%vol(D86)	max.1.5	1.0		1.2		0.8
final boiling point,°C(D86)	max.300	260.0		257.1		226.8
freezing point,°C(D5972)	max.-47	-50.3	-52.8	-57	-64.7	<-80
existent gum,mg/100mL(D381)	max.7.0	1.1		0.7		0.4
viscosity @ -20°C,mm^2/s(D445)	max.8.0	4.10		3.73		3.38
viscosity @ 40°C,mm^2/s(D445)	-	1.23	1.19	1.15	1.10	1.06
density @ 20°C,kg/m^3(D1298)	771-836	802.8	791.0	779.5	767.2	754.1
density @ 15°C,kg/m^3(D1298)	775-840	806.3	794.3	783.2	770.5	757.9
smoke point,mm(D1322)	min.25.0	27		27		35
flash point,°C(D93)	min.38	53.0		50.0		48.5
derived cetane number(ex IQT^{TM})	-	41.7	40.1	38.4	36.1	34.0
specific energy,MJ/kg(D3338)	min.42.80	43.30		43.40		43.78
energy density,GJ/m^3 @ 20°C	min.33.00	34.76		33.83		33.01
energy density,GJ/m^3 @ 15°C	min.33.17	34.91		33.99		33.18
bocle, wear scar diameter,mm(D5001)	max.0.85	0.71		0.67		0.84

in H/C ratio, governed by the much lower density of hydrogen with respect to carbon.

6.2.3 Specific Heats and Gamma

During combustion in a gas turbine, the hydrogen and carbon molecules within the fuel are reacted with atmospheric air. The final products of combustion are essentially CO_2 and H_2O, with excess O_2 and N_2 that did not take part in the reaction, and a small fraction of NO_X, SO_X, H_2 and CO are present from other reactions.

Ignoring the trace oxygenates, the quantity of CO_2 and H_2O formed in a specific combustor, at a specific operating condition, is directly proportional to the H/C ratio of the reactant molecule. With a fuel containing a higher H/C ratio relatively more H_2O is formed, and due to the lower specific heat of H_2O with respect to CO_2, this would result in a lower overall specific heat value for C_p.

$$C_v = C_p - R \tag{6.1}$$

In equation 6.1 [26] C_v and C_p are the specific heats for a gas or fluid measured at constant volume and at constant pressure respectively. R (kJ/kg.K) is the specific gas constant. Gamma (γ) is calculated using equation 6.2, and the values for the specific heats. With R the difference between the value of the numerator and denominator, a smaller value for C_p would result in a larger value for γ.

$$\gamma = C_p/C_v \tag{6.2}$$

The idealised, isentropic, specific work done by a turbine compressor can be described by equation 6.3 [26]. The properties of the gas being compressed, or in the case of a turbine expanded, are accounted for by γ and R.

$$\omega_{Comp} = \frac{\gamma}{\gamma - 1} \; R \; (T_2 - T_1) \tag{6.3}$$

In equation 6.3 T_2 and T_1 are the temperature after and before compression respectively. R is the specific gas constant of the gas, calculated according to the mass fraction of the various species in the gas stream, and is calculated for each species using the universal gas constant and the specific molar mass via equation 6.4.

$$R = \frac{R_U}{M} \tag{6.4}$$

In equation 6.4 M (kg/kmol) is the molar mass and R_u is the universal gas constant (kg/kmol.K).

An increase in the fuel H/C ratio will increase both γ and the overall gas constant R for the final gas stream at the same equivalence ratio. Hence, the properties of the gas entering into the engine turbines will differ for a fuel with a different H/C ratio.

6.3 Idealised Gas Cycle Model

The exact fuel flow rates, combustion equivalence ratios, values for γ and R of the combustion products, temperatures before and after combustion, as well as before and after expansion through the turbine necessary to produce the same power output were calculated via a theoretical model for petroleum–derived Jet A-1 and SPK.

6.3.1 Assumptions and Means for Comparison

The T63 power turbines operate in series with gas producer turbines, thus maintaining the power output from the power turbine constant, as a means for comparison, results in the power extracted by the gas producer turbines also being fixed. For the same pressure and temperature inlet conditions, using the same compressor with the same efficiency for a given energy input from the gas producer turbine, will result in a fixed mass flowrate of air, as well as a fixed temperature and pressure after compression.

Compression and expansion were assumed to be isentropic processes for the purpose of comparison. The mass flowrate of compressor air, as well as the combustor inlet temperature and pressure were assumed constant. Compressor inlet temperature and pressure were assumed to be 25°C and 1 atmosphere, while combustor inlet pressure was assumed to be 5 atmospheres absolute. It was assumed that there was no pressure loss through the combustor liner, and combustion efficiency was 100%.

The AFT model described above was used to calculate the specific gas temperature and properties for a given reactant temperature. Two separate AFT models were setup to calculate the gas temperatures and properties for the two fuels separately and simultaneously, while keeping power output from the power turbines constant.

Using Equation 6.3, the work attained via the turbine and required by the compressor could be calculated. For a given equivalence ratio for petroleum–derived Jet A-1, and a given power turbine power output (arbitrarily as the model was air mass flowrate independent), the fuel flowrate of SPK was solved to attain the same power output from the power turbine, and hence using the above mentioned AFT model, all the properties were calculated.

The model described above produced the following results.

6.3.2 Equivalence and A/F Ratios

A range of overall equivalence ratios most common in the T63 were examined for the petroleum–derived Jet A-1, and the corresponding equivalence ratios for SPK calculated via a numerical solver. The X-axis is arbitrary as the model was independent of the air mass flowrate. However, the power output was dependent on the air mass flowrate, and a flowrate of 1.3 kg/s was selected for the purpose of kW comparison. Figure 6.3 shows the calculated overall equivalence ratios for various power outputs for the two fuels.

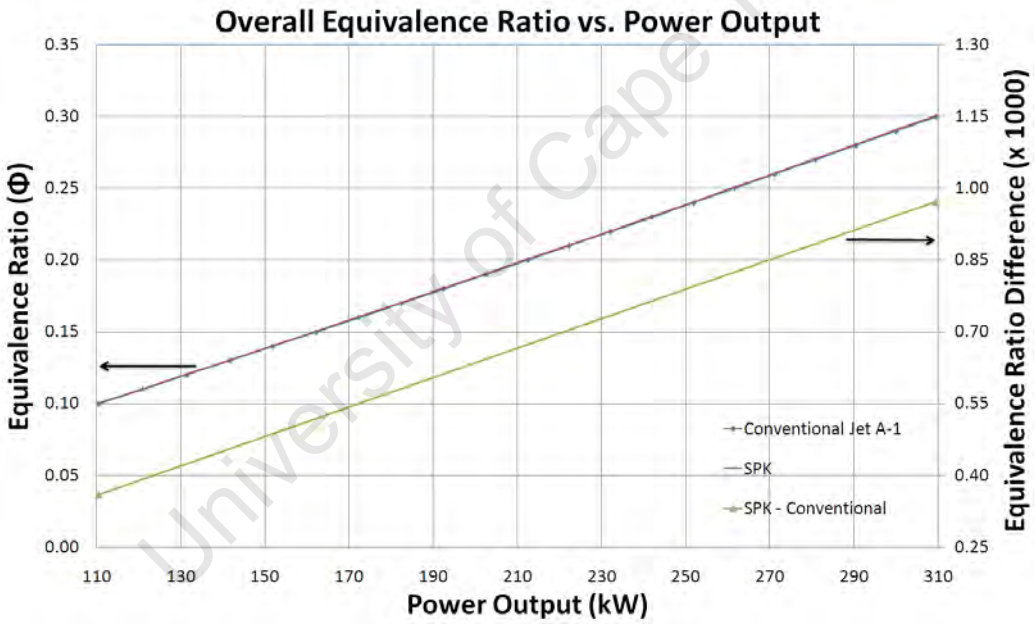

Figure 6.3: Overall engine equivalence ratio for a given power output.

At the same power output, the engine was seen to operate with a slightly higher equivalence ratio while operating on SPK, primarily due to the higher Stoichiometric A/F ratio of SPK with respect to petroleum–derived Jet A-1. This allows a slightly reduced mass flowrate of SPK to mix with the same quantity of air and attain a greater overall equivalence ratio.

The stoichiometric A/F ratio for petroleum–derived Jet A-1 and SPK were 14.666 and 15.014 respectively. Operating at the same power output

and essentially the same equivalence ratio resulted in a significant difference in the overall A/F of the engine, calculated by dividing the stoichiometric A/F ratio by the overall equivalence ratio (shown by Figure 6.4).

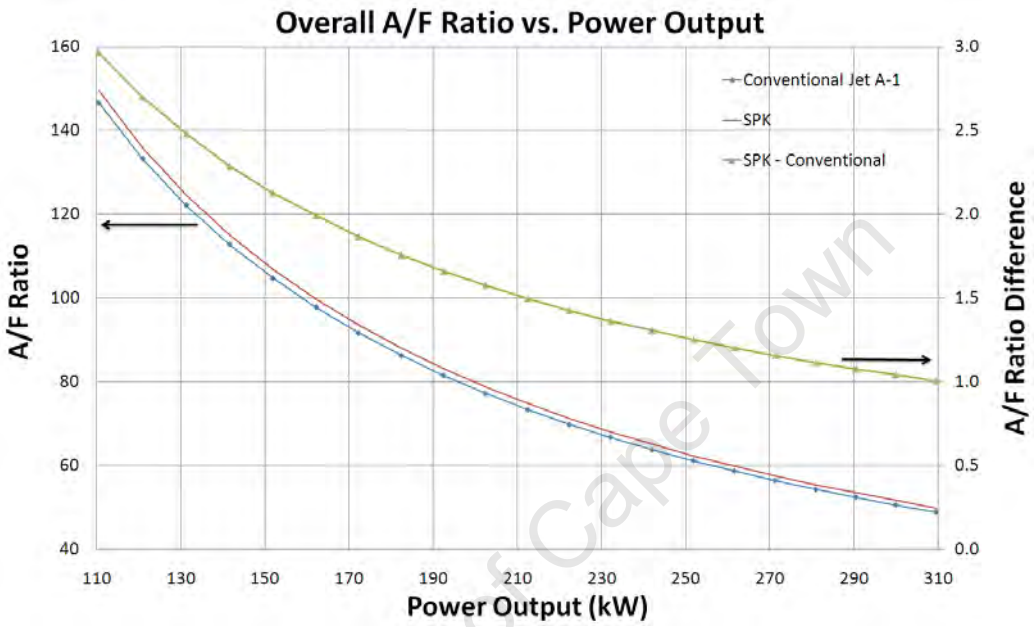

Figure 6.4: Overall A/F ratio for a given power output.

The hyperbolic curve of A/F is due to the A/F ratio tending to infinity as the equivalence ratio tends to zero. In a real engine the air mass flowrate increases with increasing power output, which linearises the curve somewhat. The calculations were done for a fixed air mass flowrate, hence, to attain more power from the same mass of air compressed, and the same pressure drop across the turbine, the temperature drop across the turbine must be increased or the properties of the fluid being expanded must be improved.

Equation 6.3 indicates that the values of γ and R are important in extracting work from a gas stream. For a given fuel, the properties for γ and R are the direct result of the H/C ratio, amongst others. Therefore, an increased mass flowrate of fuel is the only manner to attain more power output from a given mass of air, attained though a greater Δ T temperature drop though the turbine. The increased concentration of CO_2 and H_2O in the final products will modify the product properties and cannot be avoided.

6.3.3 Products Gamma and R Values

At the same equivalence ratio, the values for γ and R of the final products of combustion with SPK were slightly higher than with combustion of petroleum–derived Jet A-1. Due to these difference in the fuels, the engine operates at a slightly higher equivalence ratio with SPK to produce the same power output, shown in Figure 6.3. At the same power output, the difference in the values for γ become exceptionally marginal, shown in Figure 6.5 (Note the difference in γ was amplified by a factor of a thousand).

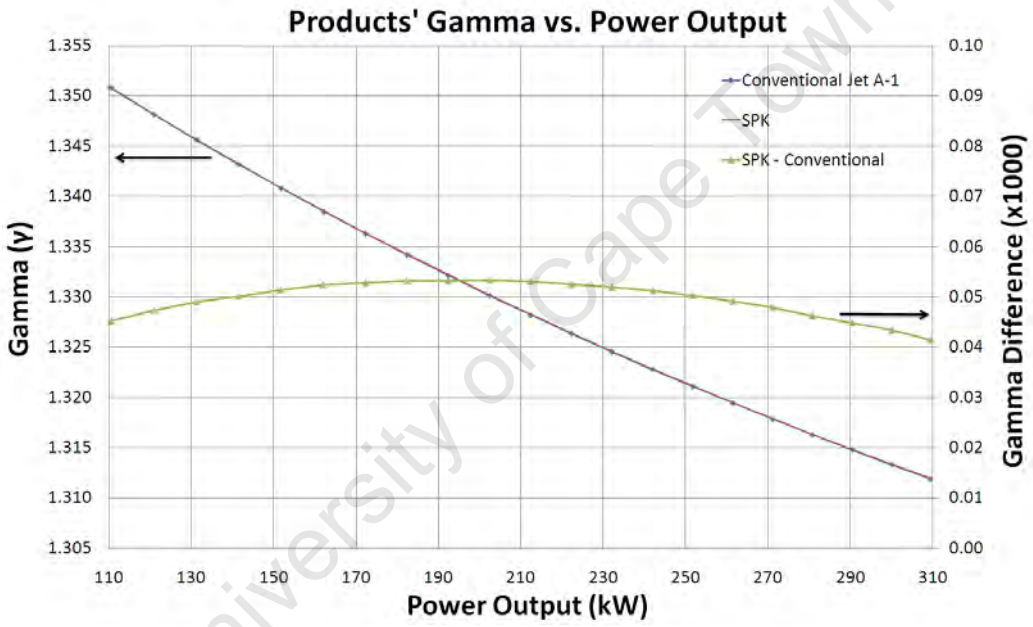

Figure 6.5: Overall values of Gamma for the final products of combustion.

At a slightly different equivalence ratio and the same power output, the SPK provided combustion product properties with a slightly great R value than petroleum–derived Jet A-1. The difference in the value of R was equivalence ratio dependent, with a higher equivalence ratio corresponding to a greater difference between petroleum–derived Jet A-1 and SPK, shown by Figure 6.6.

The differences is the values of R are directly related to the H/C ratio of the fuel, and the corresponding mass fractions of H_2O and CO_2 in the combustion products. The R value associated with H_2O were more than double that of CO_2, shown by Table 6.2. Hence, increasing the mass fraction of H_2O in the combustion products increases the overall R value, and allows for

Table 6.2: Combustion Products Properties

Species	Molecular Mass (kg/kmol)	R (kJ/kg.K)
CO_2	44.009	0.188923
H_2O	18.015	0.461521
O_2	31.998	0.259838
N_2	28.012	0.296812

an increase in the energy extracted from the combustion gases by a turbine, described by equation 6.3, all else being equal.

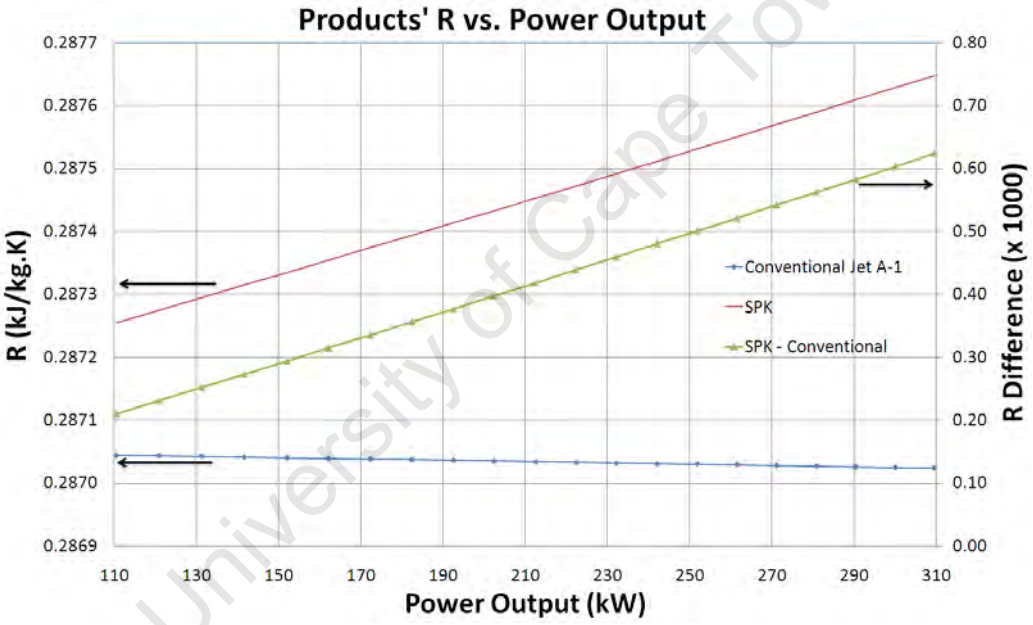

Figure 6.6: Overall values of R for the final products of combustion.

6.3.4 Efficiency and Turbine Inlet Temperature

The variation in the above mentioned properties have far reaching implication in both turbine inlet temperature and variations in overall efficiency, at the same power output. A fuel with the higher H/C ratio produces combustion products with better overall properties for energy extraction via a turbine, and thus an engine operates more efficiently. The improvement in the overall properties allowed for a reduction in the turbine inlet temperature, and a

smaller temperature drop across the turbine to result, which was offset by the increased value of R to produce the same power output. Figure 6.7 shows the overall efficiency for the two fuels, as well as the difference.

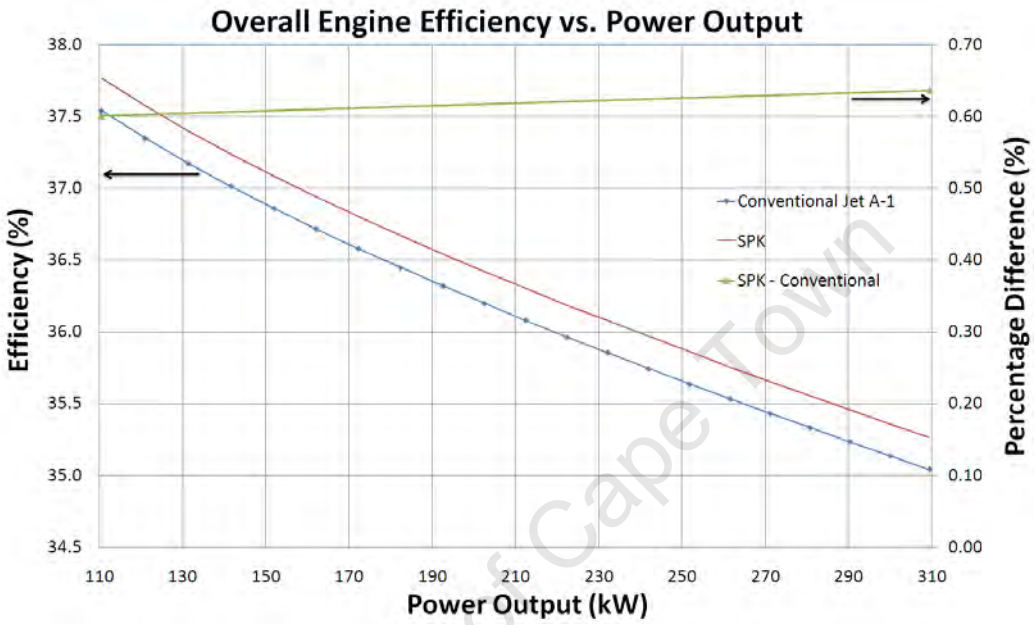

Figure 6.7: Idealised overall engine efficiency.

The efficiency was calculated for the two fuels over the range of ϕ from 0.1 to 0.3, with due consideration given to the gravimetric energy content of the actual fuel being tested.

The reduction in the turbine inlet temperature resulted in a lower final exhaust temperature, indicating the improvement in efficiency due to less of the energy input being lost to the heated exhaust. Figure 6.8 shows the combustion products' temperature prior to entrance into the turbine. The effects of AFT mentioned in section 6.1 play a large role here, as AFT is equivalence ratio dependent. The difference in temperature was diminished due to the engine operating at a slightly higher equivalence ratio with SPK, although the final product temperature was still lower with SPK than with petroleum–derived Jet A-1.

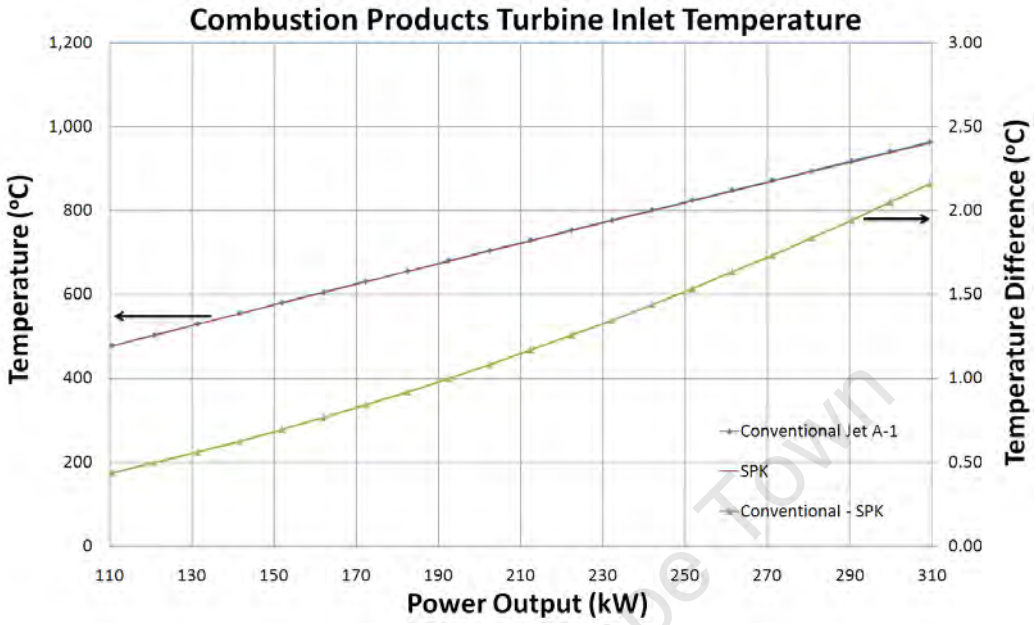

Figure 6.8: Turbine inlet temperature.

6.3.5 Fuel Flowrate

The fuel gravimetric energy density for a fuel with a higher H/C ratio is generally greater due to the much higher heat of combustion of Hydrogen with respect to Carbon. The volumetric energy density is seen to decrease for a higher H/C ratio fuel, attributed to the much greater density of Carbon with respect to Hydrogen.

The two fuels being tested, SPK and petroleum–derived Jet A-1, had gravimetric energy contents of 43.78 MJ/kg and 43.17 MJ/kg respectively. This would infer that the gravimetric fuel flowrate should decrease by 1.4% to match the calorific energy input. However, when combined with the theoretical improvement in thermodynamic efficiency, the model predicted an average gravimetric fuel flowrate reduction of 2.0%.

The modelled fuel mass flowrate is presented in % in Figure 6.9, showing an almost constant 2.0% reduction of the gravimetric fuel consumption of SPK with respect to petroleum–derived Jet A-1.

The decrease in SPK fuel flowrate was attributed to the improved efficiency of the engine, and the changing difference was due to the overall

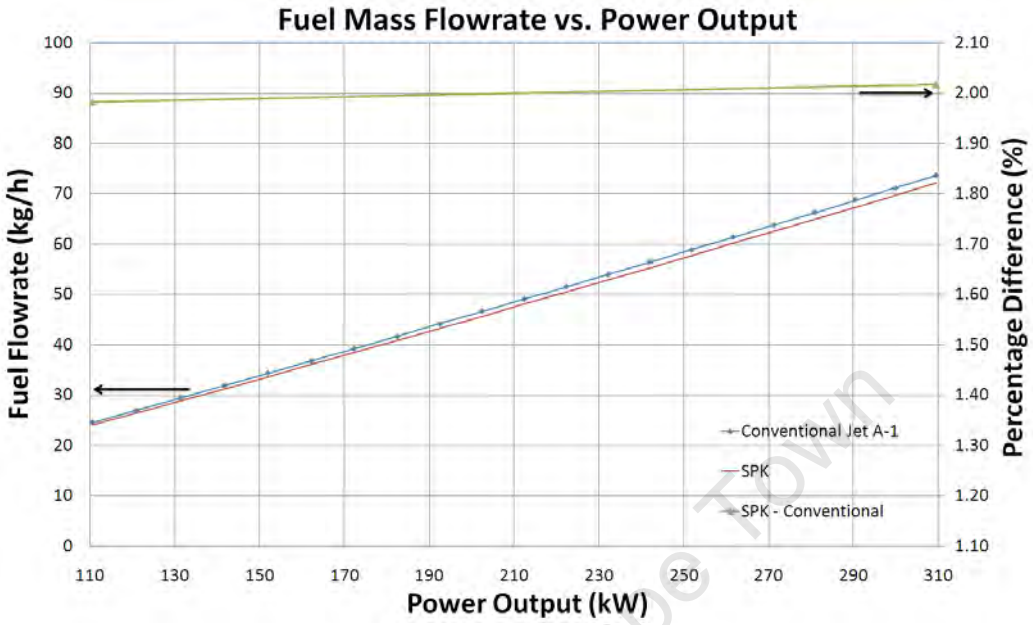

Figure 6.9: Engine gravimetric fuel flowrate.

engine efficiency increasing proportionally to the overall engine equivalence ratio / power output. The fuel mass flowrate contributes to the energy extracted by the turbine, and a diminished fuel flowrate provides less mass flowrate through the turbine. This was also offset by the improvement in the combustion product properties.

6.4 Applying Theory to Analyse the Experimental Data

To aid with the assessment of the fuel effects on engine performance, the experimental air mass flowrate through the engine was sought. The air mass flowrate combined with the measured fuel flowrate would provide the engine overall Air/Fuel ratio and hence, provide a means to link the theoretical predictions with the experimental findings.

6.4.1 Method

The AFT model described above was adapted in order to calculate the air mass flowrate through the actual engine during the experiments, without using a direct measurement. Knowing the initial reactants temperature and the final exhaust gas temperature via measurements, as well as the composition of the gas stream via an inferred equivalence ratio, the overall difference in enthalpy could be evaluated.

From this, the mass flow rate of gas through the engine could be calculated by determining the overall equivalence ratio required to balance the mechanical energy and oil heat dissipated. Knowing the fuel flowrate via measurement, and the equivalence ratio to solve the energy balance, one could calculate the air mass flowrate. Therefore, via a global energy balance of the engine the air mass flowrate through the engine could be calculated.

6.4.2 Assumptions

The composition of the exhaust stream was assumed to consist of H_2O and CO_2, with excess O_2 and N_2, as with the AFT model. The heat lost by radiation and free convection from the outer combustor case was assumed negligible. The heat lost to the oil was assumed to be equivalent to 10% of that provided to the dynamometer.

Errors associated with these assumptions would minimally effect the ability of the model to aid in the comparison of the two fuels, as the assumptions are largely not fuel specific.

Chapter 7

Measurement Accuracy and Results

During experimentation the engine was operated at two load conditions, idle and cruise. Idle refers to engine operation at 60% N_1 and 60% N_2 speeds, while cruise refers to the range of engine operation between TOT 620°C and 693°C, most common during flight. Data was captured at various cruise conditions between 75% and 100% of maximum cruise (M.C.), providing the best manner for the comparison of fuel effects. The load conditions of 75%, 90% and 100% M.C. refer to operation at 100% N_2 speed, and a TOT of 620°C, 663°C and 693°C respectively.

Prior to the incorporation of the instrumented combustor liner, fuels with varying aromatic contents were tested to determine aromatic effect on engine performance and filter smoke number (FSN). Engine performance and emissions were analysed for neat SPK and petroleum–derived Jet A-1, as well as a blend of the two with the following results.

7.1 Power

Engine power was calculated via the dynamometer load cell and rpm sensor measurements. The load cell was calibrated using known weights and a lever of known length, as per standard dynamometer calibration. A power check was provided via the engine torque pressure measurement.

Engine output power provided the means for comparison between different fuels and their associated impact on engine operation. This required the measurement of engine output power to be accurate and repeatable, as power would impact almost every measured quantity. The dynamometer load cell, an HBM Series U2A, and rpm sensor provided the repeatability and accuracy required.

7.2 Fuel Flowrate

The fuel gravimetric and volumetric flowrates were measure by a Micro Motion series 2000 fuel flowrate sensor. The density, temperature and flowrates were all recorded for completeness and to provide a cross check of the volumetric versus gravimetric flowrates. Measurement accuracy and repeatability, as provided by Micro Motion, is shown in Table 7.1. The flow accuracy includes the combined effects of repeatability, linearity and hysteresis.

Table 7.1: Fuel Flowrate Measurement Accuracy and Repeatability

Measurements	Accuracy	Repeatability
Flow	± 0.15%	± 0.05%
Density	± 2.0 kg/m^3	± 0.5 kg/m^3
Temperature	± 1°C ± 0.5% of reading	± 0.2°C

Measurement of the fuel flowrate versus engine power output, while operating on petroleum–derived Jet A-1 and SPK provided the following results.

Referring to Fig. 7.1, the mass flowrate during operation on SPK decreased by about 2.4% when compared to operations on conventional Jet A-1, at a power output of 135kW. The 45% SPK blend showed a liner reduction in the mass flowrate, proportional to the concentration of SPK in the blend, when compared to operation on conventional Jet A-1 at the same power output.

The differences in fuel flowrate between the two fuels maintained an almost constant percentage variation. The fuel flowrate measurements were highly consistent, suggesting very good measurement repeatability.

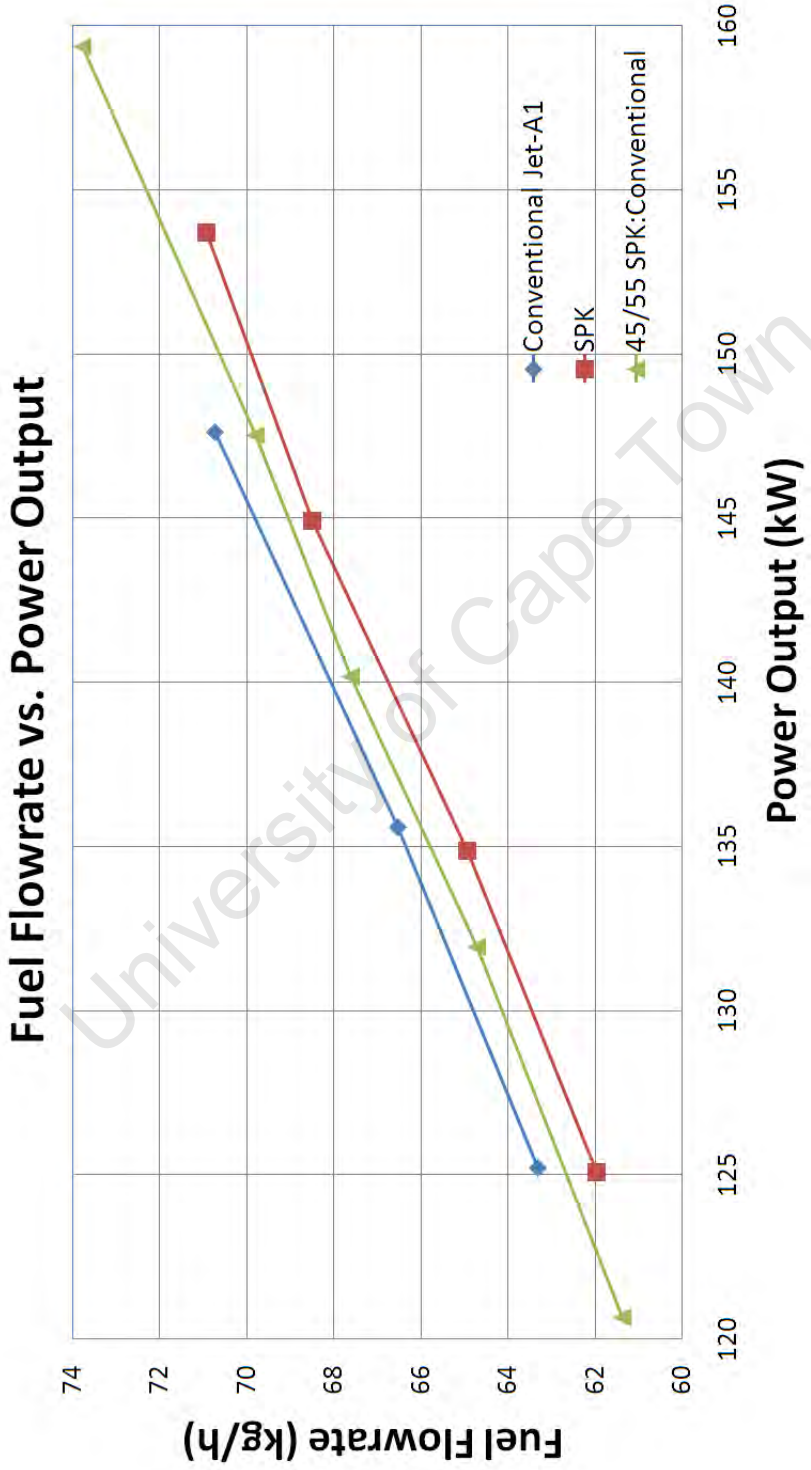

Figure 7.1: Fuel flowrate measurements of a T63 at cruise conditions.

7.3 Soot Emissions

An AVL Filter Smoke Meter was used to provide the Filter Smoke Number (FSN) and engine soot emissions associated with the engine operating condition and the specific fuel tested. The FSN was evaluated by the smoke meter via the mean average of 3 measurements, with constant volume sampling employed, and a sample volume of 1000 ml per sample used.

The Filter Smoke Meter provided smoke numbers indicating the effect of exhaust soot emissions on reflectance, with a FSN of 0 to 10 equivalent to a soot concentration of 0 to 32 000 mg/m^3. The equipment has a display resolution of 0.01 FSN / 1 mg/m^3 / 0.1%. The repeatability is $\leq$ 0.05 FSN for paper blackening results in the range from 0.5 to 6 and filter paper HP0153 [27]. Incorporating the empirically derived correlation equation provided by AVL to estimate soot emissions (mg/m^3), from the FSN, provided the correlations seen between soot and aromatic/SPK concentration, visible in Figure 7.2.

Figure 7.2 shows the soot emissions as a function of the SPK concentration for idle conditions and two cruise power settings.

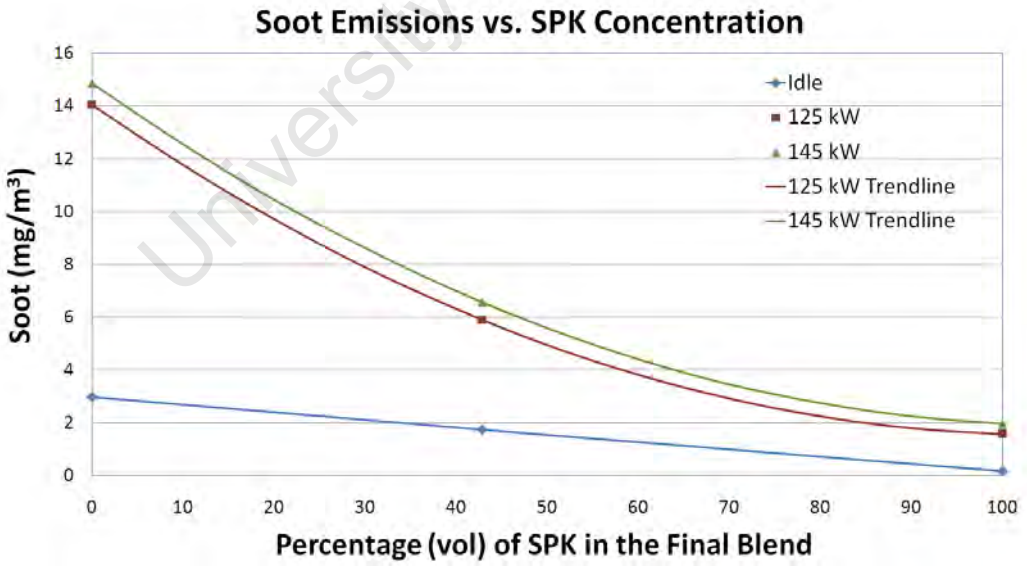

Figure 7.2: Soot emissions vs. %SPK for idle, 125 kW and 145 kW.

The experimental data indicated an apparently linear trend between aromatic content and soot emissions at idle conditions, while higher power con-

ditions appeared to show a second order polynomial correlation as expected. The data correlated well to that previously published by Moses et al. [3] on the influence of Sasol FSJF on particulate emissions. Conventional Jet A-1 produced the highest smoke emissions, while SPK provided the least. The values are provided in Tab. 7.2.

Table 7.2: Effects of Aromatic Content on T63 Smoke Emissions at Idle and Cruise

Fuel	Aromatic Content % (vol)	Filter Smoke Number				Soot Emissions (mg/m^3)			
		Idle	125 kW	135 kW	145 kW	Idle	125 kW	135 kW	145 kW
Crude Jet A-1	19.00	0.22	0.83	0.85	0.87	2.98	14.04	14.44	14.84
Blend	8.13	0.07	0.41	0.43	0.45	1.74	5.92	6.24	6.57
SPK	0.00	0.01	0.12	0.14	0.16	0.17	1.58	1.78	1.99

7.4 NO_x Emissions

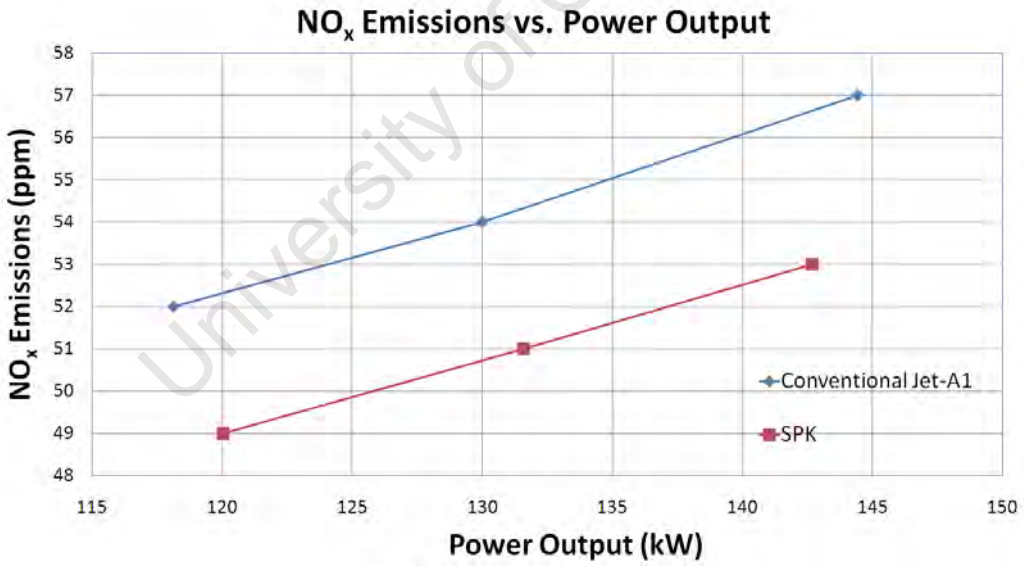

Figure 7.3: Engine NO_X emissions during operation at cruise conditions.

The engine NO_x emissions were measured using a Horiba MEXA-720NO_x analyzer. The equipment can measure both NO_x emissions and air/fuel ratio. The NO_x measurements were found to be at the very low limit of the instrument's measurement range and should therefore be regarded as tentative. However, despite this caveat, the NO_x readings exhibited a proportional

relationship with the engine power output and, as was illustrated in Fig. 7.3, the SPK was found to produce less NO_x than petroleum–derived Jet A-1 at a given power output.

7.5 Gas Temperature

To fully analyse engine performance, the inlet and exhaust gas temperatures were measured during testing. The difference in the inlet and exhaust gas temperatures, along with the knowledge of the reactants and exhaust gas composition, and the energy transferred to the dynamometer and oil, provided the means to conduct a full energy balance on the engine.

The compressor discharge temperature was measured since the combustor liner cooling film comprises compressor discharge air, and as such is fundamental to the energy balance and heat transfer analysis of the combustor liner.

All measurements were conducted at quasi-static conditions due to the effect of thermal lag, allowing time for the thermocouple readings to stabilize. Maximum measurement accuracy was ± 1.5°C for the K-Type thermocouples, and ± 1.4°C for the J-Type thermocouples, including the accuracy of the input modules in the PLC unit.

7.6 Engine Pressure

The absolute compressor discharge, intermediate liner and combustor liner pressures were measured during engine operation. A sensitive Δ P pressure transducer was incorporated to measure the pressure drop across the liner, as the accuracy of the absolute pressure transducers did not allow for calculation of the pressure drop via subtraction.

Gems pressure transducers were incorporated for the absolute measurements, and had an accuracy of ± 0.25%. At cruise pressure, ≈ 5 bar absolute, the measurement accuracy was ± 0.01 bar.

An ABB Δ P transducer was incorporated for the measurement range of 0 - 50 kPa. The sensor was specified as having a maximum deviation of

0.075%, with the quality control test showing an actual maximum deviation of only 0.025%. This ammounted to a maximum error of ± 0.0025 kPa at 10 kPa Δ P, the approximate liner pressure drop at cruise.

Figure 7.4 shows the measured pressure loss percentage across the liner when operating on petroleum–derived Jet A-1 and SPK. The pressure loss was linear with respect to power output, and SPK provided a reduction in liner pressure loss of ≈ 0.2 kPa.

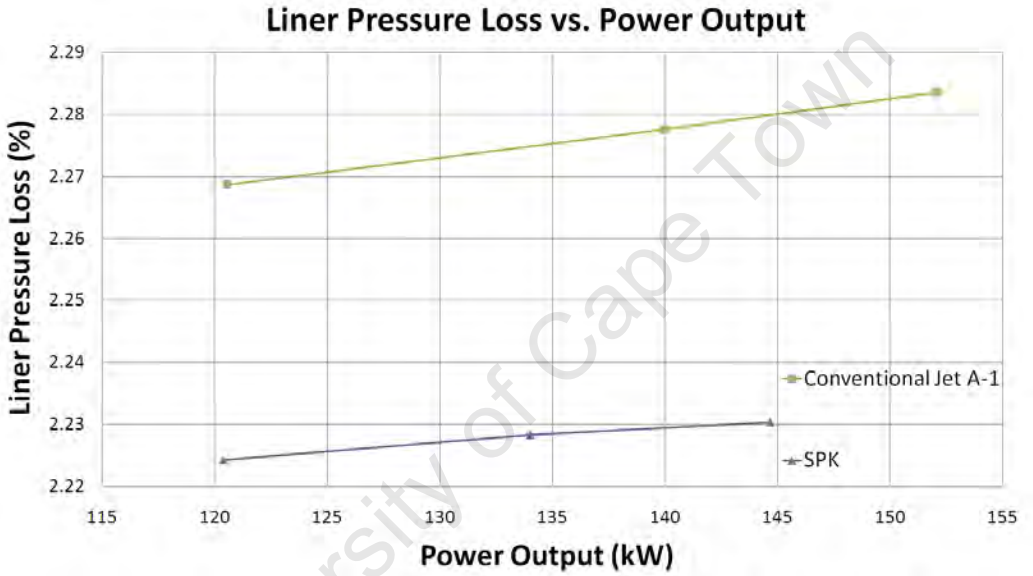

Figure 7.4: Pressure drop across the combustor liner during operation at cruise power.

The reason for the fuel-related difference in the measured combustion liner differential pressure was not immediately obvious. It was surmised that the observed trends were linked to the lower liner temperature and an associated fluid viscosity effect. (Gas viscosity decreases in proportion to the absolute temperature.)

7.7 Liner Temperature

Once the performance and emissions implications of SPK were measured and recorded, the engine was fitted with an instrumented combustor liner and

case. Temperature measurements were captured while operating on neat SPK and petroleum–derived Jet A-1 to provide the two temperature extremes.

The K-Type thermocouples attached to the surface had a maximum measurement accuracy of ± 1.5°C. Due to the attachment of the thermocouples to the cool side of the combustor liner the temperature measured would be slightly less than the inner surface temperature, although the thin liner wall would minimize this discrepancy. As the thermocouples were intended to provide comparative temperature measurements between the different fuels, the absolute value was less important that repeatability, which was essential.

7.7.1 Thermocouple Placement

Several thermocouples were attached at different locations across the combustor liner to provide information about the various means of heat transfer to the liner. The primary combustion zone temperature was measured directly downstream of a film cooling jet (Thermocouple 'E') to be able to infer a variation in thermal radiation loading as radiation is the main source of heat addition in this region.

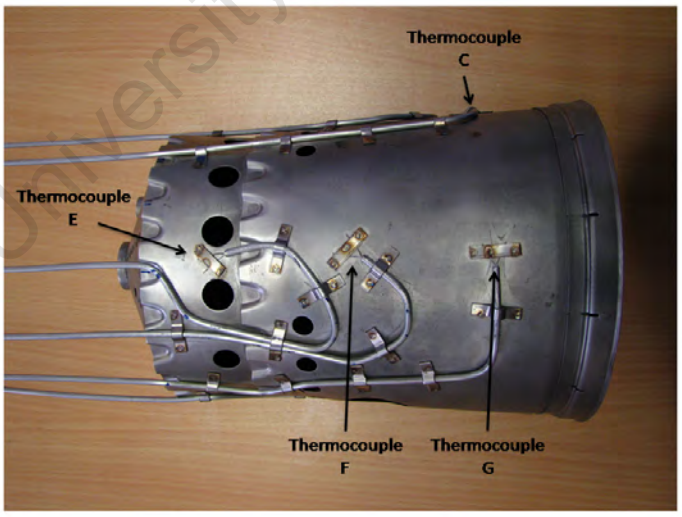

Figure 7.5: Thermocouple placement on an instrumented T63 liner.

Two thermocouples were placed at the turbine end of the combustor liner to be able to infer a variation in the mean gas temperature, and hence the adi-

abatic flame temperature (AFT). The thermocouples were 90 degrees offset from one another to measure differences in circumferential thermal loading due to internal flow dynamics. One was placed immediately downstream of the primary combustion zone thermocouple (Thermocouple 'G') and the other downstream of a quench hole (Thermocouple 'C'). Forced convection becomes the main source of heat addition at the turbine end of the combustor liner, as soot is oxidized and the film cooling air becomes fully mixed with combustion gases.

Another thermocouple was placed midway between the primary combustion zone and turbine end of the combustor liner (Thermocouple 'F') to measure the intermediate liner temperature between the forward and turbine end. In this region both radiation and forced convection are present as significant sources of heat addition.

7.7.2 Thermocouple Measurements

Figure 7.6 shows the temperature measurements that resulted from the experimentation on the T63 while operating on neat petroleum–derived Jet A-1, and SPK.

The liner was seen to attain a consistently lower temperature at all locations when operating with SPK with respect to petroleum–derived Jet A-1. Thermocouple E, which measured the liner temperature immediately adjacent to the primary combustion zone, and showed the lowest overall temperature, as well as the greatest reduction in temperature with operation on SPK. Thermocouple E showed on average a 21.3°C reduction in temperature, or a 24.47% reduction with respect to the compressor discharge air temperature. Thermocouple F showed an average 6.73°C or 3.76% reduction in temperature when operating on SPK.

Thermocouple G and C were both placed at the turbine end of the combustor liner and showed the smallest reduction in temperature. Thermocouple G showed a 4.81°C or 2.11% reduction in temperature, when changing from operation on petroleum–derived Jet A-1 to SPK, while thermocouple C showed a reduction of 5.6°C or 1.72%.

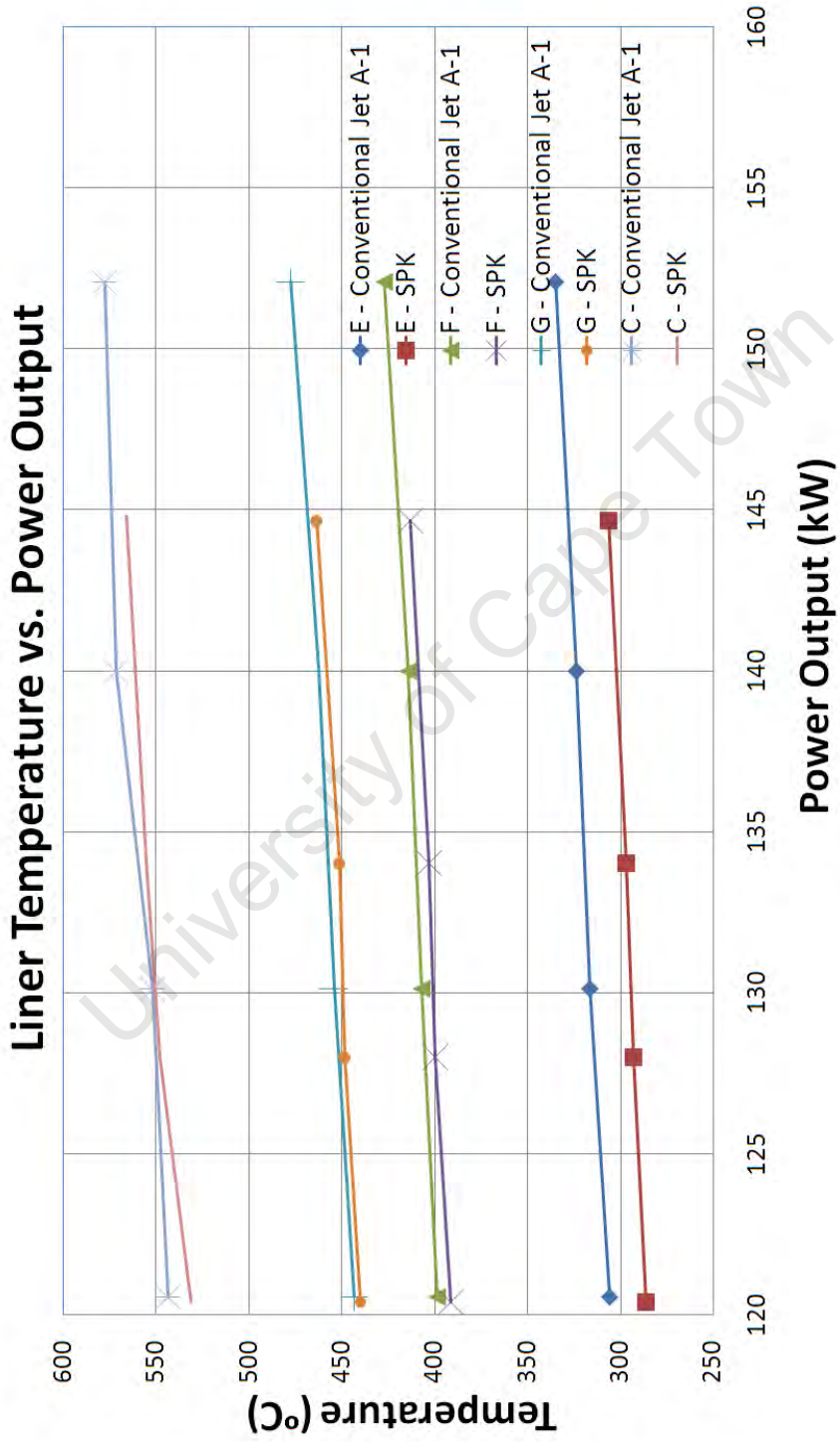

Figure 7.6: T63 gas turbine combustor liner wall temperatures at cruise conditions.

Chapter 8

Discussion of Results

8.1 Overall Engine Efficiency

The overall engine efficiency was calculated using the measured fuel mass flowrate, the power delivered to the dynamometer, and the specific energy content of the fuel. Figure 8.1 shows the trendlines of the calculated overall engine efficiency when operating on the different fuels.

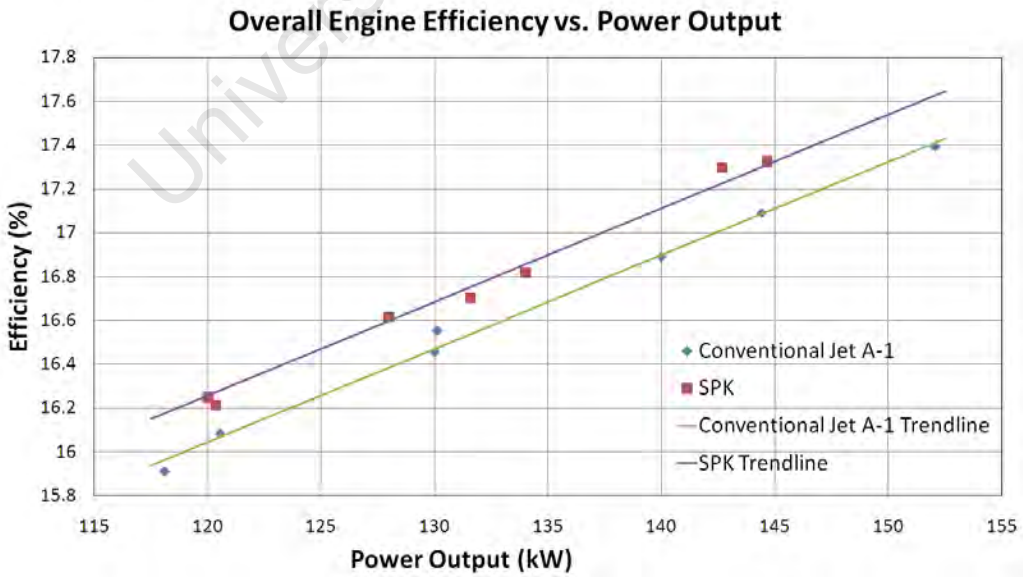

Figure 8.1: Overall engine efficiency of a T63 at cruise conditions.

The overall thermodynamic efficiency difference when operating on neat SPK was seen to increase by a mean value of 1.17% when compared to engine operation on conventional Jet A-1. The standard deviation was 0.35%. The SPK/conventional Jet A-1 blend appeared to exhibit a linear increase in efficiency with respect to the percentage of SPK in the final blend.

The gain in efficiency was attributed to a number of underlying effects, shown in Fig. 8.2.

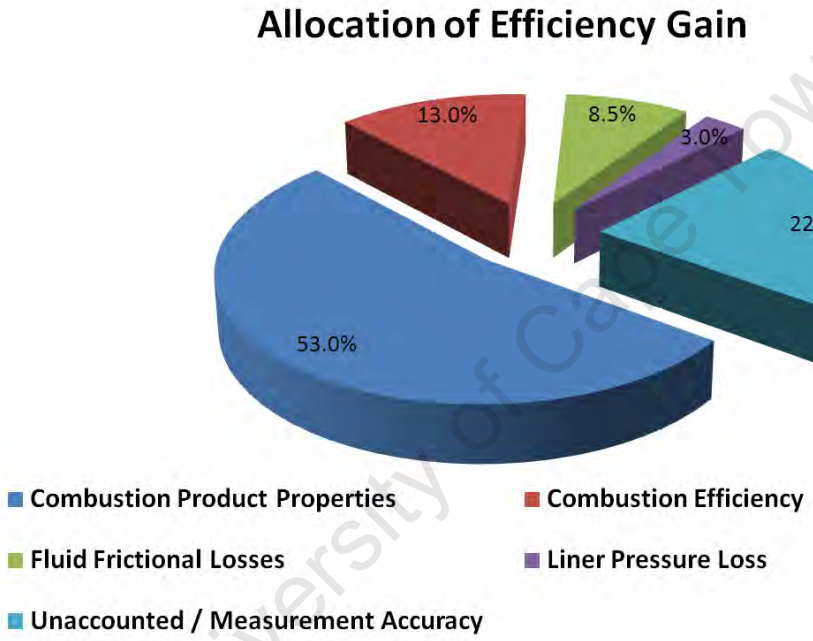

Figure 8.2: Percentage Allocation of the Measured Efficiency Gain.

- Firstly, the engine model had shown that an increase in the fuel H/C ratio would result in an intrinsic increase in the overall efficiency as a result of the changes in the thermodynamic properties of the products of combustion. As predicted by the idealised gas turbine cycle model, the SPK fuel was expected to exhibit a 0.62% improvement in the overall efficiency. This represents 53.0% of the observed total improvement.

- Secondly, soot emissions in the exhaust stream represent incomplete combustion and hence a loss of potential heat release within the combustion chamber. The literature suggests that soot from gas turbines comprises $\approx$ 96% carbon [7], from which the relative combustion efficiencies of conventional Jet A-1 and SPK could be calculated. This provided a 0.153% increase

in overall efficiency, or 13.0% of the total improvement in efficiency.

- Thirdly, the reduction in the liner pressure loss represented a 0.036% improvement in overall efficiency, or 3.0% of the total improvement in efficiency. This contribution was calculated from the measured pressure loss with the aid of the idealised gas cycle model.

- Fourthly, the fluid frictional losses within a gas turbine are significant. The viscosity of the final products of combustion changed according to temperature and composition and this was seen to reduce the pressure losses via friction and separation. The viscosity differences were estimated for the different combustion products streams at their respective calculated temperatures and these data were used to estimate the respective fluid frictional pressure losses. This calculation indicated a further component of the efficiency increase and contributed 8.5% of the total measured increase.

The aforementioned fractions of efficiency gain changed marginally depending on the exact power output, but the magnitude of their respective percentage contribution to the whole remains essentially the same through the cruise power range.

The remaining 22.5% of the overall efficiency gain was unexplained and was thought to be possibly attributable to a reduced friction factor for the turbine blades caused by a reduced deposition of nanometer sized soot particulates which would be more numerous during operation on conventional Jet A-1. This would have further reduced the fluid frictional losses within the turbine and improved the overall engine efficiency to that measured.

However, it is possible that the unexplained 22.5% of the overall efficiency gain could be absorbed in the measurement precision and accuracy limitations, whilst the efficiency gain contribution attributable to the changes in the gas properties was derived from basic thermodynamic theory, the other efficiency contributions were inferred from experimental measurements, as was the overall efficiency determination itself.

The aforementioned sources of efficiency gain are partially dependent on the engine design. The efficiency gain due to reduced soot formation, about 13%, is likely to reduce in magnitude with lean burn combustors which emit far less soot and attain a very high combustion efficiency, thereby allowing for less improvement in combustion efficiency. On the other hand, almost two thirds of the efficiency gain was derived from an improvement in the thermodynamic properties of the combustion products, which would not be

engine dependent, and would provide a similar efficiency improvement in all gas turbine engines.

The variation in liner pressure loss measured was minimal, accounting for 3% of the efficiency gain. Its origin was thought to be linked to the liner temperature, through a change in fluid viscosity in the vicinity of the combustor liner. This in turn links back to the issue of radiation and soot formation. Although modern lean-burn gas turbines emit very low levels of soot, they still produce a significant quantity in the primary combustion zone that is later oxidized prior to emission. Corporan at al. [4] described a 60% reduction in particulate number at ϕ=0.6 in an atmospheric combustor due to operation on synjet versus conventional Jet A-1 (JP-8). The efficiency gain would thus partially be expected to remain with modern lean burn combustors.

About 8.5% of the efficiency gain was deduced to be attained though a reduction in the viscosity of the combustion products. This is not engine dependent and would be expected to apply in principle to all gas turbine engines. The viscosity is composition and temperature dependent and thus would provide the greatest improvement for mixtures with lower bypass ratios that incorporate higher fraction of the combustion products and less bypass air. The reduction in combustion gas temperature associated with the SPK would also be expected to be most prominent at higher equivalence ratios, thereby providing a greater improvement in efficiency via a lower viscosity.

8.2 Fuel Flowrate

Based solely on the gravimetric energy content of the fuels, the fuel mass flowrate of SPK could be expected to decrease by 1.4% with respect to engine operation on conventional Jet A-1. However, the idealized gas turbine model revealed that the fuel mass flowrate of SPK should theoretically decrease by about 2.0% with respect to conventional Jet A-1. In practice, the experimental measurements yielded a fuel mass flowrate for SPK that was about 2.4% lower than the conventional Jet A-1 at a given cruise power output. The greater-than-expected reduction was due to the various contributions listed in the preceding section.

8.3 Engine Soot Emissions

The measurements revealed a reduction in soot of 86.8% at cruise and 95.3% at idle conditions, with operations on SPK versus conventional Jet A-1. These results were in good agreement with the soot emissions measured at the Propulsions Directorate at Wright Patterson Air Force Base (WPAFB), the latter also obtained on a T63 gas turbine [4].

The idle reduction in soot was 2.81 mg/m^3. With a volume flowrate at idle of $\approx$ 1.4 m^3/s, this would be about 3.93 mg/s. At cruise the reduction in soot was about 12.66 mg/m^3, accounting for a reduction in soot of about 35.45 mg/s when considering the volume flowrate at cruise of $\approx$ 2.8 m^3/s, and a power output of 135kW.

The reduction in FSN of 95.3% at idle thus accounted for a much smaller quantity of soot due to the small quantity of soot formed during idle. The benefit is that aircraft spend much of their time within the borders of cities idling on the tarmac of an airport, therefore this indicated a direct benefit of improved air quality in the vicinity of airports.

Cruise conditions represent the region of operation where aircraft operate for the longest period of time. Reducing the soot emissions at cruise represent a reduction in the overall soot mass emissions produced by an aircraft during its operational life.

Thermal radiation occurring from luminous sources, i.e. soot particulates, accounts for a significant portion of the total radiation heat transfer to the combustor liner. Reducing the quantity of the soot formed would reduce the magnitude of the luminous thermal radiation, thereby lowering the overall thermal loading on the combustor liner and leading to increased liner life. This aspect is addressed in greater detail in a later section. Soot particulates are also implicated with erosion of the turbine blades. A reduction in the mass and number of particulates produced by combustion will increase turbine life and thereby reduce associated operating costs.

8.4 NO_x Emissions

The NO_x measurement made herein were in good agreement with the trends shown by Pratt & Whitney as part of the emissions performance analysis of Sasol Fully Synthetic Jet Fuel (FSJF) prior to it's approval. The emissions data published claimed a 4% reduction in NO_x emissions during a simulated LTO cycle with operation on Sasol FSJF that contained 10.9% aromatics, with respect to conventional Jet A-1 [21].

When considering the effect of aromatic content on fuel H/C ratio and AFT, the reduction in NO_x measured by Pratt & Whitney would be expected to roughly double with experimentation on SPK due to the removal of the remaining 10.9% aromatics. SPK was measured to produce about 7% less NO_x on the T63 at cruise conditions.

There was no measurable difference in NO_x emissions at idle conditions, as was the case with Pratt & Whitney, attributed to the much greater overall A/F ratio at idle conditions and the resulting diminished difference in fuel AFT.

8.5 Combustor Liner Temperature

The combustor liner temperature measurements showed a reduction in the operating temperature of the liner throughout the cruise range when operating on SPK versus petroleum–derived Jet A-1. The largest reduction was seen in the primary combustion zone, with a smaller reduction in the liner temperature shown toward the turbine end of the combustor liner.

The variations in liner temperature were somewhat less than those presented in Fig. 2.1 and those presented by Moses at al. [3] on a T700 during operation on Sasol FSJF. This was attributed to the pressure ratio of the GE F101 and the T700 being significantly higher that the pressure ratio of 6.18 for the T63 gas turbine. Higher pressure ratios cause an increase in the size and number of particulates formed in the primary combustion zone [8], thereby increasing the fractional contribution of radiation heat transfer to the overall thermal loading on a combustor liner. Therefore, a similar percentage reduction in soot could result in a larger reduction in the liner temperature of the GE F101 and T700 combustors.

The pattern of reduction in liner temperature with the SPK fuel in relation to the conventional Jet A-1 appeared to be primarily associated with the magnitude of thermal radiation incident on the combustor liner, coupled with convective heat transfer arising from the products of combustion at their respective temperatures.

8.5.1 Primary Combustion Zone during Cruise

The reduction of 21.3°C adjacent to the primary combustion zone was primarily attributed to the reduction in the thermal radiation, due to the reduction in soot formation. The film cooling effectively ensures that the primary zone is shielded from the influence of convective heat transfer form the combustion products and thermal radiation from the rich primary zone is the only other means of significant heat transfer. Thermal radiation heat transfer is dependent on the number, size, emissivity, etc of the soot particulates formed in the primary combustion zone [10]. The reduction in soot formation in the primary zone inferred from the temperature measurements is not necessarily the same as that which was measured in the exhaust stream. Global soot reduction may be largely due to a reduction in the size of the particulates formed, which are subsequently more easily oxidised prior to measurement although El-Leathy et al. [17] suggested that there was no significant fuel effect on soot oxidation rates. Hence, the measure 86.8% reduction in soot emissions is effectively the difference between the soot formation and oxidation processes of the two fuels, and detail may well have been lost with a global difference measurement.

The engine model indicated that the combustion temperatures were not the same for the two fuels, with the SPK exhibiting a slightly lower overall adiabatic flame temperature. This would also influence the primary zone radiation heat transfer because the radiating soot particles are generally regarded to be in thermal equilibrium with the gas, ie, at the same temperature, and the radiation heat transfer exhibits a fourth power dependency on temperature. However, the magnitude of this temperature aspect is not sufficient to explain the 24.5% reduction in the liner temperature difference that was measured and this suggests that the soot reduction seen from operation on SPK is primarily the result of a reduction in soot formation, due to the reduction in aromatic content, with variations in soot oxidation assumed negligible.

8.5.2 Dilution Zone during Cruise

Both the thermocouples placed at the turbine end of the combustor liner, thermocouple G and C, measured approximately a 5°C reduction in liner temperature when operating on SPK versus conventional Jet A-1. At an overall ϕ between about 0.20 and 0.24 for both conventional Jet A-1 and SPK, representative of the overall equivalence ratio range during cruise, the difference in the modelled final products temperature was between 1.2 and 1.5°C. The reduction in liner temperature of ≈ 5°C was thus only partially the result of the reduced products' temperature, and predominantly the result of the thermal radiation difference in the hot primary zone, but muted by the distance and the oblique radiation incidence angle. The radiation emanating from the secondary and subsequent zones would be comparatively lessened by both the lower gas temperature and the reduced soot concentration resulting from soot oxidation.

The variation in combustion products' temperature was expected to influence the liner temperature in the downstream position since the cooling film flow becomes turbulent after about 45mm (Calculated for the measured liner pressure drop of 11 kPa and the resulting cooling film velocity of 75 m/s.). Once the cooling film becomes turbulent, it mixes rapidly with combustion gases and the combustor liner is thereafter exposed to heating via forced convection.

Thus, although radiation only accounts for a smaller fraction of the overall heat transfer to the combustor liner at the turbine end, the large reduction in thermal radiation caused the majority of the temperature reduction measured.

8.5.3 Intermediate Zone during Cruise

The intermediate zone temperature, midway between the primary combustion zone and the turbine end of the combustor liner, was measured via thermocouple F. The thermocouple showed on average a 6.7°C reduction in liner temperature when operating on SPK versus conventional Jet A-1.

The thermocouple was placed at the edge of the cooling film laminar flow boundary, where turbulent mixing begins to cause heating of the combustor liner via forced convection. Thermocouple F experienced a slightly greater

temperature decrease that thermocouples G and C due to its location, and a larger fraction of the overall heat addition to the liner in this location attributed to thermal radiation. Thermocouple F was closer to the primary combustion zone, and thus received more energy via thermal radiation than thermocouples G and C, due to the proximity to the source, and the incident angle being closer to perpendicular. Hence, a reduction in the magnitude of radiative heat addition effects the primary dilution zone more than the secondary dilution zone.

8.5.4 Liner Temperature during Engine Idle

A measurable variation in liner temperature was not detected under idle condition with operation on SPK versus operation on conventional Jet A-1. Due to the very low equivalence ratios at idle there would be a marginal difference in combustion gas temperature, leading to a negligible difference in forced convection and non-luminous radiation heat transfer.

Although there was a 95.3% percentage difference noted in the exhaust soot emission, the absolute magnitude of the soot mass emissions was minimal at 2.81mg/m^3. This said, one would still expect the liner to operate at a lower temperature with operation on SPK versus conventional Jet A-1 due to less luminous radiative heat addition. This suggested that reduction in soot emissions with SPK are possibly due to the formation of smaller soot particulates in the primary combustion zone that were more readily oxidised downstream in the dilution zone. Hence, a similar quantity of soot may have been present in the primary combustion zone during idle, combined with similar gas temperatures, leading to the similar liner temperatures measured.

Chapter 9

Conclusions

9.1 Test Cell Setup and Instrumentation

A RR-Allison T63-A-700 turboshaft gas turbine, model 250-C18 B, was installed in a test cell at the SAFL. Stable operation was attained throughout the engine operating range which allowed for accurate, repeatable data to be attained. The engine was successfully instrumented for the purpose of analysing fuel effects on engine performance.

9.2 Performance Advantages

It can be concluded that operation on SPK would provide an efficiency improvement of about 1.17% with respect to petroleum–derived Jet A-1. Of the noted efficiency gain, 53.0% was concluded the result of a fundamental performance advantage gained through use of a fuel with a higher H/C ratio, and an improvement in the combustion product properties. 13.0% of the improvement was concluded as attained through improved combustion effciency, via the complete oxidation of carbon in the form of soot, and a further 3.0% was gained via a reduced liner pressure loss. 8.5% was concluded as attained through a reduction in the fluid friction losses through the turbine section due to a reduction in the viscoty of the combustion products, and the remaining 22.5% was unaccounted for, although it could conceivable be absorbed by measurement inaccuracies.

The majority of the improvement attained through the incorporation of a zero aromatic fuel was due to the increase in the H/C ratio of the fuel, an indirect result of the reduced aromatic species. Although not directly linked, the H/C ratio of a fuel will invariable increase when reducing the aromatic content, due to the higher C/H ratio of aromatic molecules with respect to paraffinic molecules. The reduction in soot was linked to the aromatic content of the fuel, as the exhaust soot content was seen to decrease linearly with the reduction in aromatic content of the fuel, as well as the literature supporting this notion.

The liner pressure loss was linked to liner temperature and thus to flow friction losses via a reduction in the viscosity of the fluid due to a temperature reduction in the region of the boudary layer. Liner temperature was concluded to decrease primarily due to the reduction in soot associated with low aromatic fuel. Although the liner pressure loss was not directly affected by the aromatic content of the fuel, soot formation, which effects liner temperature, was directly linked. Hence, liner pressure loss was concluded proportional to the aromatic content of the fuel.

A secondary advantage offered by fuels with higher H/C ratios, or lower aromatic contents, was lower turbine inlet temperatures at the same power output. Turbine inlet temperature is one of the major limiting factors of a turbine engine, and an engine could either produce the same power output with a lower turbine inlet temperature, or more power at the same turbine inlet temperature with a higher H/C ratio fuel.

9.3 Soot Formation and Emission

A significant reduction in soot emissions was noted at both idle and cruise conditions when operating on SPK versus petroleum–derived Jet A-1. A 95.3% reduction in FSN was measured at idle, along with an average reduction of 86.8% in smoke number at cruise conditions. The reduction in soot was concluded as the result of the removal of aromatics from the fuel.

The reduction in the exhaust soot content at cruise was concluded to be the result of less soot formed in the primary combustion zone, directly linked to the aromatic content of the fuel, and quantified via the reduction in the combustor liner temperature adjacent the primary combustion zone. The influence of soot oxidation via the formation of smaller particulates that

are more easily oxidised was not quantified, although this phenomenon was expected to play a role.

9.4 Liner Temperature

A reduction in liner temperature in the primary combustion zone of 21.3°C was measured with operation on SPK versus petroleum–derived Jet A-1, with a reduction of ≈ 5°C measured at the turbine end of the combustor liner. The reduction in the primary combustion zone liner temperature was concluded as the result of less soot formation, and the resultant reduction in the magnitude of thermal radiation incident on the combustor liner. The variations in AFT and non-luminous radiation were concluded as negligible in the primary combustion zone with respect to the variation in thermal radiation. About 75% of the reduction in liner temperature at the turbine end of the liner was concluded the result of a reduction in thermal radiation, with ≈ 25% of the reduction the result of the lower combustion gas temperature, and less heat transfer via force convection resulting.

Chapter 10

Recommendations

10.1 Test Cell Setup and Experimentation

During experimentation some engine speed oscillation was still present, caused by the rotational inertia of the drive shaft and dynamometer combination being below the recommended range for the engine. Reducing engine speed oscillations would reduce data scatter and could be achieved via better dynamometer control, a physical change to the engine fuel control unit, or the incorporation of a flywheel to raise the rotational inertia of the drive train.

The current engine TOT is attained through an analogue gauge, with a reading accuracy of ± 5°C. During modelling it was predicted that the difference in TOT between SPK and petroleum–derived Jet A-1 would be about 1.5°C at the same power output. Hence, to measure the difference, a more accurate gauge should be installed that could measure gas temperature to within a maximum accuracy of ± 0.1°C.

Dynamometer load may be lost during experimentation due to unforeseeable circumstances, and result in a rapid overspeed that would be limited by the engine rapid overspeed response. It could be possible to control the engine via an electronic throttle controller that varied the N_2 throttle lever according to load, as in a helicopter. This would allow for transient cycle testing, as well as additional system protection in case of dynamometer load loss.

During experimentation with zero aromatic SPK, seal swell became an

issue due to fuel leaks that occurred in the engine fuel control unit. Old O-rings shrank due to the absence of aromatics; due to their age they did not reform to seal the high fuel pressure as required. The effect was seen within 24 hours of exposure to zero aromatic fuel. It is recommended to flush the engine with aromatic containing fuel immediately after experimentation with aromatic free fuel to prevent leakage.

10.2 Theoretical Confirmation through Experimentation

The overall equivalence ratio was estimated via a calculated air mass flowrate. It is recommended to incorporation a broadband lambda sensor that would provide a direct measurement of the overall equivalence ratio. This would allow for a more reliable estimation of the overall equivalence ratio, as well as the air mass flowrate.

To be sure that the liner pressure loss is fuel dependent, the liner pressure loss should be measured on a separate combustor liner without the attached thermocouples, thereby eliminating another variable as the attached thermocouple extension wires reduce the flow area.

The effects of thermal radiation and forced convection were inferred from the thermocouple measurements. A direct measurement via a radiation sensor would provide the confirmation of the fractional allocation of radiation and forced convection to the overall liner temperature change.

The reduction in AFT, $\approx 20°C$ in the primary combustion zone, would infer a noticeable reduction in the quantity on NO_X formed in the primary combustion zone. This could be measured via a NO_X sensor placed in the exhaust stream and would provide confirmation of the AFT model, as well as providing additional emissions data.

To properly confirm the predicted combustion efficiency and a/f ratio differences, exhaust gas sampling/measurement should be employed. This should include the measurement of CO_2, CO, NOx and UHC emissions.

References

[1] A. H. Lefebvre, "Influences of Fuel Properties on Gas Turbine Combustion Performance," *AFWAL-TR-84-2104*, 1985.

[2] D. R. Ballal and W. E. Harrison III, "A Time Scale Approach to Understanding Jet Fuel Combustion and Particulate Formation and Growth," *American Institute of Aeronautics and Astronautics*, no. 2001-1085, 2001.

[3] C. A. Moses, I. G. Wilson, and P. Roets, "EVALUATION OF SASOL SYNTHETIC KEROSENE FOR SUITABILITY AS JET FUEL," Report 08-04438, Southwest Research Institute, 6220 Culebra Road, San Antonio, TX USA, December 2003.

[4] E. Corporan, M. J. DeWitt, V. Belovich, R. Pawlik, A. C. Lynch, J. R. Gord, and T. R. Meyer, "Emissions Characteristics of a Turbine Engine and Research Combustor Burning a Fischer-Tropsch Jet Fuel," *American Chemical Society*, 2007.

[5] J. P. Holman, *Heat Transfer, 9th Edition.* New York: McGraw Hill, 2002.

[6] C. Viljoen, "Effects of blending Fischer-Tropsch iso-paraffinic kerosene (FT IPK) with conventional Jet A-1," *Sasol Technology Fuels Research*, 2008.

[7] A. H. Lefebvre, *Gas Turbine Combustion.* New York: Taylor and Francis Group, 1999.

[8] H. I. Joo and O. L. Gulder, "Pressure dependence of soot formation in diffusion flames," *AMSE Turbo Expo*, vol. GT2008, no. 50437, 2008.

[9] D. R. Ballal, M. J. DeWitt, E. Corporan, and W. E. Harrison, "Particulate Loading and Radiation in Gas Turbine Combustion," *American*

Institute of Aeronautics and Astronautics, vol. 41st Aerospace Science Meeting and Exhibit, 2003.

[10] S. C. Lee and C. L. Tien, "Optical constants of soot in hydrocarbon flames," *Eighteenth Symposium (International) on Combustion: The Combustion Institute*, vol. Pittsburgh, pp. 1159–1166, 1981.

[11] G. W. Autio and E. Scala, "The Normal Spectral Emissivity of Isotropic and Anisotropic Materials," *Carbon*, vol. 4, pp. 13–28, 1966.

[12] S. A. Mosier, "Fuel Effects on Gas Turbine Combustion Systems," *Combustion Problems in Turbine Engines; AGARD-CP-353, SPS Limited: Essex*, no. 5, pp. 1–15, 1984.

[13] C. Moses, "U.S. Army Alternative Gas Turbine Fuels Research: Meradcom," *Combustion Problems in Turbine Engines; AGARD-CP-353, SPS Limited: Essex*, no. 7, pp. 1–10, 1984.

[14] D. M. Evans and M. Noble, "Gas Turbine Combustor Cooling by Augmented Backside Cooling," *ASME*, vol. 78, no. GT, p. 33, 1978.

[15] A. H. Lefebvre and M. V. Herbert, "Heat-Transfer Processes in Gas Turbine Combustion Chambers," *Proceeding of the Institute of Mechanical Engineering*, vol. 174, no. 12, pp. 463–473, 1960.

[16] I. Glassman, *Combustion*. New York: Academic Press, 1996.

[17] A. M. El-Leathy, F. Xu, and G. M. Faeth, "Soot Surface Growth and Oxidation in Laminar Unsaturated-Hydrocarbon/Air Diffusion Flames," *American Institute of Aeronautics and Astronautics*, vol. 100, no. 2002-1116, 2002.

[18] M. Frenklach, D. Clary, W. G. Jr., and S. Stein, "Detailed kinetic modeling of soot formation in shock-tube pyrolysis of acetylene," *Twentieth Symposium (International) on Combustion: The Combustion Institute, Pittsburgh, PA*, pp. 887–901, 1984.

[19] J. Nagle and R. Strickland-Constable, "Oxidation of carbon between 1000 and 2000 °C," *Proceedings of the Fifth Carbon Conference*, vol. 1, no. 154, 1962.

[20] D. E. Hall, "A Review of Recent Literature Investigating the Measurement of Automotive Particulate; the Relationship with Environmental Aerosol, Air Quality and Health Effects," *SAE*, no. 982602, 1998.

[21] C. A. Moses and P. N. J. Roets, "Properties, characteristics and combustion performance of sasol fully synthetic jet fuel," *AMSE Turbo Expo*, vol. GT2008, no. 50545, 2008.

[22] Defense Energy Support Center: Product Technology and Standardization Division, "Petroleum Quality Information System 2002; Product Technology and Standardization Division," 2002.

[23] RR-Allison Gas Turbine, *Turboshaft Model 250-C18 A,B and C Operation and Maintenance Manual*. General Motors Corp., U.S.A., 1989.

[24] L. M. Shafer, R. C. Striebich, J. Gomach, and J. T. Edwards, "Development of an Experimental Database and Kinetic Models for Surrogate Jet Fuels," *AIAA*, no. 2006-7962, 2006.

[25] E. J. Hearn, *Mechanics of Materials 1*. Oxford: Butterworth Heinemann, 2003.

[26] Y. A. Cengel and M. A. Boles, *Thermodynamics, An Engineering Approach, 4th Edition*. New York: McGraw-Hill, 2002.

[27] AVL LIST GMBH Graz, *AVL 415S Variable Sampling Smoke Meter*. AVL, Austria, latest ed., 2000.

[28] J. E. Shigley, C. R. Mischke, and R. G. Budynas, *Mechanical Engineering Design, 7th Edition*. New York: McGraw Hill, 2004.

[29] SCHENCK, *W3S-480 Instruction Manual*. SCHENCK, Darmstadt, Germany, 1989.

[30] W. J. Bottega, *Engineering Vibrations*. New York: Taylor and Francis Group, 2006.

[31] Lovejoy,Inc, "Torsional Coupling Selection for Internal Combustion Engine Applications," *Torsional Couplings*, p. 9.

[32] J. Maree, "Shaft Dynamics," *CAE Report*, p. 19, 2005.

[33] W. J. D. Annand, "Heat Transfer in the Cylinders of Reciprocating Internal Combustion Engines," *Proc. Instn Mech. Engrs*, vol. 177, no. 36, pp. 973–990, 1963.

Appendices

Appendix A

T63 Fuel Control Systems and Operation

Almost all fuel control systems on the T63 are aimed at either sustaining N_2 speed at 100%, or preventing damage occurring to the engine. Damage prevention involves, among others, limiting engine N_1 speed, TOT and torque production. All of the above mentioned requirements are implemented by variations in fueling, and as such the only control system on the gas turbine is a fuel control system.

A.1 Introduction

The fuel control system is made up of two major components, namely the N_1 or gas producer fuel control and the N_2 or power turbine governor. Various other accumulators, check valves and filters are also present in the various pressure lines that connect the two governors to one another and to the engine.

The fuel flowrate for engine control is established as a function of compressor discharge pressure (P_C), both N_1 and N_2 speeds as well as gas producer and power turbine lever angles. All information contained herein was obtained from the operation and maintenance manual for engine series 250-C18 [23].

A.2 Gas Producer Fuel Control

The gas producer fuel control has a bypass valve, metering valve, acceleration bellows, governing and enrichment bellows, manually operated cut-off valve, maximum pressure relief valve, a lever assembly and a start derichment valve. The various circuits and components of the gas producer fuel control unit can be seen in figure A.1, depicted as the main fuel control. Figure A.1 is a schematic of a model 250-C20 B and is more modern than the engine used in the present research, however, the fundamental control strategy remains unchanged. The gas producer fuel control has a number of internal circuits, and to show this the schematic shows cross sections of the various circuits within the fuel control unit.

Fuel is supplied to the control unit from the engine fuel pump and filter assembly, and is conveyed to the metering valve, components 13. The bypass valve, shown in the schematic as 14, maintains a constant pressure differential across the metering valve by bypassing excess fuel back to the fuel pump and filter assembly. This is achieved by the spring force, adjusted via the specific gravity adjustment, being overcome by the pressure differential and the bypass valve moving to uncover the return line, thereby reducing the fuel supply pressure. Reducing the fuel supply pressure causes the fuel flowrate across the the metering valve to reduce, decreasing the pressure drop across the metering valve and results in a lower pressure differential across the bypass valve, closing the return line.

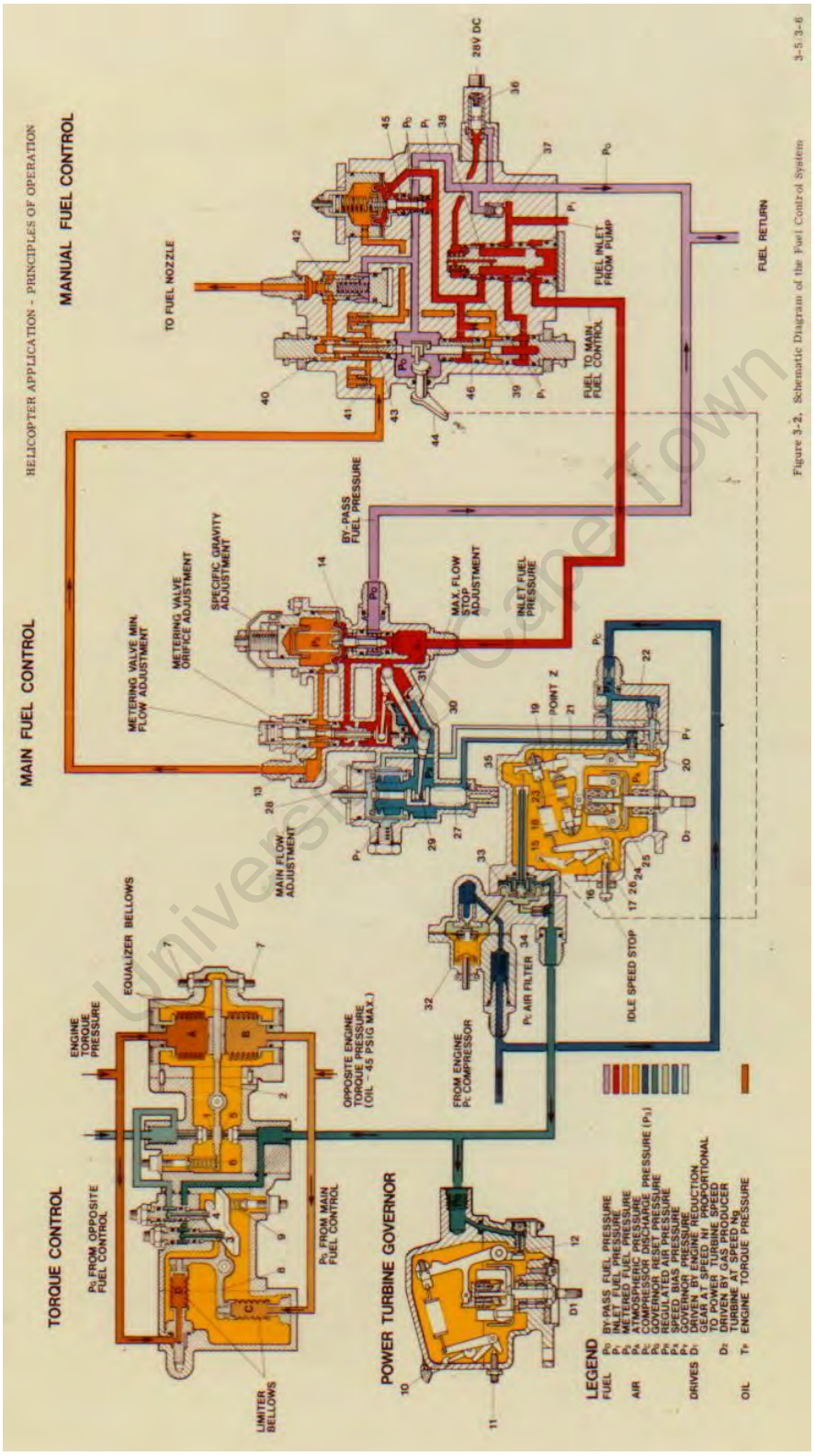

Figure A.1: Engine fuel control system schematic.

The metering valve is operated by a mechanical lever, component 30, through the movement of the governor and acceleration bellows, component 28. Metering valve area, or fuel flowrate, is a direct function of valve travel. Prior to light-off the metering valve is established at a predetermined position by the acceleration bellows, due to P_C being equal to ambient pressure.

During light-off and initial acceleration the start derichment valve is open until a predetermined P_C value is attained. When open, the derichment valve vents P_Y pressure to atmosphere. Venting P_Y allows the governor bellows, 28, to move the metering valve against the minimum flow stop. At minimum flow the metering valve provides the lean fuel scheduling required after light-off. This continues until P_C attains sufficient magnitude to shut the derichment valve via the derichment bellows. Once shut, the control of the metering valve is returned to the normal operating schedule.

During acceleration the P_X and P_Y pressures are equal to P_C up to the point where the speed enrichment orifice, feature 22, is opened by flyweight action (26). Opening the orifice vents P_X pressure to atmosphere while P_Y remains equal to P_C. The pressure differential of P_Y - P_X across the governor bellows causes the metering valve to move toward the maximum flow stop position.

Gas producer (N_1) speed is controlled by the gas producer fuel control governor. A set of flyweights, component 26 in figure A.1, operate the governor lever (21) which controls the governor bellows, P_Y, bleed at the governing orifice (20). That is the governor lever makes contact via 'Point Z', driven by the flyweight action, with the gas producer power output link (19), opening the governing orifice. The flyweight operation of the governor lever is opposed by a variable spring load, established by the throttle lever acting via a spring scheduling cam, component 17. Opening the governing orifice bleeds P_Y pressure and allows P_X pressure to control the governor bellows. The P_X influence on the bellows moves the metering valve toward minimum flow and to a position where metered flow is at steady state requirements.

The governor reset assembly, components 32 - 35, in the gas producer fuel control limits or governs power turbine speed. Although the reset assembly is located in the Gas producer fuel control unit, control of the unit is derived from the power turbine governor. The power turbine governor also provides rapid N_2 overspeed response by bleeding governor servo (P_Y) pressure from the gas producer fuel control, not shown in figure A.1.

A.3 Power Turbine Fuel Governor

The power turbine speed is scheduled by the power turbine governor lever and the power turbine speed scheduling cam. The cam sets a governor spring load which opposes a speed-weight output. As the desired speed is approached the speed weights, operating against the governor spring load, move the linkage to open the power turbine governor orifice, feature 12. The opening of the power turbine governor orifice bleeds the P_G pressure line. At higher speeds the same speed weights also open the overspeed P_Y bleed at the power turbine governor, providing rapid response to overspeed.

The governor orifice, 12, is downstream of a bleed, 34, supplied by a regulated air pressure, P_R. Opening the governing orifice and bleeding the P_G pressure line results in a lower P_G pressure. The force generated by P_R - P_G acts across a diaphragm, 33, acts on the gas producer power output link (19), through the governor reset rod (35), to supplement the weight force in the gas producer fuel governor to reduce the gas producer speed (bleed P_Y pressure). The P_R - P_G diaphragm is preloaded to establish the active P_R - P_G range. P_R pressure is supplied from engine P_C pressure by an air regulator valve, component 32 in figure A.1.

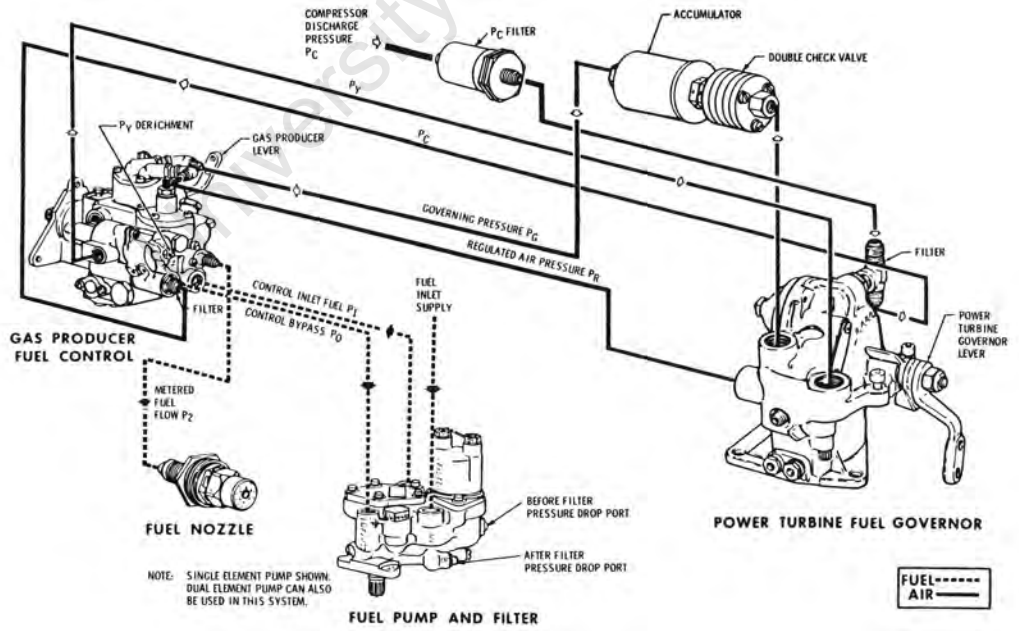

Figure A.2: Engine fuel system.

A.4 Fuel System Response

A.4.1 Test Cell Situation

The T63 gas turbine is designed for use in helicopters, where the sum of the inertial value of the rotor gears and rotor itself is approximately 3 kg.m^2. The recommended rotational inertia for safe operation of the engine is between 1.35 and 4.05 kg.m^2, to mimic that in a helicopter. In the gas turbine test cell at the Sasol Advanced Fuels Laboratory, the total rotational inertia was 0.42 kg.m^2, well below the recommended value.

Considering the operating speed of 6000 rpm, it was decided to avoid the addition of mass to attain the correct rotational inertia values so as to prevent the addition of high mass, high velocity components. These components would contain a large quantity of kinetic energy at rated speed and it was preferable to find an alternative solution.

A.4.2 Power Turbine Governor

During normal operation, at 100% N_2 speed, the fueling is controlled by the power turbine governor. If N_2 speed rises above that desired the speed weights open and bleed the power turbine governor orifice. The orifice bleeds P_G pressure, which reduces P_G pressure and results in an increase in the magnitude of P_R - P_G. The bleeding of P_G results in the reduced pressure downstream of the P_G bleed, refer to figure A.2. This pressure differential acts across a diaphragm, moving the governor reset rod to rotate the gas producer power output link and bleed the P_Y pressure line. This results in the magnitude of the P_Y - P_X reducing and the fuel metering valve being moved toward minimum flow via the lever attached to the governor and acceleration bellows. This will result in a decrease in the gas producer N_1 speed, followed by the power turbine N_2 speed.

If N_2 speed decreases below that desired the P_G bleed orifice closes, allowing P_G pressure to increase which reduces the magnitude of P_R - P_G. This results in the retraction of the governor reset rod and the spring force applied by the lever in the gas producer fuel control closes the P_Y bleed. That increases the magnitude of the P_Y - P_X pressure differential and moves the fuel metering valve toward maximum stop, thereby increasing the gas

producer N_1 speed, followed by the power turbine N_2 speed.

The power turbine governor thus provides the primary response to engine overspeed and is continually involved with fuel metering throughout normal operation. Removing the power turbine governor by disconnecting the P_R pressure line completely disables the primary N_2 overspeed governor. The engine is still able to control on the rapid response governor that directly bleeds the P_Y pressure line, however, the rapid response governor is designed to be a secondary device and only activates at about 6300 rpm.

The system, operating as designed, has a slow response time, hence the need for a rapid overspeed governor. The response is slow due to the necessity to bleed various air lines to attain the required fueling change. The main N_2 overspeed response initially bleeds the P_G pressure line before a mechanical signal begins to bleed the P_Y pressure line, enabling the necessary motion of the fuel metering valve. The bleeding of the P_G pressure line takes a significant amount of time due to the incorporation of an accumulator and the magnitude of the pressure drop is limited by the preset cracking pressure of a double check valve.

The T63 has a slow time response due to the accumulator on the P_G pressure line, incorporated to prevent yawing during flight caused by rapid engine response. The response is slow due to a slow bleed down and longer repressurise time. The magnitude of the fueling response is dependent on the magnitude of P_R - P_G and the resultant motion of the governor reset rod.

A.4.3 Effect of Reduced Rotational Inertia

The effect of reducing the rotational inertia of the drive train is to allow for more rapid speed response to a given fueling variations. This in itself is not problematic, however, if the engine fuel control system is not matched with the environment in which it operates it may lead to unstable operation.

When the rotational inertia of the system is decreased the fuel response to an under or overspeed also needs to be adjusted accordingly, unless the control system is able to sustain stable operation with more rapid speed fluctuations. The engine fuel control system is designed to operate with a high inertia drive train, requiring large fueling variations to correct N_2 speed variations. The engine when coupled to a low inertia drive train continues to enact large fuel variations to correct the speed to that desired, which results

in overshooting of the target speed due to too large a fueling response and a slow system response.

This effect was seen in the test cell when the engine was accelerated from idle, 60% N_2, to operating speed, 100% N_2. The engine accelerates smoothly until the speed weights of the power turbine governor begin to bleed the governing orifice, where operation become unstable. This indicated that the feedback emanating from the power turbine, through the power output linkage, was the source of the instability. This was confirmed when the P_Y bleed was removed and the engine taken to full power, operating solely on the N_2 overspeed governor, with negligible speed oscillation.

Stable operation was restored by installing a controlled bleed of the P_R pressure line, reducing the magnitude of P_R - P_G, but still maintaining operation of the primary power turbine overspeed governor. This modification was incorporated for all the test measurements.

Appendix B

Engine Mounting and Drive Shaft Design

In order to operate the T63 gas turbine in a test cell, it is necessary to replicate the mountings within a helicopter as well as the drive shaft connection to the rotor. The mountings must be rigid to hold the engine in place during operation with minimal motion, while the drive shaft must couple the engine to the dynamometer, with provisions for slight misalignment as a practical reality.

B.1 Engine Mounting

B.1.1 Requirements

A secure mounting is necessary to keep the engine in place with minimal motion while it operates, delivering up to 376 Nm of torque. The design torque is that delivered by the engine while operating at take-off power and 6000 rpm output shaft speed, the maximum continuous torque that will be encountered during operating.

The mounting design must allow for good alignment between the dynamometer and the engine PTO spline. The alignment requires the mountings be capable of translating the engine vertically, horizontally and for or aft as well as allowing the engine to rotate about the primary axes, providing pitch, yaw and roll. The mounting must thus allow for six degree of freedom motion.

B.1.2 General Force Calculations

The dry mass of the combined engine and free-wheeling unit is 67 kg. The engine mounts also have to support half the mass of the drive shaft and couplings, 5.4 kg, resulting in the total mass to be supported being 72.4 kg dry. The operational mass of the engine will be slightly higher due to the intake of fuel and oil, taking this into consideration the supports will be designed to support 80 kg as a conservative estimate of the operational engine mass.

The side supports are situated 414 mm apart and are responsible for providing the reaction force necessary to produce engine torque while keeping the engine stationary. The side supports are equally spaced with the PTO spline exiting the engine in the center. The side struts will be designed to be able to support the entire engine mass and provide the reaction forces and moments necessary so as to provide an additional margin of safety.

The X, Y and Z axes shown in figure B.1 were used to define the forces and moments in the supports. The Y axis is in line with the PTO shaft at it's center, while the X axis Z axes form a plane that passes through the three mounting points and is centered about the PTO spline. The center of

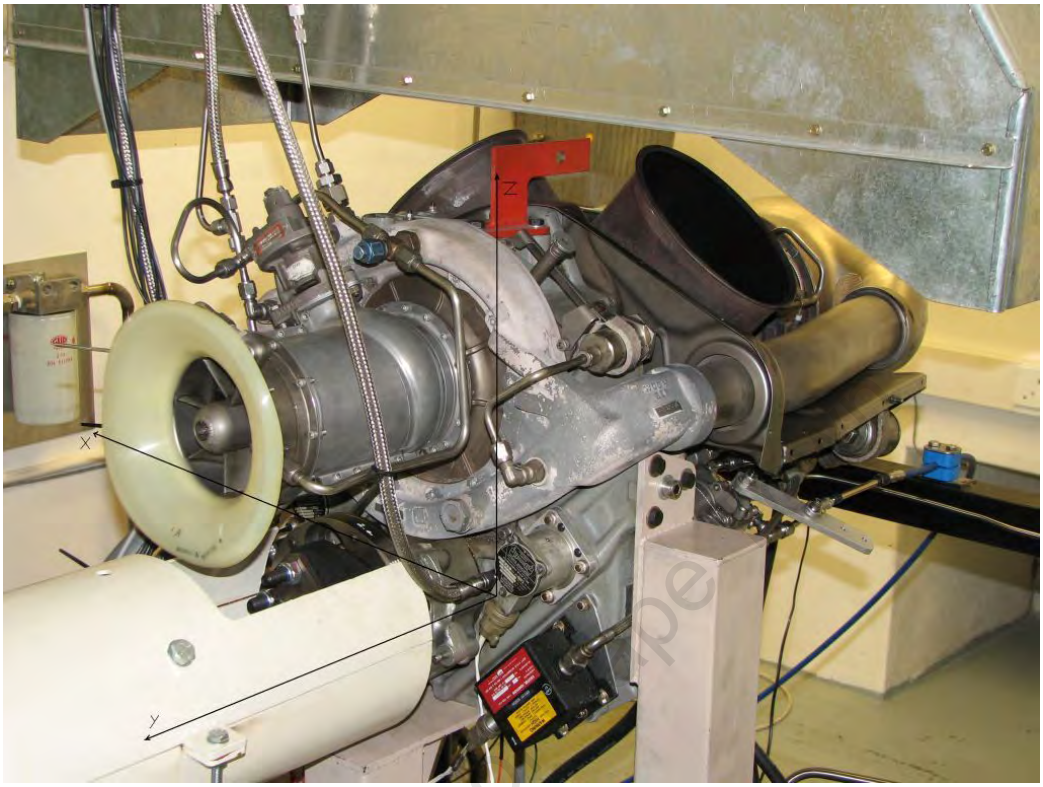

Figure B.1: X, Y and Z co-ordinate orientation.

gravity of the engine in terms of it's X direction is along the Z axis as the engine is symmetric about the YZ plane except for a few control systems. This would result in the mass of the engine being evenly supported by each of the side struts.

The center of gravity in terms of the Y axis is about -80 mm before the attachment of the drive shaft and couplings, making the center of gravity exceptionally close to the Z axes when fully operational. This results in the forces induced in the side struts being primarily axial.

Each of the side struts will support 40 kg of engine mass as well as the appropriate torque reactions force. The 376 Nm of torque converts to a couple with force 908.2 N at 0.414 m. The left strut, when viewing the engine from the front (gas generator side), will have a force in the positive Z direction exerted upon it (i.e. tension), while the right strut will having the same magnitude of force but in the opposite direction (i.e. compression). The force results from the rotation of the shaft in a clockwise direction when

look along the positive Y axis.

The result is that the left strut will have a compressive force of 392.4 N while no torque is produced and under full load the force in the strut will change to a tensile force of 515.8 N. The right strut will have the same compressive force under no load conditions and under full load will be under a compression force of 1300.6 N.

These are conservative estimates as the lower central support will also provide support to the engine's mass under no load as well as offsetting some the torque load taken by the side struts under full load. Whichever design is chosen must be capable of withstanding the above mentioned forces so as to ensure safe operation.

B.1.3 Helicopter Mounting

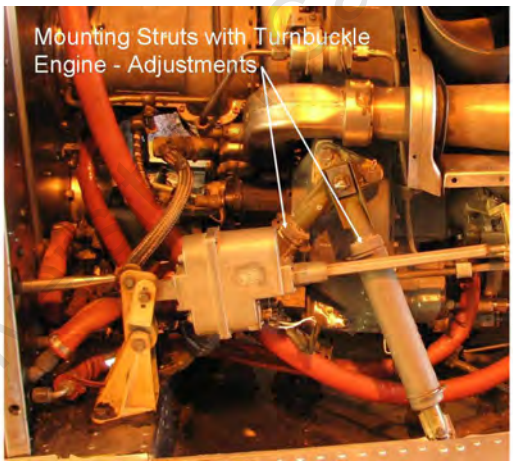

Figure B.2: T63 gas turbine engine mounted in a helicopter.

Figure B.2 shows a T63-A-700 C20 B mounted in a helicopter. The engine gearbox housing provides three triangular points of attachment for the engine, one either side of the engine, and one underneath. The triangular attachment points are all in a single plane, normal to the central axis of the PTO spline of the engine. Each mounting point has two struts attached to it, the left side mounting is shown in figure B.2.

The struts are mounted to the frame via pins and are capable of extending or contracting via turnbuckles, visible in figure B.2. This mounting design

provides the necessary translation and rotation necessary to align the engine with the rotor gearbox housing.

B.1.4 Design

Mounting Configuration

It was decided to mount the engine on three screw jacks. The screw jacks have an internal thread that gives the ability to precisely and independently raise or lower the mounting struts attached to any of the screw jacks. The screw jacks were secured to a horizontal truss which was itself secured to the main mountings which is bolted to the sprung floor. This mounting configuration gave the ability to translate the engine in any desired direction so as to attain the correct alignment and positioning, refer to figure B.3.

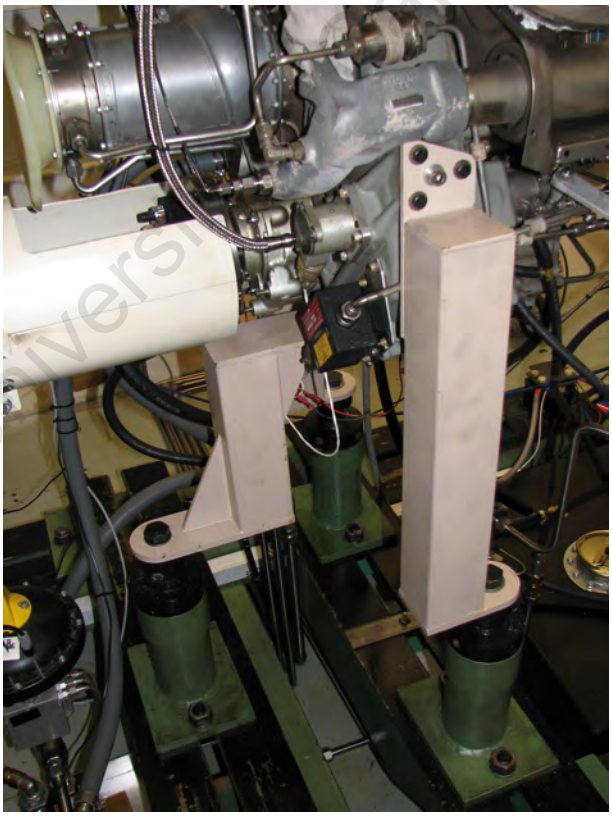

Figure B.3: T63 mounting configuration.

The two side mountings were mounted on the same horizontal truss, limiting the for and aft motion of one strut relative to the other. This necessitated the hole positioning of both struts in the Y direction (refer to figure B.1) being identical, all other variations were not crucial.

The lower central mounting point was secured via the lower strut on a separate horizontal truss to avoid the necessity of precise machining and manufacturing of the lower strut. This mounting format also provided more stable mounting by avoiding mounting the entire engine on screw jacks in a single XZ plane, as is avoided in the helicopter mounting format.

Lower Strut Forces and Structure

The lower strut was designed to be able to carry the entire mass of the engine, as during mounting and alignment of the engine the strut would inevitably be required to carry the entire mass of the engine. The strut must supply an axial force equivalent to the weight of the engine as well as a moment to balance the slight offset of the CG along the Y axis. This is represented in figure B.4.

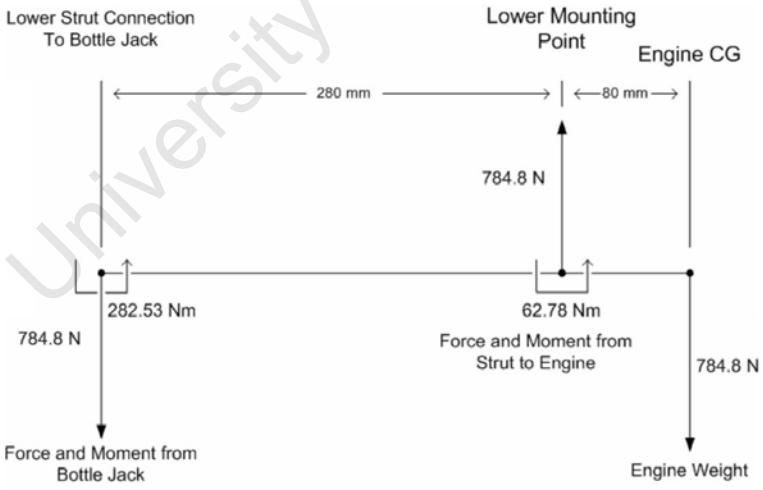

Figure B.4: Lower strut forces and moments.

Considering the offset of the lower mounting, the moment carried by the mounting at the connection to the bottle jack is much larger than that at the connection to the engine. If the lower strut carries the entire mass of the engine, conservatively assumed to be 80 kg, the moment at the screw jack

connection will be 282.5 Nm, while the moment at the engine connection will be 62.8 Nm. The lower strut must also support the weight of the engine, a force equal to 784.8 N.

The principal stresses can be obtained using [28]:

$$\sigma_{1,2} = \frac{\sigma_x + \sigma_y}{2} \pm \sqrt{\left(\frac{\sigma_x - \sigma_y}{2}\right)^2 + \tau_{xy}^2} \tag{B.1}$$

With a maximum axial load of 784.8 N and a constant moment of 172.6 Nm midway between the engine mounting and the screw jack in the vertical tube section, the stresses in the column are:

$$\begin{aligned} \sigma_x &= 1.78 \ \ MPa \\ \sigma_y &= 0 \ \ MPa \\ \sigma_1 &= 1.78 \ \ MPa \\ \sigma_2 &\approx 0 \ \ MPa \end{aligned}$$

σ_x is the axial stress, σ_y is the perpendicular stress and σ_1 and σ_2 are the primary stresses in the vertical section of the strut. A 75 mm square tube section was used with a 1.5 mm wall thickness, to calculate the above stresses. Using any of the failure theories, a Young's Modulus and Yield Strength for mild steel of 207 GPa and 280 MPa respectively, a significant margin of safety (≈ 150) is provided.

From the above calculation the 75 mm, 1.5mm wall thickness, square tube was more than capable of supporting the engine. The general structure of the strut creates a large shear force at the connection between the horizontal flat bar sections and the vertical square tube section. To avoid the large shear stress created at these 90 degree bends gussets were incorporated, these act to provide a larger area through which to transfer the force.

The flat bar incorporated was 10 mm thick, providing strong rigid mounting and a large safety margin. Drawings of the various components and their exact sizes are provided in appendix F.

Side Strut Forces and Structure

The side struts were designed to carry the entire mass of the engine as well as the torque loading during peak power production. Assuming an even weight distribution between the two side struts, they would be required to supply a force equivalent to half the engine weight (392.4 N) as well as a nominal balancing moment of 31.4 Nm at no load. The balancing moment is half the engine weight multiplied by the CG offset distance of 80 mm.

The magnitude of the compressive axial force will reduce in the left strut as the engine begins to generate torque, while the compressive axial force will increase in the right strut. The peak axial force required was calculated in the 'General Force Calculations' above to be 1300.6 N (compression), which would combined with a moment of 104 Nm to give the largest force and moment required by the side struts. Although the CG shifts closer to the mounting plane with the connection of the drive shaft and couplings, 80 mm was used to ensure an overestimate.

The maximum axial stress will be 2.93 MPa, combined with the small bending moment will produce principal stresses:

$$\sigma_1 = 2.93 \ \ MPa$$
$$\sigma_2 \approx 0 \ \ MPa$$

The above stresses are present in the 75mm square tube section, 1.5 mm wall thickness. The strut incorporates a 10 mm base plate to which the square tube is welded. The 8 mm flat bar that attaches the strut to the engine is welded to the square tube. A 150 mm length is provided to weld the flat bar to the square tube to reduce the shear stress present at this interface as well as no gusset incorporated on the lower surface due to the extremely small moment present throughout the strut. High tensile hex-head bolts, of the appropriate size, were used for all mounting connections to the engine.

B.2 Drive Train Design and Components

It was decided to incorporate a drive shaft with flexible couplings at both ends so as to ensure the natural frequency of the system was similar to that in a helicopter. A helicopter drive train employs a 'flexible' shaft with rigid couplings, while the test cell drive train had a rigid shaft, and thus required flexible couplings to reduce the overall torsional rigidity and natural frequency. The flexible couplings allow for operation with a slight misalignment and provide torsional and axial damping that extends the life of all drive train components.

B.2.1 Requirements

The requirements of the shaft and couplings are the following:

1. The combined mass of the shaft and the couplings must weigh no more than 12 kg.
2. The drive shaft must be capable of transferring 236 kW at 6000 rpm or 376 Nm of torque.
3. The drive shaft incorporated must be either a Flexible, Coupling or Needle-bearing type.
4. All components must be balanced to quality G6.3 as per DIN ISO 1940.
5. The shaft and couplings must have a combined natural frequency so as to never encounter resonance during operation.
6. 0.01 % of the outer diameter of the adapters is permissible as radial run-out at the external diameter and as axial run-out of front surfaces near the outer diameter.

The mass limitations are incurred by the incorporation of the W3S 480 dynamometer and its physical limitations. The mass of the dynamometer half of the drive shaft and couplings must weigh no more than 2, 3.4 or 6 kg when operated at 13,000, 10,000 or 7,500 rpm respectively. The power transfer requirements are those of the engine at maximum power output, namely takeoff power.

The allowable shafts are listed by the SCHENCK Instruction Manual in the Technical Data section, as well as the necessary balancing and run-out specifications [29]. The above mentioned shafts all have various pros and cons associated with their design, and the most practical design for a gas turbine engine will be discussed later.

The natural frequency of the drive shaft in gas turbine applications is not as crucial as it is with reciprocating IC engines due to the absence of a forcing function in terms of torque. The power delivered to the drive shaft is completely smooth and continuous as the torque is create by the reaction of air passing over a turbine, unlike in reciprocating engines where there is a forcing function whose frequency is proportional to the number of cylinders. With this said, the problem of resonance is that even a small force, acting in time with the natural frequency and undamped, can result in very large oscillations. The natural frequency of the system will thus be fully analysed for safety.

B.2.2 Helicopter Drive Shaft System Calculations

A number of different drive shaft and coupling arrangements are used in practice, allowing for the passing of power between the engine and the rotor gearbox housing. The rotor housing is allowed to move during operation, providing smooth flight for the passengers. This motion changes the shaft alignment with the rotor housing and necessitates the couplings and shaft being able to operate at an angular offset.

(a)Bendix Shaft (b)Test Cell Shaft

Figure B.5: Gas turbine drive shafts (a), (b).

A common shaft used is called the Bendix shaft, shown in figure B.5(a).

The shaft is about 100 mm long between the gears, and about 17 mm in diameter. Using the theory of pure torsion, the torsional rigidity of the shaft would be $\approx$ 5500 Nm/rad, assuming a shear modulus (modulus of rigidity) of 76 GPa, normal for steels used in the manufacturing of highly stressed components.

The shaft has two high rotational inertia masses on either side. The rotor has a rotational inertia in the region of 3 kg.m^2 and although the individual components of the engine gearbox and turbine wheels are small, they rotate at a much higher speed which results in their 'effective' inertia being much higher, approximately 0.27 kg.m^2. Equation B.2 was used to calculate the effective inertia of the engine gearbox components and turbine wheels.

$$I_{Eff} = I_1 + I_2 \left(\frac{\omega_2}{\omega_1}\right)^2 + I_3 \left(\frac{\omega_3}{\omega_1}\right)^2 ... + I_n \left(\frac{\omega_n}{\omega_1}\right)^2 \tag{B.2}$$

Where I_1 refers to the rotational inertia of the shaft and I_2, I_3, I_n refers to the rotating inertia of the components rotating about axis 2, 3, n at speed ω_2, ω_3, ω_n. All rotational inertia are calculated about the axes of rotation of the individual component and must be either directly or indirectly geared to the shaft so as to impact the effective inertia.

The torsional natural frequency of a system containing a Bendix shaft attached to a rotor of 3 kg.m^2, and an engine of 0.27 kg.m^2, is about 620 rpm. This mean that the natural frequency is passed under light-off, and operation between 3600 and 6000 rpm ensures operation is far removed from the natural frequency.

B.2.3 Drive Shaft

The drive shaft incorporated was 600 mm long between the outside of the triangular flanges, with a shaft OD of 38 mm and ID of 30mm. The shaft was designed with triangular flanges to incorporate the JURID flexible couplings. The shaft has a mass of 3 kg and operates with only a torsional loading and as such carries a safety factor of 8.75. The design was done in Pro-E and pictures of the shaft are provided in figures B.5(b) and B.6.

The right side of the shaft in figure B.6 is made to have a component press fitted into the shaft so as to allow the shaft to be centered via an IKO

PB 16 PILLO-BALL bearing, housed in the connecting coupling. The other side of the shaft locates another IKO PB 16 bearing internally, for the same purpose.

The shaft was machined from Bohler V155 steel designed for use with highly stressed components such a propeller shafts, connection rods, crankshafts and landing gear components. The properties provided in table B.1 are those at 20°C for a component whose diameter is 16-40 mm, as specified by Bohler. The yield shear strength was conservatively estimated to be half the yield strength, and a shear modulus of 78 GPa assumed.

Table B.1: Bohler V155 Properties, Hardened and Tempered

Yield Strength (minimum)	900	MPa
Tensile Strength	1100 - 1300	MPa
Density	7850	kg/m^3
Young's Modulus	210	GPa
Yield Shear Strength	500	MPa
Shear Modulus	78	GPa

The drive shaft with couplings and bolts attached was balanced by ABB. The system was balanced to within the limits set by G6.3 ISO 1940 to have a final imbalance of 183 mg and 138 mg on the outer radius of the adapter couplings on either side of the shaft.

B.2.4 Critical Speed

During operation, as a shaft rotates, eccentricity causes a deflection due to centrifugal force and this deflection is resisted by the rigidity of the shaft, EI (E is the Young's Modulus and $I = \pi D^2/64$ is the second moment of area). A specific rotation frequency exists for each shaft such that the eccentricity become unchecked resulting in an ever increasing deflection until failure occurs. Equation B.3 was used to calculate the first and lowest critical whirling speed.

$$\omega_1 = \left(\frac{\pi}{l}\right)^2 \sqrt{gEI/A\gamma} \tag{B.3}$$

Where l is the shaft length, g is gravitational acceleration, A is the cross-sectional area and γ the specific weight.

The critical speed of the shaft with properties mentioned above was calculated to be 13,537 rpm. This positions the first and lowest critical whirling speed of the shaft more than double the operational speed, as recommended by Shigley, Mischke and Budynas [28].

B.2.5 Adapter Couplings

The adapters provide connection between the flange of the Free-Wheeling unit of the gas turbine and the dynamometer to the drive shaft. The Free-Wheeling unit flange is shown far left in figure B.6, while the dyno flange is shown on the far right. The various adapter couplings incorporated were machined from Bohler M300 and M120 Stainless Steel.

Figure B.6: Complete drive shaft and couplings.

The components were all bolted together using hex-head high tensile steel bolts. M12 bolts attach the flexible couplings to the shaft and to the appropriate adapter, with M10 bolts attaching the coupling to the dyno. Four 1/4

inch UNF (Unified National Fine) thread bolts were used to attach the Free-Wheeling unit to the couplings. These are the same bolts used in the engine and provide the weakest point in the system, ensuring that if failure were to occur the 1/4 inch bolts would shear first. It is preferable to have the drive shaft disconnect at the engine side to prevent the shaft from being whirled about as the engine continues to produce power under no dynamometer load.

The 1/4 inch bolts were conservatively assumed to have a solid diameter of 5 mm. A torque of 376 Nm, with bolts on a PCD of 53.95 mm in a worst case scenario (when friction between the members no longer carries the shear load), requires two bolts to carry 3.485 kN each. The torque is generally passed by only two bolts due to machining imperfections that are unavoidable. This equates to a single shear stress of 177.53 MPa, well below the shear stress of high tensile steel (minimum of 300 MPa depending on exact chemical composition and heat treatment).

B.2.6 Flexible Coupling

The couplings incorporated were used on both ends of the drive train to connect the shaft to the adapter couplings. The properties of the couplings are displayed in table B.2.

Table B.2: Jurid Coupling: Type GD 80 Properties

Maximum Speed	13000 rpm
Permanent Inflection Angle	3 °
Torsion Power	445 Nm
Torsion Power Maximum	890 Nm
Trashing Power	4450 Nm
Rotational Rigidity (Static)	6000 Nm/Rad

The rotational rigidity of the couplings were measure during a prior project at the Sasol Advanced Fuels Laboratory and was shown to be 6000 ± 300 Nm/rad during a static test. The test procedure was to secure the one end of the coupling and apply a known torque via a torque wrench, measure the angular deflection, and then calculating the nominal rotational rigidity.

Although the static versus dynamic rigidity of the couplings is somewhat different, it has been shown that there is a correlation between the two. R + W Coupling Technology have shown a general trend in that the dynamic

torsional stiffness at T_{KN} (the rated torque of the coupling) is approximately double the static torsional stiffness at 50% T_{KN}. A secondary effect is the heating of the rubber via hysterisis during operation, whereby the rotational rigidity of the rubber decreases as the temperature of the coupling increases. The rigidity properties were measured at room temperature, about 20°C, as the rubber heats during operation the reduction in torsional rigidity will cause the dynamic torsional rigidity to move back towards the static torsional rigity measure at room temperature.

B.2.7 Drive Train Resonance

The drive train includes the drive shaft, flexible couplings, rigid adapters and the engine and dyno components rotating with the drive shaft. The flexible couplings are considered in both analogies to be flexible or spring member, while the engine and dyno components are considered to be rotating masses of the appropriate rotational inertia on either end of the system.

The adapter couplings are considered non-existent as they are essentially completely rigid due to their extremely short length and large diameters while also have a very small rotational inertia (< 0.001 kgm^2). The rotational rigidity of the shaft was calculated to be 16,274 Nm/Rad using equation B.4, this is more than double the rigidity of the flexible couplings but in the same order of magnitude.

$$Rotational \;\; Rigidity, k_T \;\; (Nm/Rad) = GJ/L \tag{B.4}$$

Where G is the modulus of rigidity, J is the polar second moment of area and L the length. Hence, the two different analogies will considering the drive shaft first as a flexible member and secondly as a rigid member.

Flexible Shaft

The shaft as a flexible member combines with the two flexible couplings to create three spring members in-line. Using basic spring theory for series connected springs, equation B.5 [30], these three member were combined to form a single spring with a spring constant representative of the three individual springs, shown in figures B.7(b) and (c).

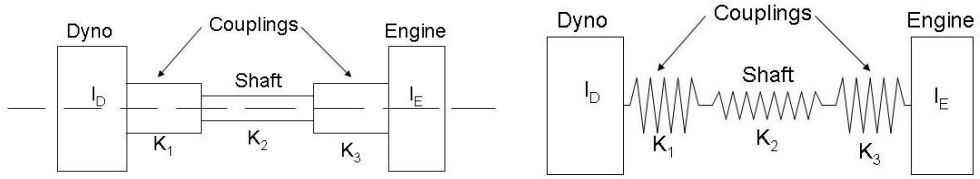

(a)Basic representation (b)Flexible members as springs

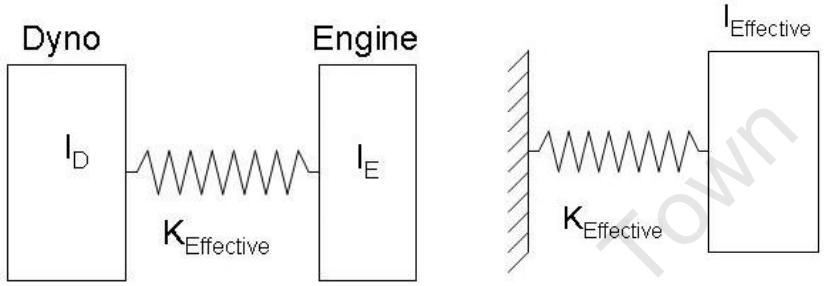

(c)Single spring representation (d)Single spring and mass

Figure B.7: Drive train analogy (a), (b), (c), (d).

$$k_{eq} = \frac{1}{1/k_1 + 1/k_2 + 1/k_3} \tag{B.5}$$

k_{eq} is the equivalent spring constant calculated from springs $k_{1,2and3}$, and the rotational rigidity of the various series connected 'flexible' components. The rotational inertia of the masses is also combined to provide a system with a single degree of freedom which can easily be solved, shown in figure B.7(d). The effective inertia is calculated using equation B.6 [31].

$$I_{eq} = \frac{I_D.I_E}{I_D + I_E} \tag{B.6}$$

Where I_D is the inertia of the dynamometer and I_E is the inertia of the engine, estimated using equation B.2 and knowing the rotational speeds of the various components. The natural frequency of the system can now be calculated using equation B.7 [30].

$$\omega_n = \sqrt{k_{eq}/I_{eq}} \tag{B.7}$$

Using a rotational rigidity for the couplings of 12,000 Nm/rad, double the static torsional rigidity and a safe overestimate according to R + W Coupling Technology. An inertia valves of 0.42 kgm^2 for the dyno and 0.27 kgm^2 for the engine, the natural frequency was calculate to be 1565 rpm. Without the two flexible couplings the natural frequency is 3015 rpm, relating the degree of flexibility of a steel shaft.

Rigid Shaft

When the shaft is assumed to be a rigid member the system become that shown in figure B.8(a). The system has two natural frequencies, one where the shaft oscillates internally between the spring members as in figure B.8(b) and the other where the outer masses begin to oscillate with ever increasing rotational displacements as in figure B.8(c).

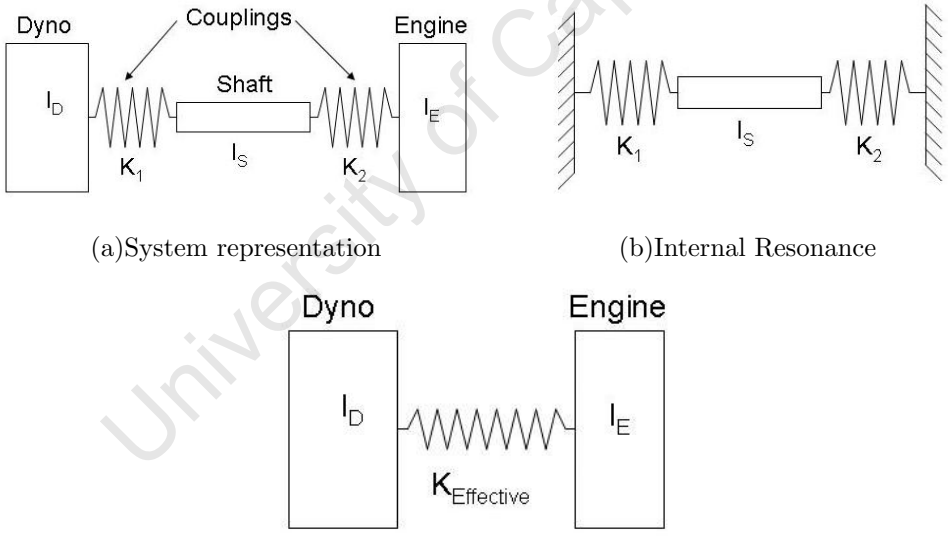

(a)System representation

(b)Internal Resonance

(c)External Resonance

Figure B.8: Solid shaft drive train resonance analogy (a), (b), (c).

The two natural frequencies can be calculated using equations B.10 [32].

$$\omega_1^2 = \frac{K_1}{I_D}, \quad \omega_2^2 = \frac{K_1}{I_S}, \quad \omega_3^2 = \frac{K_2}{I_S}, \quad \omega_4^2 = \frac{K_2}{I_E} \tag{B.8}$$

$$\omega_a = (\omega_1^2 + \omega_2^2), \quad \omega_b^2 = (\omega_3^2 + \omega_4^2) \tag{B.9}$$

$$\omega^2 = \frac{1}{2}(\omega_a^2 + \omega_b^2) \pm \frac{1}{2}\sqrt{(\omega_a^2 - \omega_b^2)^2 + 4\omega_2^2\omega_3^2} \tag{B.10}$$

The two natural frequencies were calculated using the same rotational rigidities and inertias mentioned about, with the inertia of the shaft being 0.00086 kgm^2. The two critical speeds were 1830 rpm and 50,321 rpm for 'external' and 'internal' resonance respectively. To ensure the number were correct another calculation was done using first principles, similar to those done for the flexible shaft scenario above, with good numerical agreement.

B.2.8 Conclusion

The designer can confidently conclude that the drive shaft, adapter couplings, flexible coupling and all the fasteners are capable to transfer the necessary torque from the engine to the dynamometer.

The critical speed of the system will be a maximum of 1830 rpm, half the minimum sustained operational speed of the engine. The secondary critical speed of the shaft was calculated to be in excess of 50,000 rpm, well beyond the operational envelope of the engine. The critical whirling speed of the shaft was calculated to be 13,537 rpm, more than double the highest sustained operational speed.

The system can be said to be safe for sustained operation between 3600 and 6000 rpm, as required.

Appendix C

Test Cell Systems

A T63-A-700 gas turbine when operated as intended, in a helicopter, has a number of systems built into the helicopter to enable engine operation. When the engine is removed from a helicopter it becomes necessary to simulate the functioning of the various sub-systems that enable operation. The sub-systems required are those necessary to condition and supply fuel and oil, enable duel throttle control, provide a plentiful supply of fresh air and a manner to simulate engine operation under varying load. It is also necessary to monitor engine operation in terms of turbine inlet temperature and various pressures and turbine speeds.

C.1 Fuel Supply System

C.1.1 Requirements

The requirement of the engine is to have the correct quantity of fuel delivered, in the correct condition, and in a safe manner. The requirements necessitate the fuel system having the following properties:

1. To supply fuel at a variable flowrate, between 61 and 221 lb/hr (27.7 - 100.2 kg/hr) at idle and takeoff respectively.
2. To present the fuel to the engine with a slight positive pressure ($\sim$ 6 - 10 psi gauge or 0.4 - 0.7 bar gauge).
3. Fuel supplied to the engine must be free of all air bubbles and foreign objects, i.e. contaminant free.
4. The system must allow for the changing of fuels from one test fuel to another.
5. System design must limit the quantity of fuel outside the fuel store, specifically inside the test cell.
6. The fuel supply side must be able to draw fuel from fuel barrels as well as be able to change fuel supply source during operation.
7. The operator must be able to fully control fuel supply from outside the test cell.
8. The entire fuel supply system must be safe, meaning easy to operate and fail safe where possible.

The engine requires the flowrate to maintain operation, while the pressure and absence of air ensures that the high-pressure fuel pump does not cavitate. Foreign objects will cause blockages in the engine and cease operation. A fuel store is specifically designed with a bunted volume and an extraction system to contain leaks and prevent the buildup of toxic fumes as well as the formation of a combustible mixture. Fuel is safest when stored in a specially designed room and minimizing the quantity outside the room will minimize risk of incidents as well as the magnitude of any that occur. Fuel is specifically not wanted inside the test cell as there are a number of sources of

ignition within a test cell for exposed fuel as well as a number of high speed components that could fail and rupture fuel lines or tanks.

In case of an emergency it is imperative to stop the fuel supply as soon as possible and then to limit the quantity of fuel available to the fire if possible. This is achieved by including both manual and electronic shut-off valves immediately upstream of the engine.

The operator must be capable of switching fuel supply sources during operation as the gas turbine consumes a significant quantity of fuel and would consume the usable portion of a fuel barrel ($\sim$ 120 liters) in about 70 minutes at cruise conditions. Fuel barrels/drums are the most common packaging for liquid fuels and being able to operate directly from the fuel drums limits the time and effort required for fuel changes. As the test cell is intended for fuel research purposes it will be necessary to operate on a number of different fuel, requiring the fuel system to be fully purged of the prior test fuel to avoid contamination.

C.1.2 Design

The fuel system was designed to meet all the above requirements and figure C.1 is a schematic of the final design.

The entire fuel supply system comprised 316 Stainless Steel and fuel resistant flexible hose. Flexibility was required where attachments were made to the fuel drums, the fuel flow meter and to the engine. The system was constructed from 1/2 inch tube, keeping the internal diameter of the tube 9 mm throughout. These dimensions kept the flow in the piping at 1 m/s for the necessary supply plus circulation, thereby limiting the boost pressure required. The system was designed to operate at up to 1 bar pressure gauge, 2 bar absolute, throughout. This was sufficient pressure to attain the necessary flow rates and supply pressure to the engine.

The fuel supply side was designed with quick couplers to make the change of fuel source as quick and easy as possible. A generic connection adapter was made that fits securely into the position of the filler cap, providing a connection point for the supply, return and ventilation lines. The boost pump was placed immediately outside the fuel store, limiting the sources of ignition as well as a flame arrester placed on the ventilation line to prevent any external flame traveling to the drums.

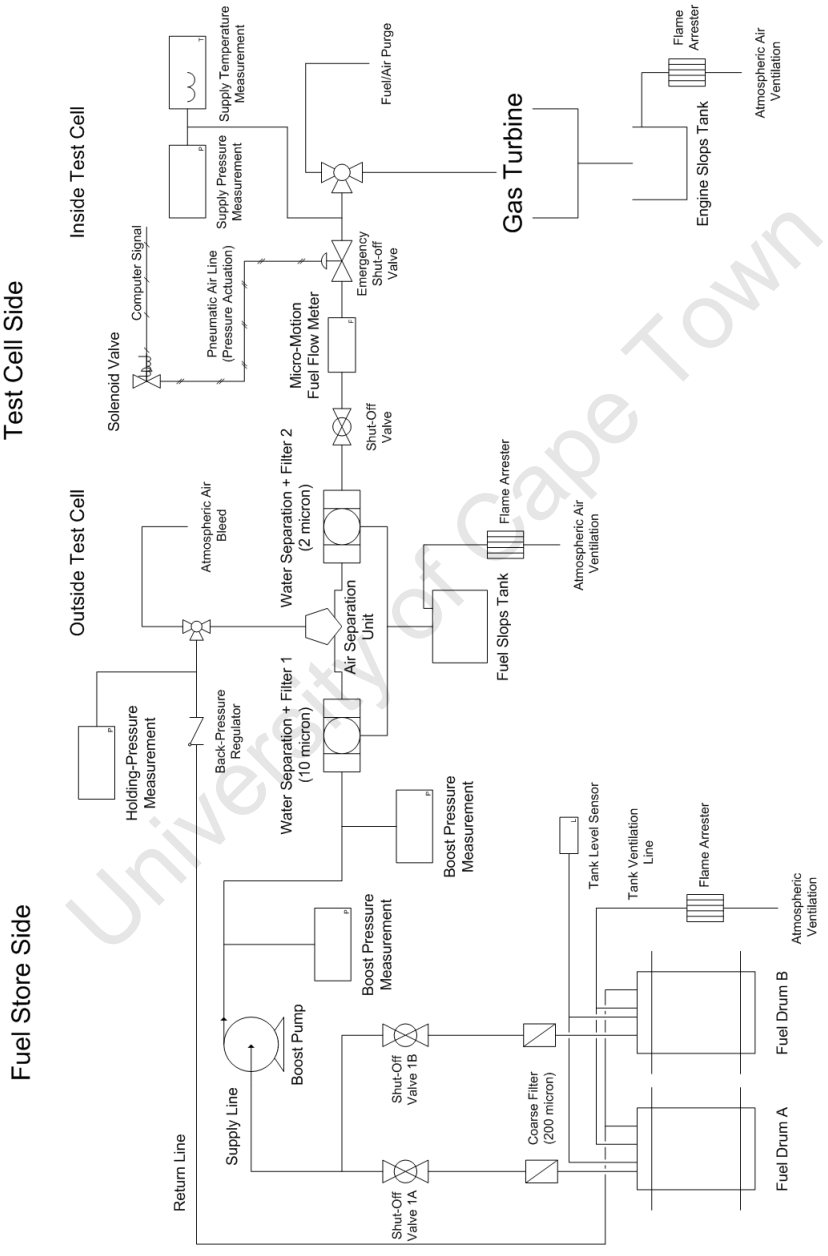

Figure C.1: Fuel supply system schematic.

The portion of the fuel system upstream of the boost pump was the only section in which air could be entrained as it was the only section below atmospheric pressure. Two shut-off valves were included to prevent the intake of air into the fuel system by preventing a pressure drop forming across the quick coupler that was currently not in use.

Mechanical pressure gauges were incorporated on the supply line to prevent personnel from working on the fuel line while it was pressurised which would result in fuel spillage. The supply line was about 20 meters long and as such a gauge was incorporated on either side, adjacent to the pump and outside the test cell where the fuel preparation occurred. Water was separated as well as further filtration of the fuel to remove particulates larger than 2 microns, reducing the need to check, clean or replace the 5 micron fuel filter in the gas turbine. An air separation unit was also designed and incorporated to remove any air that was entrained in the fuel stream and circulate it back to the fuel drum. A variable back-pressure regulator was included to prevent fuel preferentially flowing back to the drum, and a pressure gauge fitted upstream to verify the holding pressure. A 3-way valve and air bleed point was required to drain fuel from the air separation unit and the fuel filters. The fuel filters being able to be drained from their underside and the air separation unit drained under gravity through the fuel filters.

The air separation unit also acts as a tee, separating the supply line to fuel going to the engine and fuel circulated back to the fuel source. The fuel that flows along the line toward the engine is that used by the engine and as such the flowrate in this line is approximately the fuel flowrate though the engine fuel nozzle. The engine is capable of circulating fuel internally and as such the flow rates are not exact, however, at steady state operation they would be equivalent, making the placement of a fuel flow meter on this line appropriate. A second fuel filter was placed directly after the air separation unit in the stream going to the engine to do final filtration of the product going to the engine as well as a manual shut-off valve incorporated in case of an emergency.

Fuel then flows into the test cell where it immediately passes through an emergency shut-off valve. The valve incorporated here was an angled seat, normally closed, pneumatically operated shut-off valve. The pneumatic line used was shop air ($\sim$ 7 bar) and the supply of shop air was controlled via a solenoid valve, also normally closed that received a signal from the controlling computer when desired. Separating the electrical signal from the fuel avoids another potential source of ignition. Once inside the test cell the temperature

and supply pressure of the fuel are measured and read into the controlling computer to supply real-time information of the fuel supply. The 3-way valve is incorporated immediately before the engine to allow air bleeding and fuel purging right up to the engine when required.

C.1.3 Components

In case of a component becoming faulty, misplaced or theft occurring it is preferable to replace the component with the originally specified component as to ensure the system operates as designed.

Table C.1: Summary of the Fuel System Components

Section	Part Name	Description	Part Number	Company
Supply	Safeway Quick Couplers	3/8" Quick Connector	SS105-3 + SS101-3	Hyflo
	Flexible Hose	3/8" Fuel Resistant Hose		Hyflo
	Stainless Steel Tube	1/2" SS Tube	SS-T8-S-035-6ME	Swagelok
	Fuel Pump	Fuel Boost Pump		Avon Aero
Preparation	Fuel Filter	Racor Turbine Series	500FG Fuel Filter	Cape Filter
	Fuel Flow Meter	Micro-Motion Flow Meter	2000 series	
Test Cell	Angled-Seat Valve	2/2 Way Piston-Operation	Type 2000	burkert
	Solenoid Valve	3/2 Way Mini-Solenoid	Type 6012	burkert
	Pressure Transducer	Fuel Pressure Measurement	2200 Series	Atlas

All components not mentioned in table C.1 are standard Swagelok components and can be ordered from Johannesburg Valve and Fitting, Cape Town.

C.1.4 Operation

The fuel system is capable of operating normally, where it supplies fuel to the engine as required and circulates the excess back to the fuel drum, purging the existing fuel in lieu of a fuel change and changing fuel supply source during operation. The fuel supply system also enables the user the ability to shut-down the fuel supply instantly in an emergency.

Normal Operation

In order to safely operate the fuel system the following procedure must be followed:

1. Check all fittings and piping to ensure they are appropriately connected and secure.
2. The supply and return fuel lines should be attached to the fuel drum currently in use and only the shut-off valve in line with the supply from the drum currently in use open.
3. The shut-off valve between the fuel filter and the flow meter must be in the open position, allowing fuel flow to the test cell. The 3-way valve between the air separation unit and the back pressure regulator must be pointing in the direction of the regulator (i.e. not open to atmosphere).
4. The 3-way valve between the engine and the emergency shut-off valve must be oriented to enable flow to the engine and not to the purge point. The line must be firmly secured to the fuel inlet on the engine.
5. Switch on the PLC and controlling computer to enable operation of the boost pump and emergency shut-off valve.
6. Ensure that there is sufficient fuel in the drum by referring to the level sensor.
7. Lift the emergency shut-off valve in the test cell and switch on the boost pump using the operating system ETA.

The system will be seen to be active by an increase in the reading of the fuel supply pressure transducer and the noise of the fuel pump. To shut down the fuel system merely switch off the pump.

Fuel Change During Operation

To safely change the fuel supply source during operation the following procedure must be followed:

1. Position the new drum to be used adjacent to the drum currently in use.
2. Open the new drum and remove the filler cap before insert the filler cap fitting with the quick couplet attachments.
3. Take the spare supply and return quick couplers and attach them to the new drum.
4. Open the supply line ball valve to allow the pump to draw fuel from both drums.
5. Leave both valves (labeled shut-off 1A and 1B in figure C.1) open for at least 30 seconds to ensure no problems arise before closing the valve on the old supply drum.
6. Remove both supply and return quick couplers from the old drum and attach the level sensor lead to the new drum.

Purging the Fuel Line

To ensure all fuel from a prior test is out of the system, and the new fuel is not contaminated, the following steps must be followed:

1. Place the new fuel drum in place as the primary source and connect up the supply line, remembering to connect the return line to a slops drum to prevent contamination.
2. Drain the fuel from the fuel filters and air separation unit by opening the underside drain of the fuel filters and empty the contents ($\sim$ 3 liters) into a fuel slops drum.
3. Close the filter underside drains and run the boost pump for about 10 seconds to fully purge the supply line up to the 10 micron fuel filter.
4. Repeat step 2 and ensure you drain at least 1 liter of fuel here, the volume in the supply line.
5. Run the boost pump again and make sure at least 1.5 liters drains into the slops tank to fully purge the return line.

6. The return line to the slops must be disconnected and the 3-way valve in the test cell turned to purge to remove the ~ 0.5 liters remaining in the supply line.

7. Return all valves to normal operating position and connect the return line to the supply drum.

Step 6 is optional as during the start and warm-up procedure the remaining 0.5 liters will be consumed, ensuring tests to follow will be completed on the new fuel only.

Emergency Shutdown

In an emergency it is often necessary to stop fuel supply as soon as possible and isolate the fuel supply from the problem area, however, rapid shut-downs will likely result in irreversible engine damage. If it is deemed necessary to shut-off the fuel supply instantly the following procedure should be followed:

1. Immediately click on the emergency shut-off valve icon in ETA, followed by the fuel boost pump icon.

2. Proceed to turn off the ball valve outside the test cell between the fuel flow meter and the 2 micron fuel filter.

At this stage the test cell is isolate from the fuel supply and the engine will stop running if it has not already been stopped.

Hazards

The ability of the fuel system to do the various tasks requires ball valves to be manually moved from one position to the next, creating the possibility that one may forget to return a valve to its original operating position. This may result in the system failing to deliver fuel as required or fuel spillages, the following considerations should be noted to avoid potential hazards.

- Failure to place either of the two 3-way valve in the correct position or attach the fuel line to the fuel inlet on the engine as described in the

section 'Normal Operation' would inadvertently result in fuel spillage occurring when the boost pump is activated.

- Failure to open the shut-off valves necessary to supply fuel to the test cell or to circulate fuel would result in the internal relief valve of the boost pump recirculating fuel internally.
- Failure to check that all fittings are secure and all pipes are connected as per design could result in fuel spillage.

If valves are forgotten in the closed position they will cause the fuel system to circulate as designed, however, if valves are left in the purge position or hoses and fittings left off, fuel spillage will result.

C.1.5 Troubleshooting

If the fuel system is not operating as desired the problem may be one of the following:

No pressure generated inside the test cell when the pump is activated

- Check that all the valves are in the correct position as described in 'Normal Operation'.
- Check to see that the pressure gauge is properly attached and operational and that the gauge is not the problem.
- Check to see that the pump has not lost prime, indicated by a pressure reading on the gauge adjacent to the pump, if so one must re-prime the pump or replace the fuel drum with a full drum.
- If the above does not resolve the problem there may be a blockage or a leak in the system .

No pressure generate by the pump when activated

- Check that all the valves are in the correct position as described in 'Normal Operation'.

- Check the second mechanical gauge to ensure that it is not the malfunctioning of the gauge.
- Check to see if there is sufficient fuel in the current fuel drum, if not replace.
- Check to see that the pump has not lost prime by pressing in the internal mechanism of the supply quick coupler, if so one must re-prime the pump.
- If none of the above are observed the pump may be faulty, remove the pump and examine the brushes.

The pump does not respond when activated in ETA

- Ensure ETA is on-line by clicking the top left button that looks like a traffic light.
- Check that the fuel boost pump power has not been disconnected by checking the 24V DC power supply inside the test cell, the relay connections in the PLC and the connections to the pump.
- If all connection are good check that the relay is working by activating and deactivating it in ETA. Either by hearing a click or by using a multimeter across the contacts to measure 24V DC one can check the relay operation.

The emergency shut-off valve does not respond when activated

- Ensure ETA is on-line by clicking the top left button that looks like a traffic light.
- Verify the operation of the solenoid, one should hear a clicking sound when it is opened and closed.
- If the solenoid if operational check that the air line is still pressurised.
- If the solenoid is the problem check the power supply via the PLC.

C.2 Oil System

C.2.1 Requirements

The oil system is required to supply the engine with oil for lubrication of rotating components as well as cooling. The requirements necessitate the system having the following properties:

1. To allow the high-pressure (HP) internal oil pump to draw as much oil as is needed.
2. To cool the oil and prevent the oil-out temperature exceeding 107°C.
3. Provide a tank facility that stores no less than 10 quarts (∼9.5 liters) of turbine oil, providing thermal inertia and settling time.
4. Provide the various links between the tank and the engine (supply, return and ventilation).
5. Ensure lubrication to the one way clutch mechanism and PTO Spline not lubricated from the engine's internal oil pumps.
6. To supply oil free of any foreign matter, including air.

The oil is a critical fluid and a loss in cooling and lubrication provided by the oil would result in permanent damage to the turbine wheels that are cooled by the oil and well as damage to the gears and bearings that are lubricated. The temperature increase causes a reduction in the viscosity of the oil, limiting the lubrication provided, as well as permanent oil degradation occurring at extreme temperatures.

The tank provides a reservoir where air entrained in the oil, as it passes through the various bearings and gears, is able to be removed. The tank also provides the oil system with thermal inertia so as to avoid the oil supply to the engine heating or cooling too rapidly.

The tank is linked to the engine via a supply and return line, as well as the engine and tank ventilating with one another to avoid pressure variations in the air space above the oil.

The one way clutch mechanism is a part of the Free-Wheeling Unit that attaches to the PTO spline of the T63 and provides a flange for the attachment of a shaft or coupling. Both the PTO Spline and the one way clutch mechanism must be lubricated. The unit is lubricated from an oil pump in the main rotor gearbox housing and as such must also be simulated in the test cell.

The necessity for clean oil is that the oil is pumped through extremely small pipes as well as passing though extremely small orifices in various shafts and bearings. Sufficiently sized foreign matter would block these openings, preventing lubrication of the component and leading to more rapid wear and failure.

C.2.2 Design

The oil system was designed to meet all of the above mentioned requirements in as simple, effective and reliable manner as was possible. Figure C.2 is a schematic of the final design:

The oil supply tank and heat exchanger are positioned slightly above the engine in a helicopter, creating a gravity assisted feed of the engine's HP oil pump. The pipe length is short, about 2 meters, so to mimic the intended operational setup the tank in the test cell was positioned slightly above the engine and in close proximity. The supply oil is filtered to reduce the chance of particulates becoming lodged in the engine oil system, and reduce the need to routinely check the engine oil filter unit.

The oil heat exchanged was place on the oil line that returns oil from the engine to the primary oil tank as in normal operation. The heat exchanger was selected because of its low pressure loss and ability to remove the required heat from the oil, estimated to be $\sim$10 kW. The 3-way mixing valve on the oil return line was incorporated to give a measure of control over the degree to which the oil was cooled, allowing engine-out oil to optionally bypass the heat exchanger depending on the oil-out temperature, measured via a thermocouple. The cooled-oil temperature is also detected by a thermocouple and the signal is read via the PLC into the controlling computer.

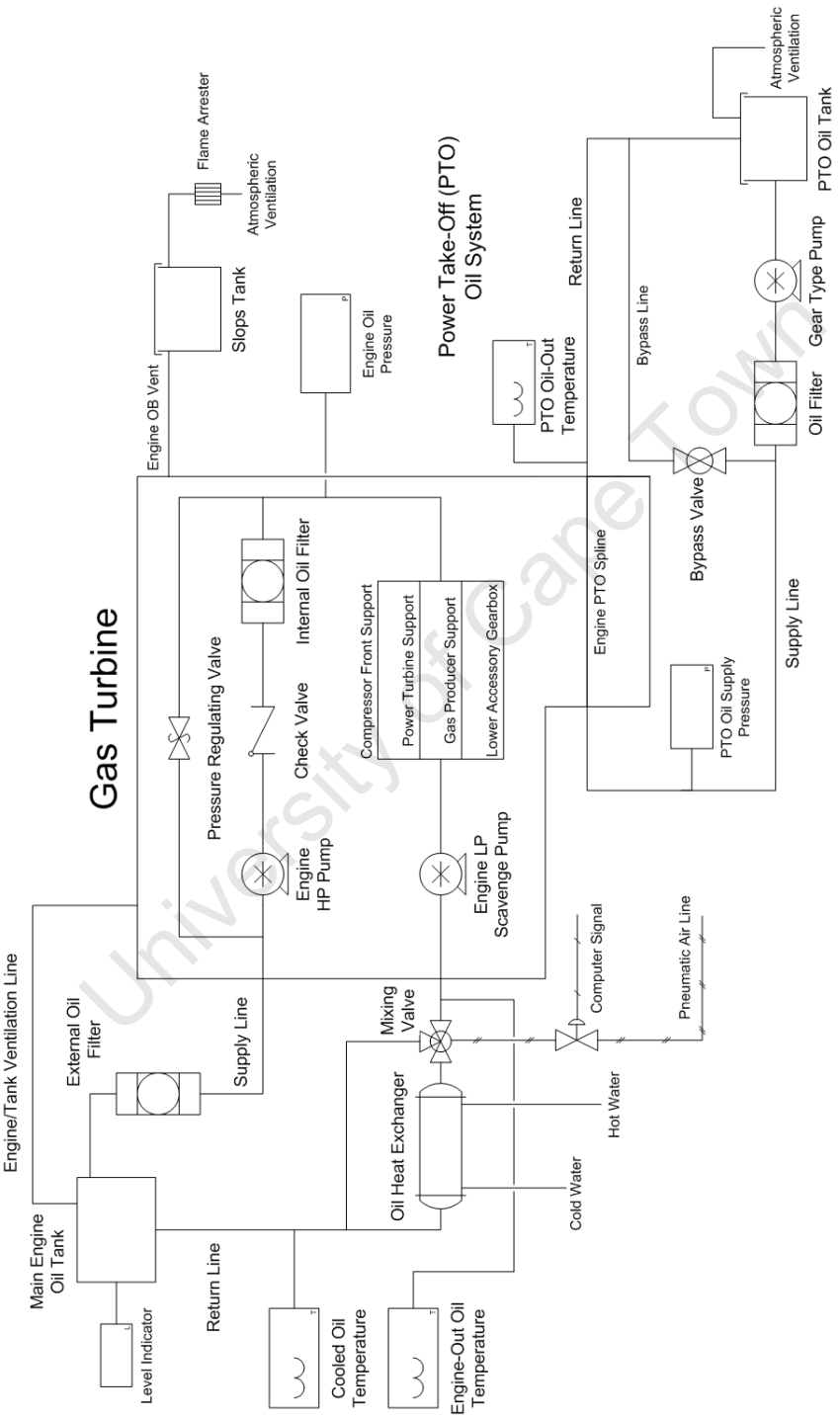

Figure C.2: Oil supply system schematic.

The engine oil pressure, the correct value being essential for engine operation, is continually measured via a mechanical pressure gauge visible from the control room, and a pressure transducer to ensure the pressure is always maintained within limits.

The engine and the primary oil tank vent with one another, with the engine venting to atmosphere via the OB vent. Inside the test cell this ventilation point was piped to a slops tank and the tank was ventilated via a filter.

The PTO oil system operates completely independently of the primary oil system and has its own storage tank, supply pump, filter element and supply and return pipes. The tank is vented locally and has a pressure transducer that is linked to the controlling computer to indicate operation of the system as well as a thermocouple to monitor oil exit temperature. The bypass valve is incorporated due to the small flowrate required through the PTO Spline and one-way clutch mechanism, requiring a portion of the flow be bypassed.

Engen Mobile Jet Oil 2 was used as it was the most easily available gas turbine engine oil that adhered to the MIL-L-23699 specification. The Jet Oil 2 was used in both the primary and PTO oil systems. Although it is permissible to use separate oils as the two systems are completely separate this reduced the chance of accidentally contamination an oil system.

Although the oil changes are made slightly more challenging, no shut-off valves were included in the system to remove the possibility of operating the engine with one or more shut-off valves in the closed position, starving the engine of oil. This does include the possibility that if an leak occurs there is no manner to isolate the system, however, considering the system contains only 10 liters of oil, the quantity is minimal.

C.2.3 Operation

The sole purpose of the oil system is to provide the engine and PTO shaft with lubricating oil while removing excess heat.

Normal Operation

In order to safely operate the system and prepare it for the operation of the gas turbine the following steps should be followed:

1. Check the level of oil in both the primary and PTO oil tanks by removing the filler cap and lid respectively. The primary oil tank has a dip stick demarcated with increments to enable the user to determine whether or not the tank is sufficiently full, while the PTO tank must have no less than 30 mm of oil above the supply tube inlet.
2. Check that all piping between the oil storage tanks and the engine are properly connected and that there are no disconnected pipes, be sure to check each thermocouple and pressure tapping connections.
3. Check that the bypass ball valve on the PTO oil line is partially open, if not open half way.
4. Switch on the PTO oil pump which operates on mains AC.
5. Wait a moment and ensure that the oil is flowing as intended and make sure the pressure transducer is registering a positive pressure on the controlling computer ($\sim$ 0.5 - 1 bar gauge).
6. If the pressure is below 0.5 bar gauge further restrict the oil bypass route by closing the ball valve a small amount, if above 1 bar reduce the restriction as required.

The oil system is now ready for the operation of the gas turbine, follow all necessary procedures and checks to ensure the gas turbine internal oil pressure remains within limits during operation.

Oil Change

Every 6 months or 200 operating hours the oil system must be drained and refilled with new oil, the following procedure should be used:

1. The primary and PTO oil tanks are designed with drain plugs to enable the contents to be easily removed from their underside without spillage

of difficulty. Remove the drainage plugs and drain the entire contents of both the primary and PTO oil tanks.

2. Remove the oil filters on both lines and empty the contents into the oil slops before disposing of the oil filters.

3. Fill the new oil filters with oil, wipe a thin film onto the rubber seals, and place the filters onto their respective seats.

4. Fill the primary tanks to the indicated 'full' point and the PTO tank to 30 mm above the inlet point.

5. Place the return line from the primary oil system in a separate container and motor the engine until about 3 liters of oil have been collected, after which fill the supply tank to supplement the drained oil.

6. Motor the engine again and ensure a positive pressure indication is seen.

The PTO oil system is not critical and as such draining the tank and oil filter will replace about 70% of the oil in the system and provide sufficient lubrication for a further 6 months or 200 hours. If so desired the rear connection of the Free-Wheeling Unit can be disconnected and the oil contained herein drained for a full change.

Hazards

If the oil system fails to deliver oil as required permanent engine damage may result. The following considerations should be noted prior to operation to ensure safe and continual operation of the system.

- Failure to ensure the oil levels are as should be may result in the supply to the engine reducing, lowering engine oil pressure and diminishing the cooling capacity and lubrication the oil provides.

- Failure to check the piping and connection may result in an oil leak with the same consequences as mentioned above.

C.2.4 Troubleshooting

If the oil system fails to operate as intended the following may be the problem:

Oil temperature continually increasing

- Check that the engine operating pressure is still within limits to ensure oil flow is maintained and no obstruction has occurred in the oil pathway.
- Compare the engine oil-out temperature to the cooled-oil temperature to check if the heat exchanger is malfunctioning. If the temperatures are similar the oil is either being bypassed or partially cooled (Note temperature drop).
    1. If bypass is expected check the position of the mixing valve and the signal from the controlling computer.
    2. If under cooling is expected check that the needle-valve on the cooling water supply is fully open. Check the water-out temperature of the dyno to determine the temperature of the water, if above 40°C ensure the 'Normal Operation' of the water system has been fully implemented.
- If none of the above are observed to be the cause, remove the heat exchanger and clean thoroughly, if the problem persists replace the heat exchanger.

C.3 Water System

C.3.1 Requirements

The water system is necessary to provide cooling to the dynamometer and the oil cooler. The following requirements are necessary:

1. The system must provide the necessary flow rates to avoid boiling of the water as is passes through the test cell.

2. Sufficient cooling to sustain the overall water temperature and thus remove the heat generated by the dynamometer and the oil cooler, a maximum of 250 kW.

3. Supply pressure must always be maintained.

4. The water must be free of foreign objects.

If water flows too slowly through a system as it provides cooling it will boil, reducing the cooling effectiveness of the system and leading to further unwanted heat buildup. The quantity of the water in the system creates a significant thermal inertia and as such the system could operate above it's cooling capacity for short periods, although this is not recommended or sustainable.

The dynamometer measures water exit temperature, however, without knowing that the water is flowing the internal temperature of the dyno could be much higher than the water exit temperature indicates. This necessitates the need to monitor the supply pressure to ensure water flow. If the dyno fails to register water pressure or registers too high a water exit temperature, the dyno immediately switches to no-load operation.

The system should preferentially be free of foreign matter as particulates will cause erosion of the piping system, a reduction in the cooling capacity of the oil heat exchanger and potential blockages.

C.3.2 Design

The water system incorporated made use of the existing water supply and cooling system and nothing was added to the water system outside of the test cell. Figure C.3 is a schematic of the water system incorporated:

In order to ensure that water never overflows the temporary storage tank, the pump that drains the storage tank is much larger than the pump that supplies the test cell. The test cell supply pump is able to supply $\sim$2.7 l/s of water at $\sim$2 bar gauge pressure, while the scavenge pump that sends the water to the cooling tower is able to pump water at $\sim$11 l/s. This system ensures that the test cell supply pump always has water as the pump draws water from the main storage point, the cooling tower.

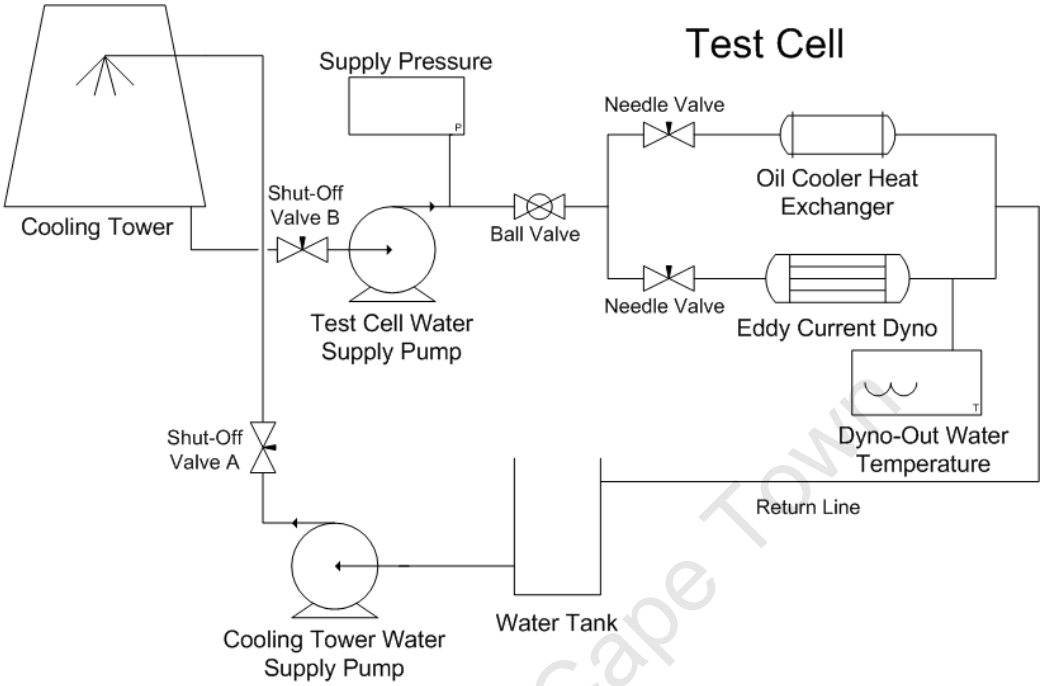

Figure C.3: Water supply system schematic.

The cooling tower is capable of producing about 500 kW of cooling via forced convection and evaporation. It is continually filled with water, via the water mains and a mechanical level sensor, as water is lost to spillage and evaporation.

A ball valve is incorporated to act as a shut-off valve as soon as the water line enters the test cell, followed by needle valves to meter the flow for each application. After use the water drain under gravity to the water tank, where it is pumped to the cooling tower.

Shut-Off Valves A and B are incorporated out of necessity, the cooling tower is situated at a greater elevation and as such without the valves water would drain under gravity back to the water tank and cause it to overflow after the cooling tower supply pump had been switched off.

C.3.3 Operation

The water system is intended to supply the Gas Turbine Test Cell with water, and remove any heat that has been added.

Normal Operation

During normal operation the system supplies water at the desired temperature to the test cell. The following procedure should be followed to enable safe and continuous operation:

1. Ensure all pipes within the test cell are secured as desired and unused connections are shut.
2. Check that the Continuous-Flow Combustion Rig has been isolated via the two shut-off valves, on the right side of it's control panel on the wall.
3. Switch on the cooling tower fan on the DB board outside the Gas Turbine Control Room.
4. Check that the fan is operational and there is sufficient water in the cooling tower. Open the fresh water supply valve if not already open.
5. Fully open shut-off valve A and switch on the cooling tower supply pump.
6. Check that the water tank has fully drained if full.
7. Fully open shut-off valve B and switch on the test cell supply pump.
8. Check that the pressure gauge within the test cell is registering and for any leaks that may have started.
9. Monitor the dyno outlet water temperature during operation to ensure the temperature remains below 40°C.

The flow of water into the water tank will indicate flow though the test cell, and a pressure gauge reading will indicate proper functioning. There should also be the sound of falling water within the cooling tower.

Shutdown

To switch off the water system follow the following procedure:

1. Ensure that the gas turbine has been switched off and no longer needs water supply. Consult whoever is operating the Continuous-Flow Combustion Rig as the water system is shared before proceeding to switch off the system.
2. Switch off the test cell supply pump, followed by shut-off valve B.
3. Switch off the cooling tower supply pump, followed by shut-off valve A.
4. Switch off the cooling tower fan on the DB board.

Hazards

The water system when used unappropriately can cause water spillages which can short and damage electrical equipment. The following are operational hazards that may occur if one is not made aware:

- The order in which the pumps are switched on is extremely important, although the water tank will take about 45 seconds to fill from empty, it is best to operate the pumps in the correct order.
- Failure to check the test cell for loose and or open water supply points could result in damage to various electronics.
- Failure to switch on the cooling tower fan will result in the run-away temperature of the water, leading to loss of load on the dyno.
- If the refill valve is left close the quantity of water in the system will decreasing. Although this is a slow process on hot,windy days a significant quantity of water loss will occur.

C.3.4 Troubleshooting

If the water system fails to operating as intended on of the following may be the problem:

Pumps not switching on when activated

- Ensure that the pump is plugged into the correct starter.
- Check on the DB board, adjacent to the Control Room, that the pumps have not been switched off.
- If the starters are active, apparent from an audible clicking when activated, the pumps are likely drawing too much current and causing the starter to trip.
- If nothing happens when the start button in engaged the starter is likely faulty. Contact an electrician.

Low pressure and or flow rates when the system is activated

- Check that the shut-off ball valve in the test cell is fully open.
- Ensure that the shut-off valve B is fully open.
- Check that the Continuous Flow Combustion Rig is isolated.
- Scour the system for leaks.
- Check the pump for improper functioning and the entire system for blockages.

C.4 Electrical System

C.4.1 Requirements

The requirement of the electrical system is to provide the engine with electrical power for the starting procedure, provide the fuel boost pump with power as well as all subsidiary requirements. The requirements necessitate the system having the following properties:

1. The power supply must be from a direct current source and between 14 and 29 Volts.

2. The source must be capable of supplying up to 500 amps (Cranking Amps).

3. The system must be mechanically controlled from the control room.

4. The system must be safe to operate and minimise the risk of electrocution.

All engine systems are designed to run on a DC power supply and can handle voltage variations between 14 and 29 volts, hence this specification must be met at all times. The starter motor must be capable of motoring the engine to 17% N_1 speed in about 12 seconds, with 17% being ∼8700 rpm. This process requires between three and four hundred amps on average. The power was specified to be no less than 500 amps so as to provide leeway for cold days as well as other systems power demands.

The control of start must be controlled from the control room to allow the user to be in a safe room when operating the engine.

C.4.2 Design

The schematic in figure C.4 represents the electrical system used for controlling the engine and the various sub-systems. The system met all requirements.

In order to switch on the main current to the starter motor and the spark circuit, a relay was use. For safety the master had to be activated as well as the starter switch before the relay would close. The starter switch was a Dead Man's Switch so that upon release it would return to the off position, ensuring that the starter switches off instantly in case of an emergency. The engine has the starter motor and the spark circuit attached to the chassis, requiring only the supply of power to operate. The starting circuit usually draws 400 amps, and the spark circuit draws about 4 amps.

The engine also has built in magnetic chip detectors to detect when a component, such as a gear, has been broken or chipped so as to alert the pilot that the engine has been damaged. The magnetic chip detectors work by having a magnetised center surrounded by a steel cylinder. If any steel components break, the steel chip would be attracted by the magnetic center and, if large enough, will complete the circuit by connecting the outer ring

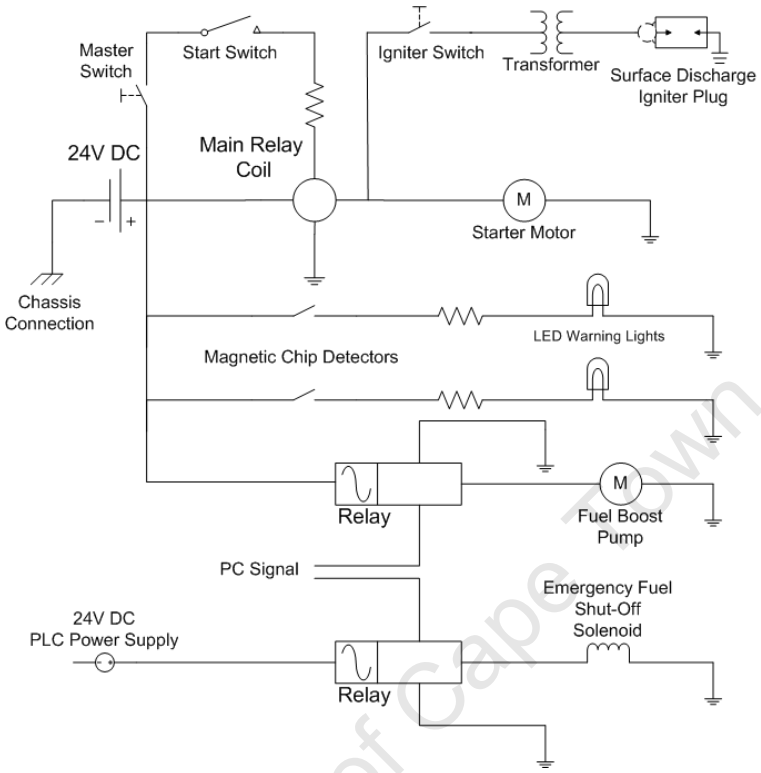

Figure C.4: Electrical system schematic.

with the inner. A circuit was created incorporating both magnetic chip detectors, a resistor to limit the current to 7mA and LED's to form a display in the control room.

The fuel boost pump draws about 81 watts, 3.5 amps from a 24 volt source. It was connected to the main 24 V DC source that was already available in the test cell. The emergency shut-off valve also required power, supplied from the 24 V DC power supply in the PLC as the current demand was low.

C.4.3 Operation

The electrical system is intended to enable the operation of the T63 gas turbine, it's sub-systems and necessary safety systems and should not be used for any other purpose.

Normal Operational

The normal operational of the electrical system involves getting the system ready for use, as the system is required for the operation of a number of different systems, as well as providing the power for the starting of the gas turbine. The following procedure should be used to ensure the electrical system if ready for use:

1. Check that all connections to the 24 V power supply (2 x 12 V batteries) in the test cell are secure and that the batteries have sufficient charge by looking at the indicators on their upper surface.
2. Make sure there is no spilled fluids, especially in close proximity to any electrical wiring.
3. Ensure that the connections to the starter motor are secured to the engine and the motor is itself secure.
4. Check the connection to the low tension capacitor discharge ignition exciter is secure, and check the leads connecting to the magnetic chip detectors.
5. Check the DB board to make sure that all appropriate switches are active.
6. Open the PLC and in the top left corner switch on breakers 1, 2 and 4 (If not already done).
7. Switch on the controlling computer as well as the dyno controller.

As the electrical system does not itself serve a function other than to enable other systems operation, these checks should be completed first and the starting of the engine and other systems only done following their prospective checks and procedures. After testing is complete the controlling computer, dyno controller and PLC should be switched off.

System deactivation

When not in use for an extended period of time, as research test cells often are, or while being maintained, it is preferable to deactivate the system to

avoid unwanted operation and accidents. The following procedure should be used:

1. Switch off all computers and sensors operating on mains power.
2. Remove the positive lead connecting the battery to the relay with a spanner and cover it using any non-conducting material.
3. Place the lead adjacent to the battery.
4. Open the PLC and in the top left corner switch off breakers 1, 2 and 4.

The system is now completely inert and is safe to use, although it must be reminded that batteries are never inert and will conduct current whenever a circuit is completed between their terminals.

Hazards

If the above mentioned checks are not performed when necessary the following problems may occur:

- Batteries not fully charged will be unable to spool the engine to a high enough speed for safe starting, either resulting in a hot-start or a multitude of other problems.
- Spilled fluid may result in short circuits in the electrical system and in the worst case electrocution of the user.
- Loose connection may fail to make connection and result in improper operation of the associated system/sensor.
- The direct connection of the battery terminals is extremely dangerous and the batteries may under no circumstances be used to place tools or other equipment when inside the test cell.

C.4.4 Troubleshooting

The electrical system is relatively straight forward and any problems with operation would likely result from discontinuities in the related circuit. Using the circuit diagram figure C.4 and follow the circuit wiring until the problem is found.

C.5 Ventilation System

C.5.1 Requirements

The ventilation system is required to supply the engine with the air necessary for operation as well as dilution air to cool the exhaust gases. The requirements necessitate the ventilation system having the following properties:

1. Sufficient air supply to maintain the engine requirements at takeoff power, as well as enough bypass air to cool the exhaust stream below 200°C.
2. Sound attenuation.
3. Both a supply and an exhaust fan.
4. Variable speed control of both fans as well as separate startup/shutdown.
5. Safe removal and exhausting of the dangerous exhaust gases.
6. Monitoring of the exhaust mixed temperature.

Takeoff power is the maximum power point at which the engine will be operated, and as such this is the maximum demand condition in terms of air supply for the engine and dilution purposes. System design at this condition will ensure safe operation at all other conditions. Dilution below 200°C was required because of the exhaust fan limitations.

The noise generated by a gas turbine during operation is immense. To limit engine noise all means of sound waves escaping the test cell must be taken into account and the magnitude of the sound emissions reduced.

Two fans were required to be able to adjust the pressure within the test cell and keep it as close to ambient as possible. Two fans also allow the pressure drop required by each fan be halved, for a given flowrate. Incorporating two fans does not in itself make pressure adjustments possible, hence variable speed drive (VSD) were incorporated on each of the fans. The VSD's were necessary as the exhaust fan and ducting incorporated are used in two other research rigs, where only the exhaust is required to operate and at a much lower speed.

The diluted exhaust gases temperature at takeoff power approaches 200°C and contains high concentrations of exhaust gases as well as being produced at $\sim$ 8 m^3/s. The volume, temperature and contents make the exhaust hazardous and full dilution necessary in such a manner as to be harmless to all.

The exhaust temperature, if allowed to attain too high a temperature, will damage the extraction fan and further reduce the air supply to the test cell. The temperature of the exhaust stream is directly proportional to the air mass flow rate, as a greater volume of air would further dilute and cool the neat exhaust gas. Monitoring the exhaust gas temperature at a given engine operating condition would thus communicate the operation of the ventilation system via a single temperature reading.

C.5.2 Calculations

The mass flow rate required through the test cell necessary to supply the engine and sufficiently cool the neat exhaust stream had to be calculated. The takeoff power condition was used for the air mass flow rate calculation as this condition corresponded to the maximum air flow requirement.

The fuel consumption of the engine at takeoff power is 0.697 lb/shp.hr, with the engine producing 317 shp (236.4 kW). This corresponds to a fuel consumption of 100.2 kg/hr. The density of Jet-A1 has to be within a certain range, however, as one fuel will differ from the next the engine accounts for this by varying the fuel flow as required to make rated power. The specific energy density of Jet-A1 does not vary much, usually between 43 and 44 MJ/kg.

Using 43.5 MJ/kg specific energy and 100.2 kg/hr flow rate, this results in 1.21 MW of fuel energy used to produce 236.4 kW of shaft power. There

is also about 12 kW of heat lost through the oil system (∼5%), resulting in 962.35 kW of fuel energy used to heat air.

Using a global energy balance, looking at the air mass flow through the test cell as well as the energy variations in the air and water flow through the test cell one can calculate the ventilation requirement. 236.4 kW and ∼12 kW are removed from the test cell via the water system, with the remaining energy input added to the air stream. Assuming a maximum air temperature supply to the test cell of 30°C and not wanting the exit temperature to exceed 175°C results in a ΔT of 145°C between inlet and outlet. The exhaust temperature was chosen to avoid the maximum 200°C operating temperature of the extraction fan and provide reaction time in case one or both fans were to shut-down unexpectedly.

Assuming a C_p value of 1005 J/kg.K, and using the quantity of energy calculated above and the formula:

$E = \dot{m}\ C_p\ \Delta T$

the necessary air mass flow rate was calculated as 6.6 kg/s. Using the ideal gas law,

$PV = mRT$

the supply flowrate of 5.5m^3/s at 20°C and exhaust flowrate of 8.4m^3/s at 175°C. The supply and exhaust fans were specified accordingly.

C.5.3 Design

The two fans used were capable of delivering the necessary flowrate as well as attenuators included in the supply line to inhibit sound escaping the test cell. Variable speed drives were incorporated on both fans to proved full speed control as well as separate startup and shutdown for their intended operation with adjacent research rigs.

The exhaust stream was monitored via a thermocouple to ensure the temperature did not exceed 200°C. The actual exhaust was ducted into a tall, sealed chimney that exhausted the gases to atmosphere no less than 12m above the nearest building ventilation intake duct.

C.5.4 Operation

The purpose of the ventilation system is to provide the gas turbine test cell with sufficient air for the engine to operate as well as to keep the exhaust gas temperature below 200°C. The two fans can be operated separately as is necessary for the use of the fans with adjacent research rigs.

Normal Operation

The following procedure should be followed to startup the ventilation system for gas turbine operation:

1. Walk through the test cell and ensure there are no loose items that may be swept into the ventilation system.
2. Ensure that there are no blockages in front of the inlet or exhaust and firmly secure the test cell doors.
3. Switch on the orange DB board containing the supply and exhaust fan variable speed drives.
4. Ensure both emergency stop switches are out, located on the orange DB board outside the operating room and on the control box in the control room.
5. Note the pressure inside the test cell from the ambient pressure transducer.
6. Dial both the speed indicators to about 20% and start the fans one at a time.
7. Slowly increase the speed of the fans one by one to attain full ventilation (Full ventilation is reached when one of the fans reaches 100% and the test cell pressure is as it was before the fans were activated).

In terms of safety the pressure inside the test cell must be close to atmospheric so the test cell doors can be easily opened and closed in case of an emergency. To avoid the unwanted escape of exhaust gases into the control room or the adjacent rooms, the test cell should be operated at a slight lower pressure than atmospheric.

Hazards

If the necessary checks are not completed prior to, or during operation, the following mishaps may occur:

- Loose and light-weight items not seen that become ingested by the ventilation system will likely themselves be damaged and cause further damage to fans and their motors.
- Failure to monitor the exhaust gas thermocouple will result in the over temperature operation of the exhaust fan in case of a fan shutdown or malfunction.
- Currently if the exhaust fan switches off during operation of the CFCR there are no attached warnings as they are separate systems. The flow is minimal, however, the contents are potentially toxic and the buildup of the gases dangerous. Regular checks must be made(10 minute intervals) to ensure safe operation until the installation of a flow sensor with a built in warning is complete.

C.5.5 Troubleshooting

In the result of a system failure, check the following switches and components:

1. Ensure that the emergency stops are not activated by pulling them outwards with a light tug.
2. Check that the power supply from the main distribution board to the VSD's is on.
3. Check the VSD DB board to ensure the board is on.
4. The board may be opened to ensure the proper operation of the variable speed drives by their visual displays. Reset if an error message is displayed or otherwise contact the suppliers (ANA Digital Systems).
5. If the system is still not operational contact an electrician.

Under no circumstances touch anything inside the main DB board or the power cables connected to the fan motors in an attempt to fix the system.

C.6 Load Control

C.6.1 Requirements

The requirements of the load control system are as specified according to the operation of the T63 and are as follows:

- Operation at speeds up to 7200 rpm.
- Capable of applying a varying load to allow engine operation of up to 250 kW power output.
- The dynamometer should be a Model 1014-T1 or Model 8123-T1 Dynamic dry-gap, water-cooled, eddy current brake or equivalent.
- The combined dynamometer and shafting moment of inertia must be between 1.0 and 3.0 slug-ft^2 (1.35-4.05 kg.m^2)

To simulate the real world operation of the engine a dynamometer must be incorporated. The dynamometer must be able to apply load and operate throughout the normal operating envelope of the engine. The engine is designed to operate at 60% N_2 speed at idle and 100% N_2 speed at all other times. 100% N_2 speed corresponds to 6000 rpm outsput shaft speed, meaning 60% corresponds to 3600 rpm. This means that the dyno must be capable of applying a small quantity of load at idle conditions ($\sim$15kW) and up to 236 kW at 6000 rpm.

In a situation where the load is instantaneously lost the engine over speed governor usually limits the engine output shaft speed to 120% N_2 or 7200 rpm. It is possible that the speed may increase above the 20% overspeed limit and in so doing it is preferable that the dyno not be damaged, hence, a higher upper operating limit would be favourable for safety and to reduce the likelihood of machine damage in the case of an overspeed.

The shaft and couplings tend to have a very low inertia, $<$0.1 Nm^2, requiring the dyno to have a considerable rotational inertia in order to physically simulate the real world operational conditions for which a helicopter engine was intended.

C.6.2 Selection

Being available in the research group and meeting all the requirements, a W3S 480 SCHENCK dynamometer was incorporated in the test cell. Type W3S is a heavy-duty eddy-current dyno with three rotors designed and built for the testing of racing engines.

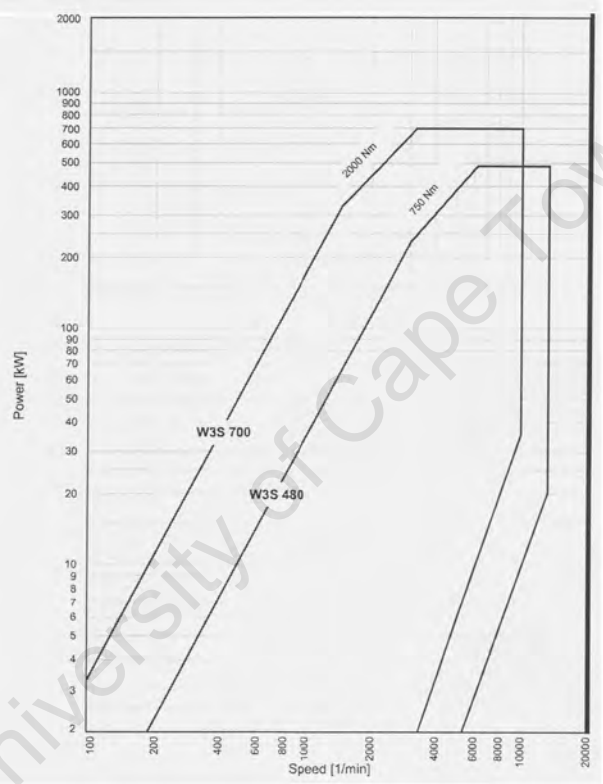

Figure C.5: Eddy-current dynos - type W3S 480 and W3S 700.

The engine operate between 98 and 102 % N_2 speed at all conditions other than ground idle and flight autorotation. This means that the dynamometer is required to apply load sufficient for the engine to produce between 15 and 236 kW at essentially a constant speed of 6000 rpm output shaft speed. Figure C.5 shows the operational envelope of the selected dyno. The above mentioned power developed by the engine at rated speed is well within the operational limits of the dyno. The engine idles at 60% N_2 speed (3600 rpm output shaft speed), produces about 15 kW to sustain engine idle speed. If it is desired to produce more power N_2 speed must first be advanced to and sustained at 100% (6000 rpm output shaft speed).

The mass of the shaft and coupling are limited by the operational speed of the dynamometer. If it is desired to operate at 13,000 rpm the mass of the shaft and couplings for the dyno half of the shafting is 2 kg. This increases to 3.4 kg at 10,000 rpm and 6.0 kg at 7,500 rpm. Considering that the engine will operate at 6000 rpm while producing power this provides a conservative mass allowance for the lay shaft and couplings of 12 kg.

The rotational inertia of the W3S 480 dyno is 0.42 kg.m^2, outside of the recommended limits but far greater than the rotational inertia of an equivalent size water brake dyno.

Appendix D

Operational Procedures

The operation of the various sub-systems is explained in detail in Appendix C (Test Cell Systems), while the interaction of the various sub-systems and the procedures to be followed to ensure safe operation of the gas turbine are contained herein.

D.1 Pre-startup Checks

Prior to activating any engine sub-systems the following checks must be completed:

1. Check the engine Log Book to ensure all maintenance work is complete and the engine is operational.
2. If maintenance has been performed check that the specific component has been reinstalled and all associated connection made/bolts fastened.
3. Check the floor of the test cell for any loose items that could be ingested by the engine and remove them.
4. Look at the first/seconds stage of the gas generator to ensure no foreign objects are present to be ingested. Check the shaft guard and free-wheeling unit for small items of debris.
5. Check all electrical and mechanical sensing lines are secured and unable to be disconnected, burned or ingested by the engine.
6. Ensure all mechanical and electrical connections to the boom box are secure.
7. Ensure the air supply path to the test cell is free of obstructions.

D.2 System Activation

Once the pre-startup checks are complete the various engine subsystems must be activated in the following order, stepping through the individual 'Normal Operation' procedures listed below:

1. Electrical
2. Oil
3. Water
4. Ventilation
5. Fuel

D.2.1 Electrical

Normal Operational

1. Check that all connections to the 24 V power supply (2 x 12 V batteries) in the test cell are secure and that the batteries have sufficient charge by looking at the indicators on their upper surface.

2. Make sure there is no spilled fluids, especially in close proximity to any electrical wiring.

3. Ensure that the connections to the starter motor are secured to the engine and the motor is itself secure.

4. Check the connection to the low tension capacitor discharge ignition exciter is secure as well as the leads connecting to the magnetic chip detectors.

5. Check the DB board to make sure that all appropriate switches are active.

6. Open the PLC and in the top left corner switch on breakers 1, 2 and 4 .

7. Switch on the gas turbine controlling computer as well as the dyno controller.

D.2.2 Oil

Normal Operational

1. Check the level of oil in both the primary oil tanks by removing the filler cap and in the PTO oil tank by removing the tank cover plate. The primary oil tank has a dip stick demarcated with increments to enable the user to determine whether or not the tank is sufficiently full, while the PTO tank must have no less than 30 mm of oil above the supply tube inlet.

2. Check that all piping between the oil storage tanks and the engine are properly connected and that there are no disconnected pipes, be sure to check each thermocouple and pressure tapping connections.

3. Check that the bypass ball valve on the PTO oil line is half way open, if not open to this position.
4. Switch on the PTO oil pump which operates on mains AC.
5. Wait a moment and ensure that the oil is flowing as intended and make sure the pressure transducer is registering a positive pressure on the controlling computer ($\sim$ 0.5 - 1 bar-gauge).
6. If the pressure is below 0.5 bar gauge further restrict the oil bypass route by closing the ball valve a small amount, if above 1 bar reduce the restriction as required.

D.2.3 Water

Normal Operational

1. Ensure all pipes within the test cell are secured as desired and unused connections are shut.
2. Check that the Continuous-Flow Combustion Rig has been isolated via the two shut-off valves, on the right side of it's control panel, on the wall.
3. Switch on the cooling tower fan on the DB board outside the Gas Turbine Control Room.
4. Check that the fan is operational, by viewing it though the transparent inspection hatch on the cooling tower, and there is sufficient water in the cooling tower. Open the fresh water supply valve if not already open.
5. Fully open shut-off valve A and switch on the cooling tower supply pump.
6. Check that the water tank has fully drained if full.
7. Fully open shut-off valve B and switch on the test cell supply pump.
8. Check that the pressure gauge within the test cell is registering and for any leaks that may have started.
9. Monitor the dyno outlet water temperature during operation to ensure the temperature remains below 40°C.

D.2.4 Ventilation

Normal Operational

1. Walk through the test cell and ensure there are no loose items that may be sucked into the ventilation system.
2. Ensure that there are no blockages in front of the inlet (remove the gas turbine inlet cover if not already done) or exhaust and firmly secure the test cell doors.
3. Switch on the orange DB board containing the supply and exhaust fan variable speed drives.
4. Ensure both emergency stop switches are pulled out, located on the orange DB board outside the operating room and on the control box in the control room.
5. Note the pressure inside the test cell from the ambient pressure transducer.
6. Dial both the speed indicators to about 20% and start the fans one at a time.
7. Slowly increase the speed of the fans one by one to attain full ventilation (Full ventilation is reached when one of the fans reaches 100% and the test cell pressure is as it was before the fans were activated).

D.2.5 Fuel

Normal Operational

1. All fittings and piping must be checked to ensure they are all appropriately connected and secure.
2. The supply and return fuel lines should be attached to the fuel drum currently in use and only the shut-off valve in line with the supply from the drum currently in use should be open.
3. The shut-off valve between the fuel filter and the flow meter must be in the open position allowing fuel flow to the test cell and the 3-way valve between the air separation unit and the back pressure regulator

must be pointing in the direction of the regulator (i.e. not open to atmosphere).

4. The 3-way valve between the engine and the emergency shut-off valve must be oriented to enable flow to the engine and not to the purge point. The line must be firmly secured to the fuel inlet on the engine.

5. Switch on the PLC and controlling computer to enable the boost pump and emergency shut-off valves to be operated if not already done.

6. Ensure that there is sufficient fuel in the drum by referring to the level sensor.

7. Lift the emergency shut-off valve in the test cell and switch on the boost pump using the operating system ETA.

D.3 Light-off

It is recommended to read the entire light-off procedure in the maintenance and operations manual to gain a full understanding of all aspects of the engine behavior. Light-off is a rapid process and the operator must already possess all necessary knowledge.

All the above 'Normal Operation' procedure lists for the various subsystems should have been complete at this stage. The following is the procedure for normal starting of the engine, that is in ambient conditions above 4°C.

D.3.1 Normal Starting

The following procedure should be used for all engine starts in the gas turbine test cell:

1. Rotate both N_1 and N_2 throttle levers to their respective minimum/off positions.
2. Check that the engine fuel supply pressure is reading ≈ 0.5 bar.
3. Ensure the residual TOT be no more than 150°C when light-off is attempted.
4. Switch on the master and spark switches.
5. Energize the starter and ignition exciter by pressing down the start switch.
6. At 15% N_1 rotate the N_1 throttle controller to the idle position.
7. Initiate the dynamometer in Commissioning mode and increase the current as needed to load the engine.
8. De-energize the starter and ignition exciter when 58% N_1 speed is reached and the start is complete when a stable N_1 speed of 59 - 65 % is reached.
9. Check that the oil pressure is within limits, if not immediately shutdown.
10. Adjust the dyno load until 60 % N_2 speed is attained.

D.4 Engine Operation and Shut-down

It is recommended to read the engine operation section of the maintenance and operations manual to gain a full understanding of all aspects of the engine behavior so as to be able to deal with problems that occur immediately and in the correct manner.

Prior to the addition of load, other than that used to keep the N2 speed at 60%, the N1 governor lever must be advanced to the fully open position.

1. If the engine oil pressure is within limits, and the temperature $\geq$50°C, as well as all other test cell temperatures and pressures within limits, the N1 governor lever may be slowly advanced to the fully open position.
2. As the N_2 speed approaches 100% the engine speed may begin to fluctuate, this can be eliminated by opening the P_R pressure line bleed valve slightly.
3. Once 100% N_2 speed is reached the P_R pressure line can slowly be opened until the engine speed begins to rise above 100% N_2 speed. Close the P_R pressure bleed until the speed decreases to 100% N_2 speed, this ensures that the power turbine governor still has overspeed control.
4. Load can now be slowly applied to the engine, continually checking the N_2 speed with the power turbine governor lever.
5. Continually monitor all systems to ensure the engine and all subsystems stay within limits.
6. Once testing is complete return the load to idle load and rotate the power turbine lever to the minimum position.
7. Bring the engine to idle by rotating the N_1 gas producer lever to idle.
8. Trim the load to settle the N_2 speed at 60%.
9. Idle the engine for no less than 2 minutes.
10. Rotate the N_1 gas producer lever to the off position and monitor the TOT gauge for afterfires.

If an afterfire occurs, visible by a rapid rise in the TOT gauge, motor the engine with the N_1 gas producer lever in the off position and the spark switch in the off position for 10 seconds.

D.5 Engine Operating Limits

It is recommended to read the entire section on 'Operation' in the operation and maintenance manual for a full understanding of the all the engine operational limitations. The most important and common are listed below.

D.5.1 Speed

N_1 Gas Producer

Maximum Continuous	104 %	No specific checks required
15 seconds or less	104 - 105 %	No specific checks required
More than 15 seconds	104 - 105 %	Turbine and Compressor Inspection
Not Permitted	Over 105 %	Turbine and Compressor Inspection

N_2 Power Turbine

Loading	TOT	CS limit	15 second limit	Component Affected
Auto-Rotation	N/A	108 %	110 %	Turbine
N/A	617°C	105 %	107 %	Turbine
N/A	699°C	104 %	106 %	Turbine
N/A	746°C	103.5 %	105.5 %	Turbine
N/A	773°C	103 %	105 %	Turbine
Loss of Load	N/A	N/A	120 %	Turbine/Gearbox

General

- N_2 speed must be maintained below 71% under ground idle conditions.

- Avoid steady state operation at any flight or ground condition, other than ground idle, at engine N_2 speed below 98% or above 102%.

D.5.2 Measured Gas Temperature, TOT

Operational Condition	TOT Limit	Time	Component Affected
Steady State	749°C	5 min @ Takeoff	Turbine
	749°C	30 min	Turbine
	≤693°C	Continuous	None
Startup/Shutdown	≤749°C	Unlimited	None
	749-927°C	10 sec	Inspect Turbine
	927-999°C	Not allowed	Inspect Turbine
	Over 999°C	10 sec	Remove Turbine
Power Transient	≤693°C	Continuous	None
	693-749°C	5 min	None
	749-843°C	6 sec	None
	843-927°C	Not allowed	Inspect Turbine
	Over 927°C	Not allowed	Remove Turbine

D.5.3 Output Shaft Torque Limit

Torque	Pressure	Power	Time Limit
434 Nm	752 kPa	273 kW	10 sec
397 Nm	689 kPa	250 kW	30 min
337 Nm	586 kPa	212 kW	Continuous

D.5.4 Oil Pressure and Temperature

N_1Speed	Pressure	Temperature
≥ 97 %	758 - 897 kPa	107°C max
78 - 97 %	621 - 896 kPa	107°C max
≤ 78 %	345 kPa	107°C max

General

- During the start a positive indication must be seen when 59 % N_2 speed is reached.
- During cold weather start 1034 kPa main oil pressure is permissible following the engine start, however, when the 896 kPa limit is exceeded operate with minimal power until normal oil pressure is attained.
- The minimum starting oil temperature is -40°C, while the minimum flight operation temperature is 0°C.

Appendix E

Heat Transfer Theory

Heat transfer to and from the combustor liner occurs via two means, forced convection and radiation. This appendix provides the reader with the various equations and methods used to determine the magnitude of radiative and convective heat transfer to and from the combustor liner.

E.1 Introduction

Liner wall temperature is attained where the balance is found between radiative and convective heat attained from hot combustion gases, and that lost by conduction to film cooling air and radiation to the surrounding casing.

Radiation heat transfer to the liner happens from both luminous and nonluminous sources. Luminous radiation is emitted from soot particles while nonluminous radiation is that emitted from certain heteropolar molecules such water vapor and carbon dioxide.

Through turbulent mixing in the boundary layer the cooling film is broken down and hot combustion gases are brought into contact with the liner wall. Heating of the liner via forced convection occurs wherever the cooling film is breached. The liner is, however, cooled via forced convection by the same cooling film until the temperature in the boundary layer exceeds that of the liner, resulting in a non-isothermal liner wall. The liner also looses heat via cold-side forced convection and radiation with the surrounding case.

The equations and theory are intended to allow for a comparison between different fuels and their respective effects on heat transfer to the combustor liner.

E.2 Method of Liner Analysis

To understand what a variation in any one of the various liner temperature measurements infers, the heat transfer mechanisms associated with the specific area of the liner must be analysed.

E.2.1 Radiative Heat Addition

Immediately downstream of the position where cooling air is injected into the combustor liner, the cooling film is completely intact and the only source of heat gain at this location is radiation from the combustion gases. In these areas the liner looses heat via forced convection both inwards and outwards, as well as transmitting energy via radiation to the surrounding case.

This would allow one to infer a variation in the quantity of radiative heat addition to the liner wall if a temperature variation were noted in this region when changing fuel.

The assumptions associated with this approach are the following:

1. The cooling film is complete, hence no heat is added via forced convection.
2. The liner does not conduct heat axially, radially or circumferentially.

The combustor liner is thin ($\approx$ 0.5 mm), making the quantity of heat conducted axially, radially and circumferentially minimal.

E.2.2 Convective and Radiative Heat Addition

Common practice is to reinforce the cooling film every 40 - 80 mm [7] to prevent combustion gases coming into contact with the line wall. The downstream end of the liner does not require film reinforcement at such regular intervals due to the flow acceleration suppressing the hot stream turbulence. This results in a portion of the can being completely protected from the combustion gases via the cooling film and all the heat addition is these regions being via thermal radiation.

In regions immediately upstream of film cooling reinforcement, convective heat addition would become more prominent and may not be assumed negligible. Recirculation and dilution holes disrupt film cooling air, creating regions of recirculation immediately downstream that entrain combustion gases, bringing them into contact with the liner wall. On the T63, in regions immediately downstream of the film cooling strips where the various sections of the liner have been spot welded together, there are discontinuities in the cooling film due to construction.

The spot welding is done is such a manner so as to minimize the area affected, and adjacent cooling films are allowed time to coalesce to prevent the discontinuities, however, discontinuities in the cooling film are present. Figure E.1 shows heat marks associated with the increase in heat transfer from the combustion gases where the cooling film is incomplete or breached. The increased heat transfer is only apparent immediately downstream of spot

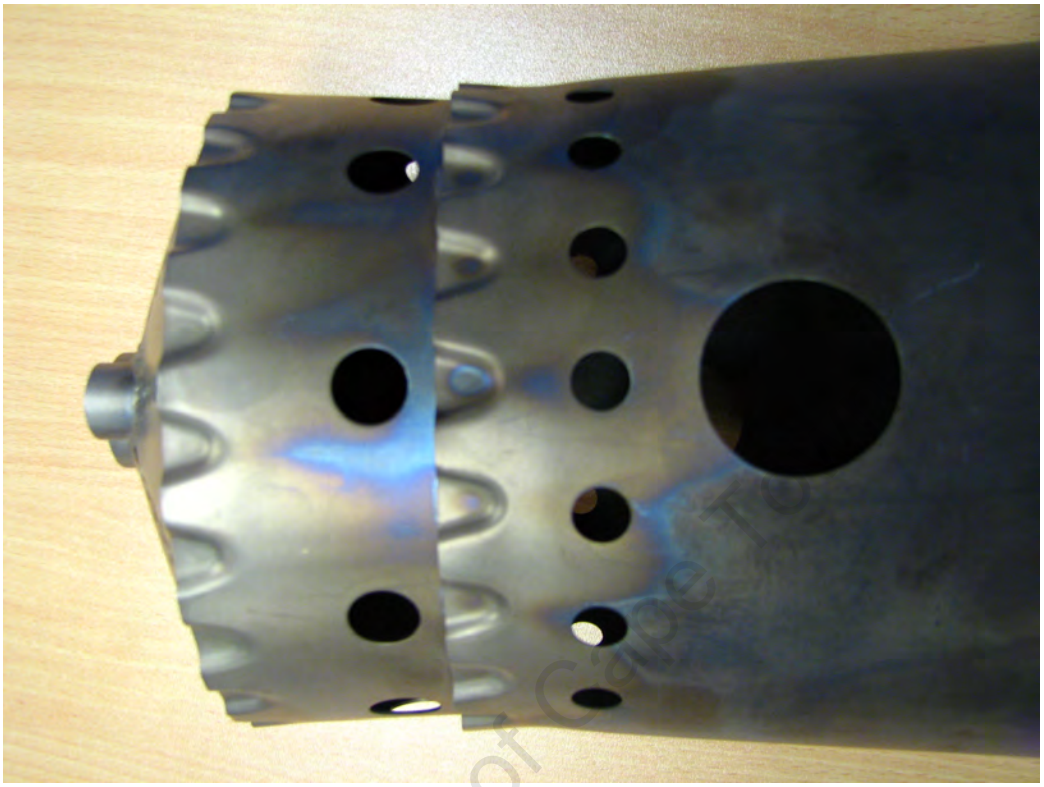

Figure E.1: T63 combustor liner.

welded joints, and is also not present downstream of all connection points. The heat scours are present on the side of the liner with the igniter, as shown, and opposite the igniter. These are the two sides of the combustor case that receive the air supply from the gas generator, and as such appear to receive preferential air flow. The primary recirculation holes on the liner adjacent the air supply scrolls are slightly smaller than those 90 degrees remove, to attempt to account for this, however the flow is partially asymmetric.

In these regions it would be incorrect to assume negligible influence of forced convection on liner temperature. It is, however, assumed for the purposes of this analysis that the magnitude of heat transferred to the liner via forced convection, at a specific operating condition, remains unchanged when operating on crude derive Jet-A1 and SPK.

Assuming the above means that the the different fuels have similar:

- Evaporative time scales

- Auto-ignition time scales (Cetane number)
- Heat release rates
- Heat of combustion

The properties of Jet-A1, SPK and various blends of the two are provided in table 6.1. The table shows all blends and neat fuels to comply to the Jet-A1 specification, except for density. Complying to the Jet-A1 specification implies that the specific fuel would perform as required, allowing for stable combustion throughout the necessary operational range.

If the flame position and structure, as well as the magnitude of the pressure perturbations within the combustor remain similar, combustion instability would be avoided and heat transfer to the combustor line would remain the same.

E.3 Combustor Liner Heat Transfer Equations

Knowing the temperature of the air after compression, as well as the pressure drop across the liner and the discharge coefficient of the various liner holes, an estimate of the specific heat transfer coefficients associated with the liner can be calculated. Knowing the heat transfer coefficients one can calculate the quantity of heat lost by the liner wall via convection. Calculating the radiation heat transfer to the case one can thus estimate the quantity of heat required to sustain liner temperature.

E.3.1 Internal Forced Convection

The convective heat transferred to the cooling film from the liner wall was calculated using:

$$q_{conv} = hA(T_w - T_\infty) \tag{E.1}$$

where T_w and T_∞ are the wall and free-stream temperatures respectively, A is the area and h the heat transfer coefficient.

The coefficient was calculated assuming the combustor liner to resemble an isothermal flat plate, heated over it's entire length and the flow regime to be laminar. The flow regime was assumed to transition from laminar to turbulent at Re = 5x10^5. Assuming the above allows for the incorporation of Equation E.2 from Holman [5].

$$h_x = 0.332k \;\; Pr^{1/3} \left(\frac{u_\infty}{\nu x}\right)^{1/2} \left[1 - \left(\frac{x_0}{x}\right)^{3/4}\right]^{-1/3} \tag{E.2}$$

$$Re_x = \frac{u_\infty x}{\nu} \tag{E.3}$$

$$Nu_x = \frac{h_x x}{k} \tag{E.4}$$

h_x (W/m^2.°C) refers to the local value of the heat transfer coefficient in terms of the distance x (m) for the leading edge of the plate. k (W/m.°C) is the thermal conductivity, u_∞ (m/s) and ν (m^2/s) are the free-stream velocity and kinematic viscosity respectively. Pr is the dimensionless Prandtl number.

With the Reynolds and Nusselt numbers defined by equations E.3 and E.4, and assuming $x_0 = 0$, equation E.2 becomes E.5

$$Nu_x = 0.332 Pr^{1/3} Re_x^{1/2} \tag{E.5}$$

Equation E.5 along with E.4 and E.3 allow for the calculation of the local heat transfer coefficient. Using equation E.6 allows for the calculation of the mean or average heat transfer coefficient, $\overline{h}$.

$$\overline{Nu}_L = \frac{\overline{h}L}{k} = 2 \;\; Nu_{x=L} \tag{E.6}$$

The properties of the fluid are calculated at the so-called film temperature T_f, defined as the arithmetic mean between the wall and free-stream temperature,

$$T_f = \frac{T_w + T_\infty}{2} \tag{E.7}$$

Cooling Film Gas Velocity

The free-stream velocity, u_∞, is required for the calculation of the convective heat transfer coefficient. The velocity is governed by the liner pressure drop, which is a function of the gas flowrate and effective area of the combustor liner.

The liner pressure drop was initially calculated using the combustor liner and case area measurements, gas properties and mass flowrate at the various operational conditions combined with the equations provided in Lefebvre [7].

Before analysing the temperature data the liner pressure drop was measured during operation of the T63 to ensure the most accurate possible estimation of the convection heat transfer coefficient.

E.3.2 Internal Radiation

The combustor liner is made from the nickel-base alloy, Nimonic 75, with an emissivity of ≈ 0.7 at typical wall temperatures. The surrounding stainless steel case was assumed to have an emissivity of ≈ 0.8 [7]. The exact values are dependent on the material composition, temperature and degree of oxidation, however, for the purpose of comparison the exact values of emissivity are not essential.

The magnitude of heat transfer via radiation was calculated assuming no convective heat addition, for the specific regions mentioned above, measuring liner temperature, and calculating the magnitude of heat lost by the liner. Liner wall temperature was initially calculated explicitly using a correlation developed by Annand for reciprocating internal combustion engines [33]. Annand proposed that the radiation heat transfer term could take the form:

$$\dot{q}_R = \beta\sigma(\overline{T}_g^4 - T_w^4) \tag{E.8}$$

where σ is the Stephan-Boltzmann constant, $\overline{T}_g$ is the mean gas temperature and T_w is the wall temperature. Coupled with a term to calculate the convective heat transfer, Annand could predicted the total heat transfer to the wall. Initial approximate values for β were in the region of 0.6 [33],

although later estimates produced values for β as high as 1.6, generally seen to exceed experimental thermal radiation findings.

Assuming a value for β of 0.6, and a mean gas temperature in the combustion zone of 1800 K provided liner wall temperature in good correlation with known values from Lefebvre [7].

E.3.3 Cold-Side Forced Convection

Air is delivered to the cold-side of the combustor liner via the compressor discharge air tubes, passing through the outer case. The air is injected radially and immediately turns to flow circumferentially around the liner or axially along the liner until passing through the liner holes. Air delivery was assumed radially even, being delivered adjacent to the primary recirculation and dilutions holes by 12 outer case openings. This presents the majority of incoming air with minimal distance to traverse before passing through an opening in the liner wall.

Axial and circumferential flow along a liner of large radius approximates that of flow along a flat plate. The can radius is 140 mm, not exceptionally large, however, the nominal distance traversed along the surface ($\approx$ 40 mm) prior to air passing through the liner allows the local region to be approximated as flat.

Considering the argument above, the convective heat transfer from the cold-side of the liner will be approximated using the same equation as those used for the internal convective heat loss. The mean flow velocity will be assumed proportional to the pressure loss across the outer case, measured during experimentation.

E.3.4 Cold-Side Radiation

The combustor liner exchanges thermal radiation with the surrounding combustor case. The nature of the exchange was assumed to resemble that of two concentric cylinders. Figure E.2 provides the means to calculate the radiation shape factors for this exchange.

Noting the radial and longitudinal dimensions of the liner and case, it was

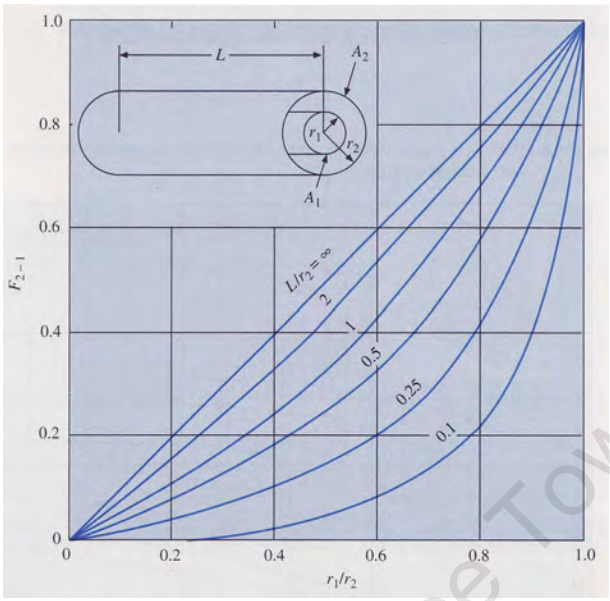

Figure E.2: Radiation shape factor for concentric cylinders [5].

calculated that the shape factor from the case to the liner was 0.85. Using reciprocity, the shape factor for the liner to the case was calculated to be 0.98. Essentially all the radiation leaving the inner liner is absorbed by the outer case immediately opposite the liner, and as such the relationship can be assumed to be that of two infinite parallel cylinders.

$$q = \frac{\sigma A_1 (T_1^4 - T_2^4)}{1/\epsilon_1 + (1/\epsilon_2 - 1)(A_1/A_2)} \tag{E.9}$$

where σ is the Stephan-Boltzmann constant, ϵ and A the respective surface emissivities and areas, with T the temperatures.

E.4 Radiation Sensor

To differentiate between radiation and forced convection heat transfer to the combustor liner, one of the two must be independently measured. The radiation heat transfer was measured via a specifically designed sensor, designed only to respond to thermal radiation. The sensor was designed specifically for incorporation in the T63 gas turbine, being 20 mm long, 9mm in diameter

and peering into the main recirculation/combustion zone through the main dilution hole in the liner wall.

E.4.1 Components

The sensor is made up of several components. The main sensing element can be seen in the center of figure E.3(a). It incorporates a long thin shaft and an elongated surface, with the base allowing for the location of two 3 mm diameter K-Type thermocouples. The upper surface of the sensor is separated from the cooling effects of forced convection via a 2mm fused silica lens. To prevent conduction heat loss from the sensor upper surface, other than that along the thin shaft, the lens is held away from the sensor surface via a collar. The sensor, collar and lens are all held in place via the screw on cover. The cover has a step, adjacent to the thread, to allow for attachment to the flange on the sensor, so as to secure the sensor element to the base.

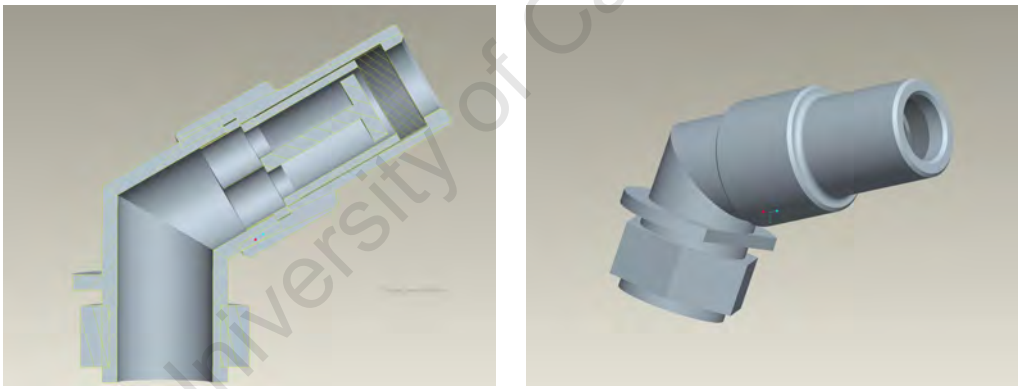

(a)Cross-Section of the Radiation Sensor (b)Radiation Sensor

Figure E.3: Radiation sensor design figures (a), (b).

The flange on the lower side of the sensor locates the sensor, with the nut threaded from the aft side of the case surface securing the sensor. The threaded components are fixed in place with high temperature thread lock.

E.4.2 Operation

Incident thermal radiation is absorbed by the surface of the sensor, heating the surface. As the surface is heated the heat is conducted via the thin

shaft to the base, where it is dissipated through conduction to the sensor outer surface, and forced convection to the passing air stream. Measuring the temperature difference between the sensor surface and base provides the means to calculate the magnitude of thermal radiation incident on the sensor.

The sensor was machined from 316 Stainless Steel, providing the emissivity and thermal conductivity. The shaft length and diameter are 6 mm and 1 mm respectively. With the above knowledge and the conduction heat transfer equation E.10, the total heat conduction q could be calculated. Knowing the total heat conducted, q, and the surface area of the sensor, A, as well as the material properties, one can calculate the incident thermal radiation.

$$q = -kA\frac{\delta T}{\delta x} \tag{E.10}$$

Where k (W/m.°C) is the thermal conductivity, A (m^2) is the cross-sectional area, δ T is the temperature difference and δ x is the length along witch heat is conducted.

E.4.3 Heat Transfer Calculations

Sensor dimensions were calculated from the estimated flame radiation necessary to sustain liner temperature previously calculated. The maximum temperature difference was wanted to increase sensitivity of the sensor, hence, the sensor was designed to attain a theoretical maximum surface temperature of 750°C. The sensor surface temperature and all calculations made herein were determined for operation with a 20% aromatic fuel at 90% maximum cruise, relating to the highest radiant thermal loading to be encountered during testing.

The magnitude of radiation at the liner surface, along with the respective mean distance from the radiation source, were used to estimate the magnitude of thermal radiation at the sensor location, $\approx 105 kW/m^2$. The surface diameter of 4.5 mm would thus receive 1.62 W of heat energy assuming the surface emissivity of the liner similar to 316 Stainless Steel and the transmittance of fused silica to be 95%.

The 1.62 W heat input was determined as the net heat exchange on the upper surface of the sensor, absorbed energy only through radiation.

The sensor must thus transmit a net 1.62 W of heat energy, via radiation and conduction along the shaft. The portion transmitted via radiation is absorbed by the sensor lower surface and the collar. Using figure E.4 one can determine the fraction of radiation leaving the underside of the upper surface transmitted to the base.

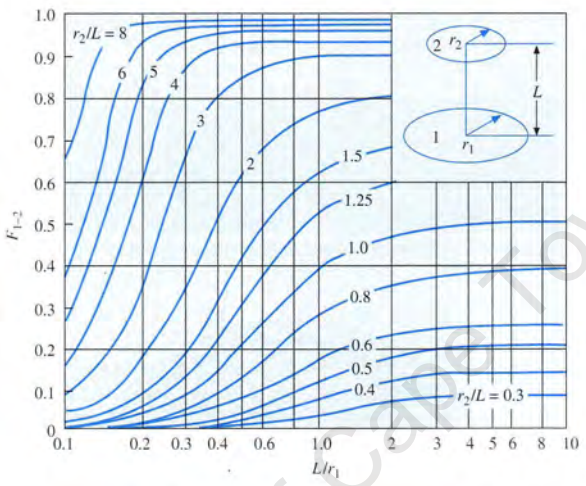

Figure E.4: Radiation shape factor for parallel disks.

Considering that the sum of the two fractions must be 1, the fraction of thermal radiation transmitted to the collar can be calculated. The result was 1.37 W of the thermal energy being conducted via the shaft, 0.22 W lost to the collar, and a further .03 W transmitted via radiation to the base. The total measured quantity at the base would thus be 1.40 W, or 86% of the incident thermal radiation. This would provide a theoretical temperature difference of 510°C, based on compressor discharge gas temperature.

Appendix F

Drawings

This appendix contains the assembly drawings of the various components designed and incorporated in the Gas Turbine Test Cell. The manufacturing drawings of the more complex components are included following their respective assembly drawings.

F.1 Engine Mounting

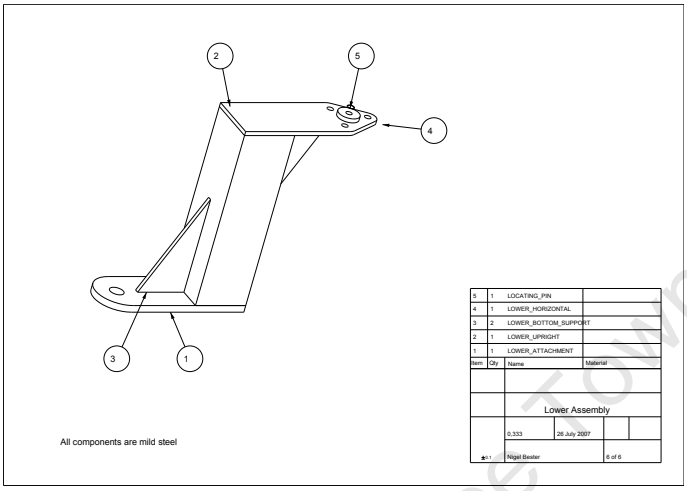

Figure F.1: Lower engine mounting assembly drawing.

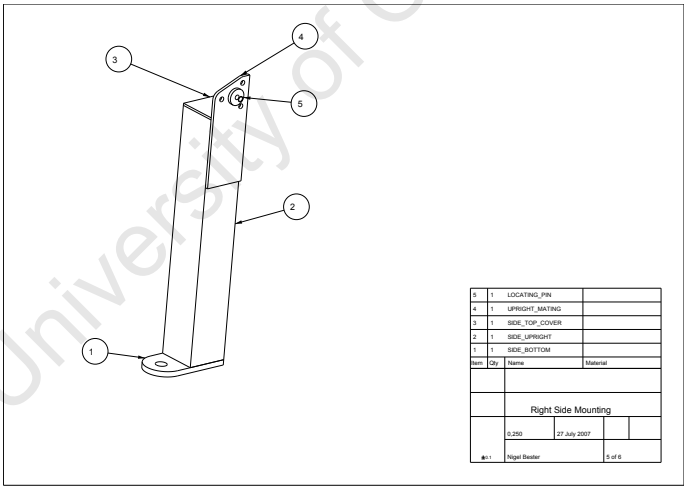

Figure F.2: Right side engine support assembly drawing.

F.2 Air Separation Unit

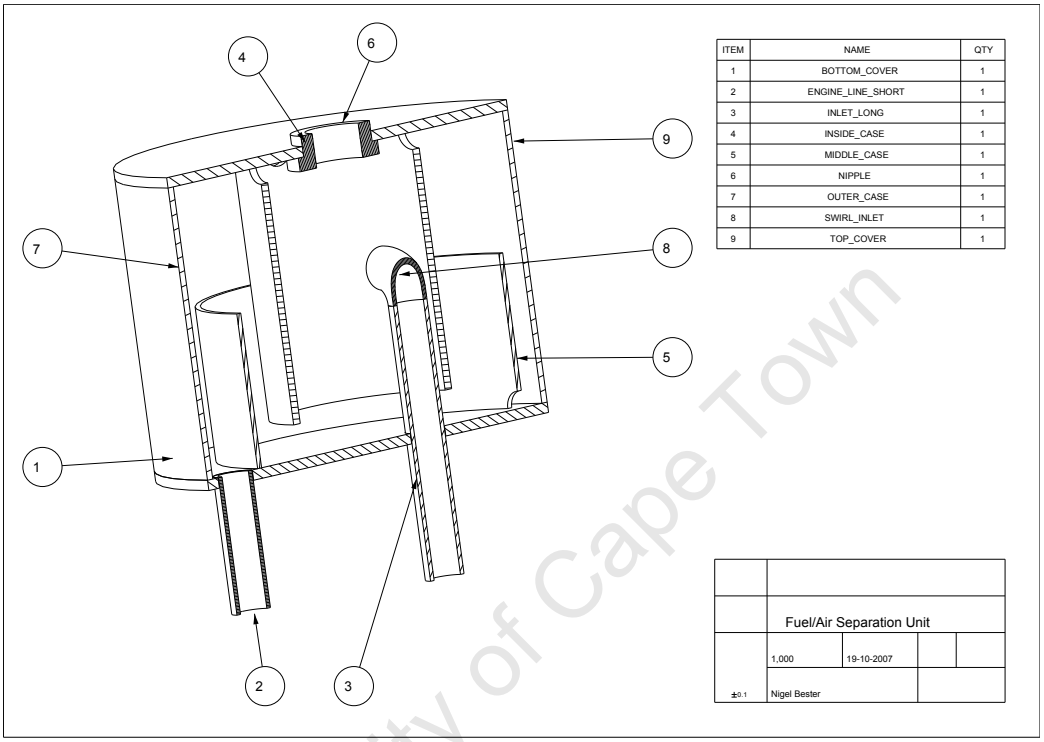

Figure F.3: Fuel/Air separation unit.

F.3 Radiation Sensor

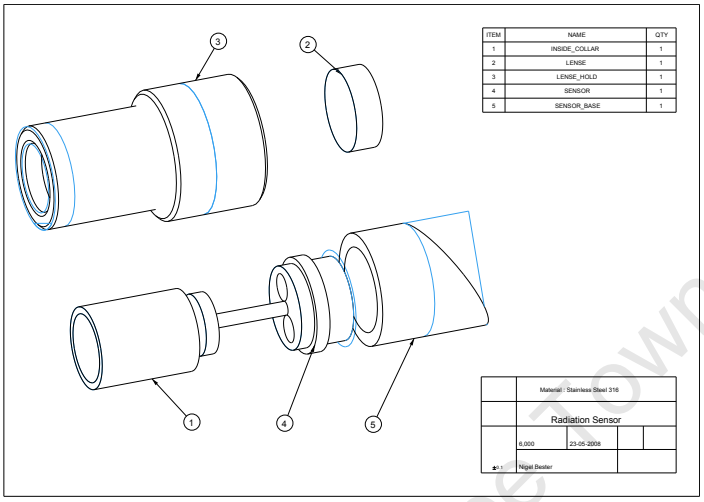

Figure F.4: Radiation sensor assembly drawing.

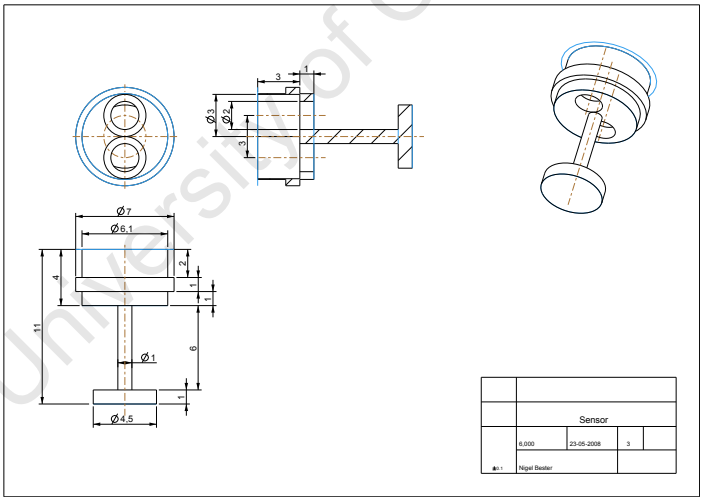

Figure F.5: Sensor manufacturing drawing.

F.4 Drive Shaft and Couplings

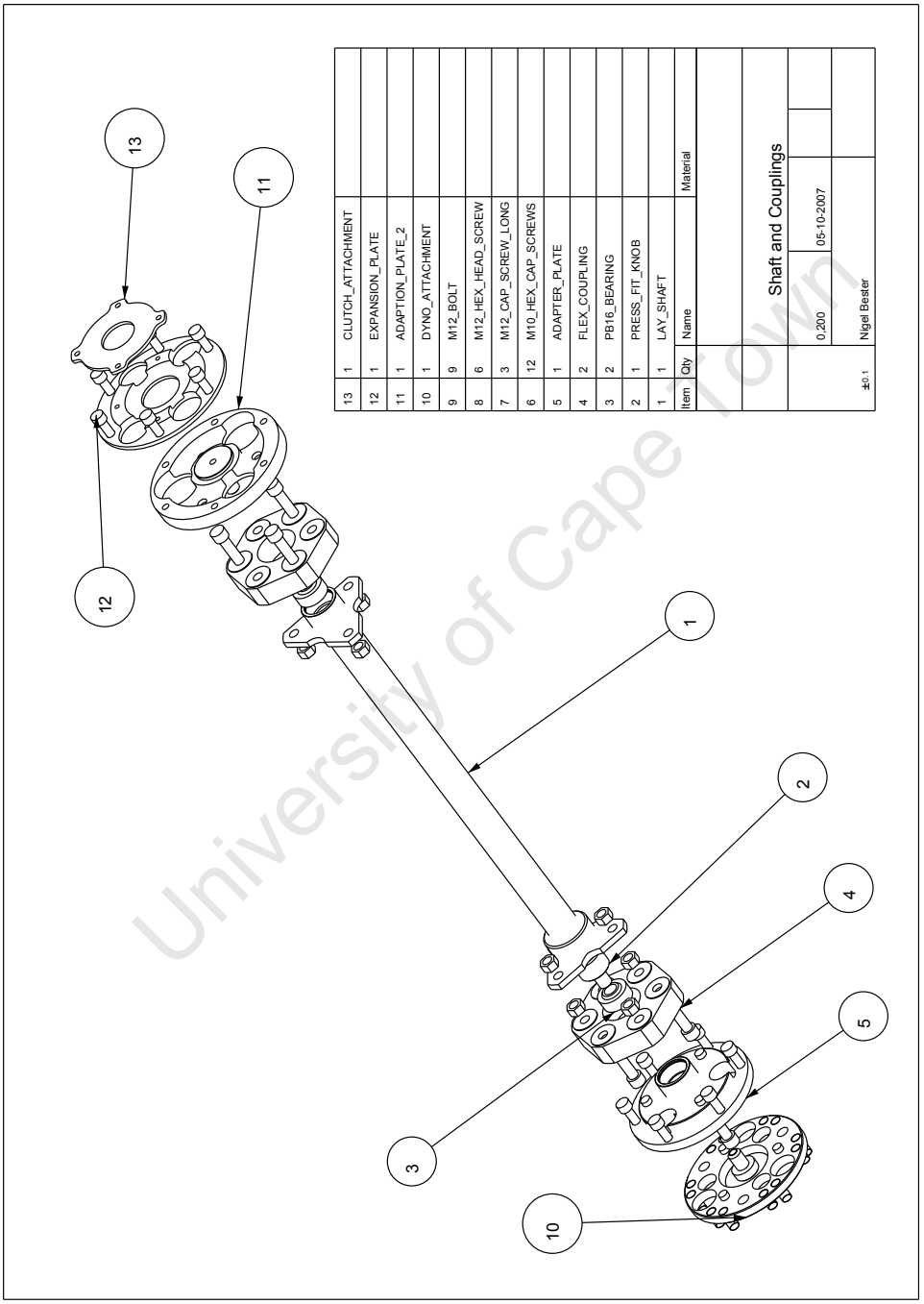

Figure F.6: Drive shaft and couplings assembly drawing.

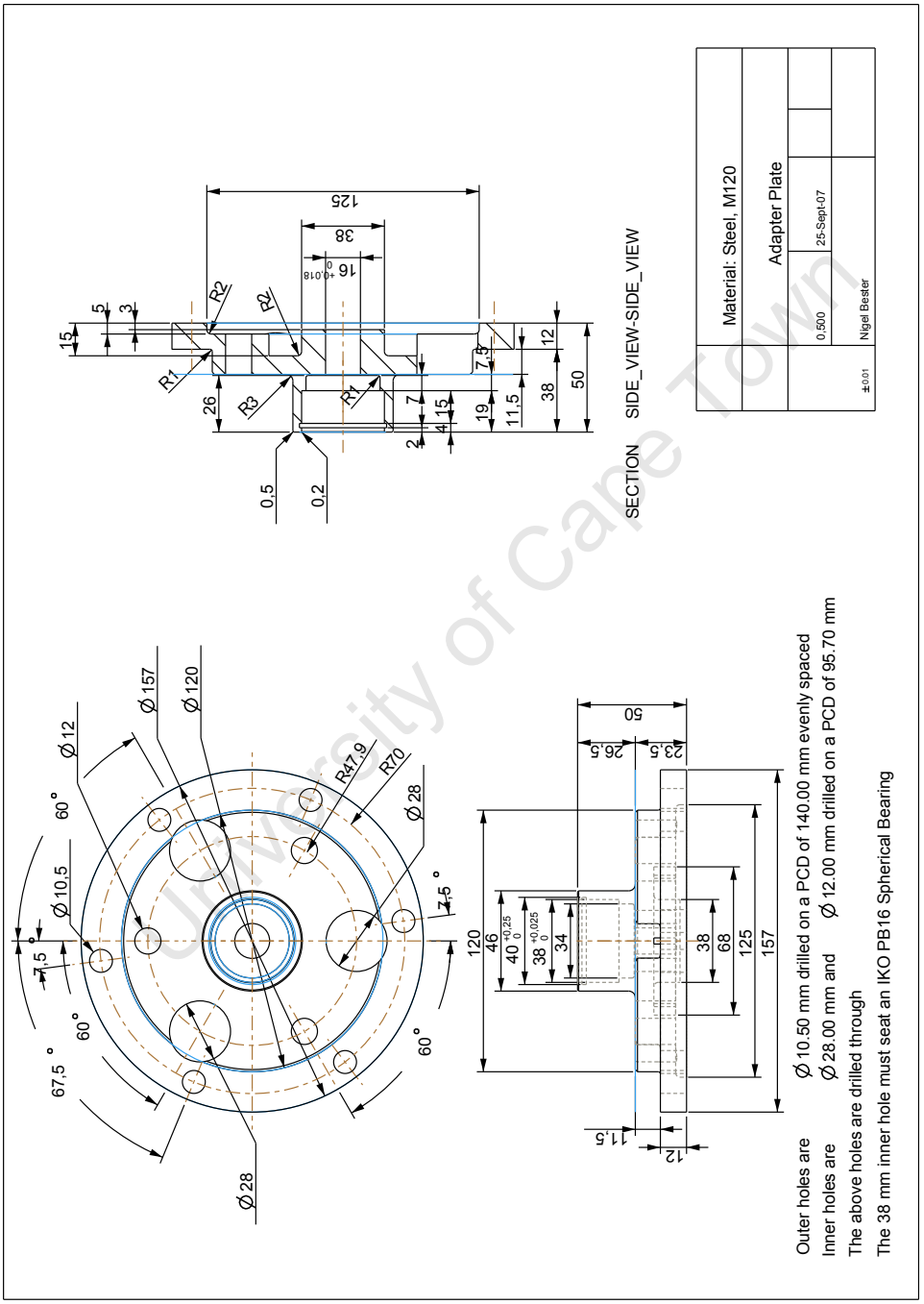

Figure F.7: Dyno–shaft adapter plate manufacturing drawing.

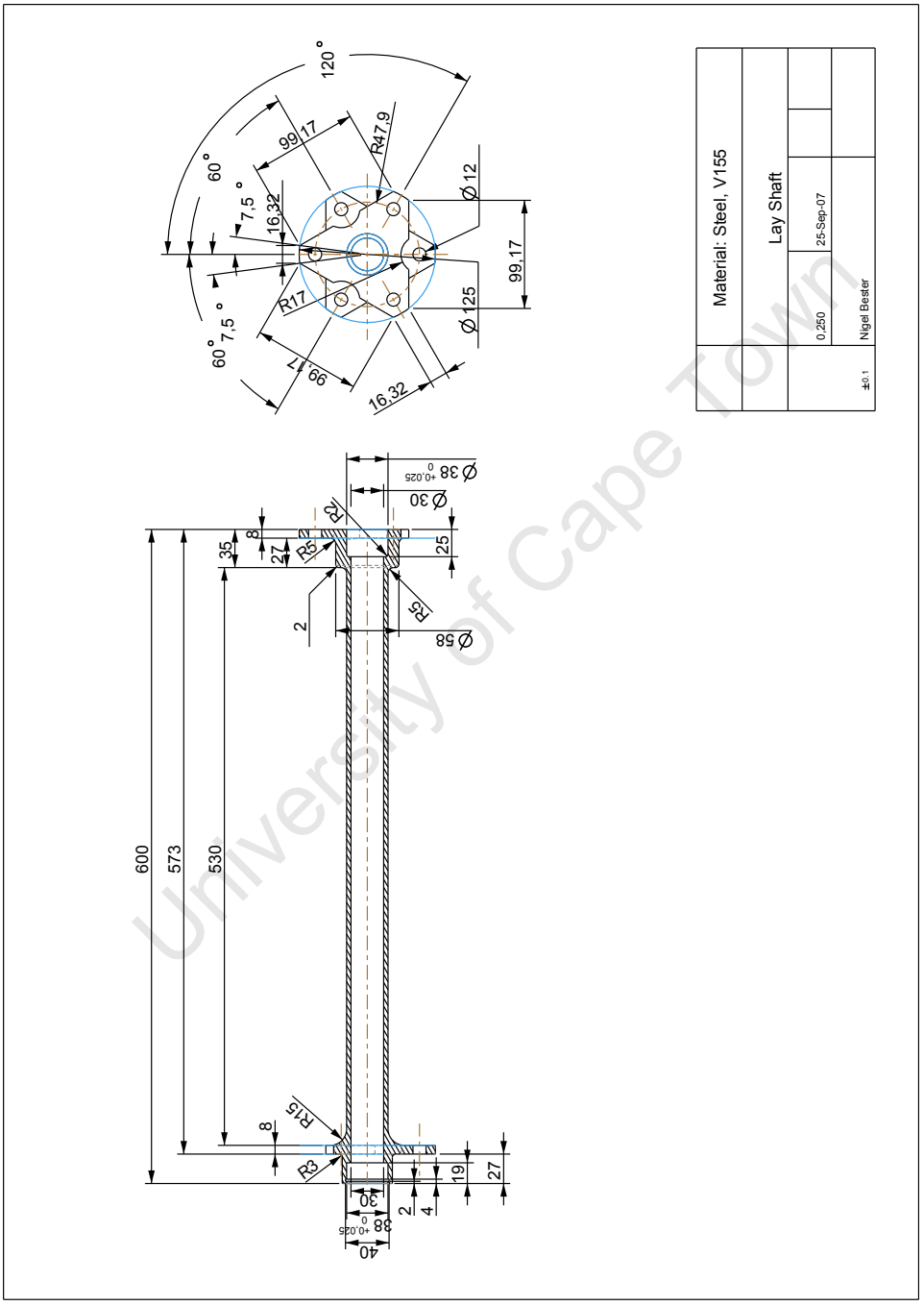

Figure F.8: Drive shaft manufacturing drawing.

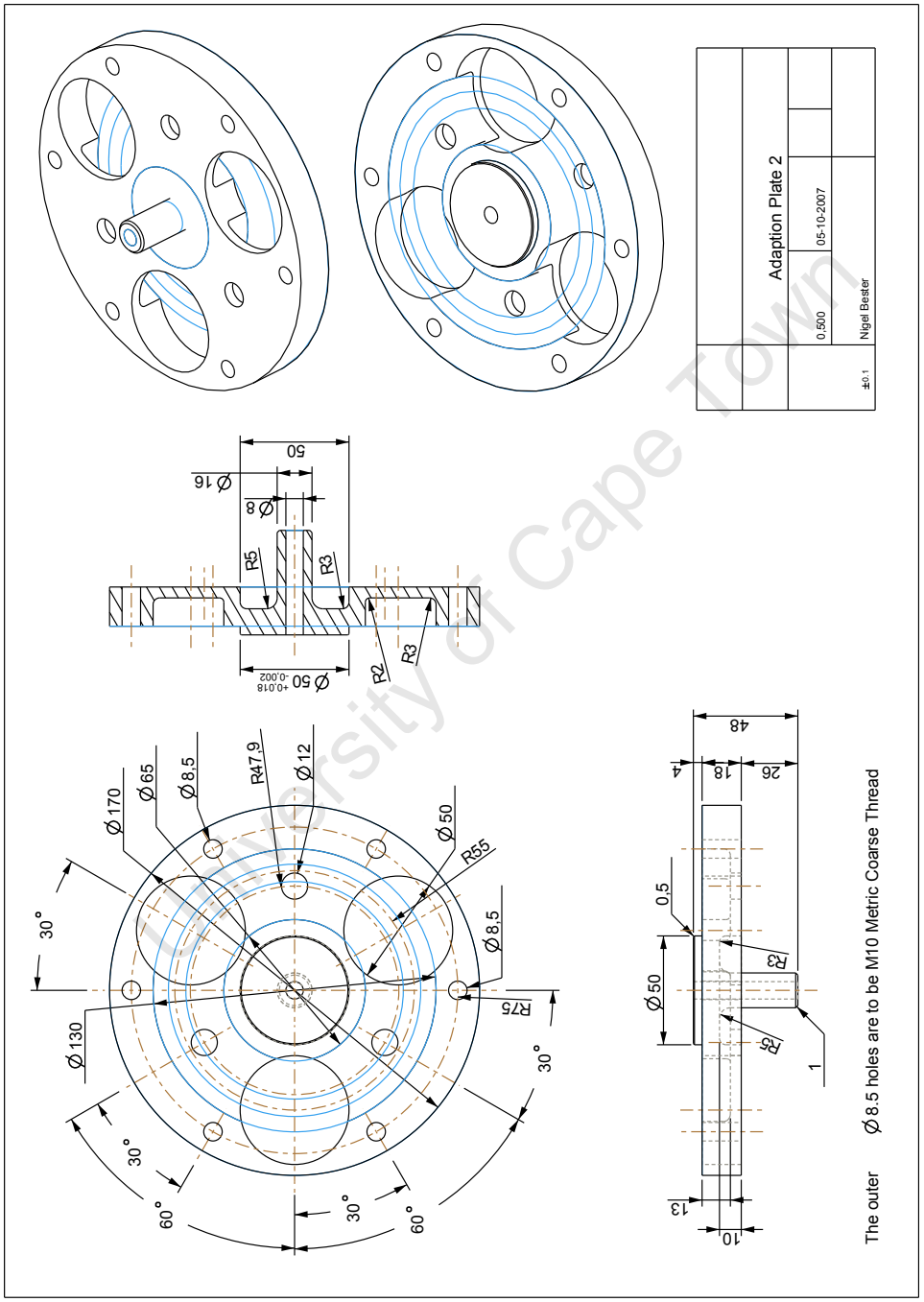

Figure F.9: Shaft–coupling adapter plate manufacturing drawing.

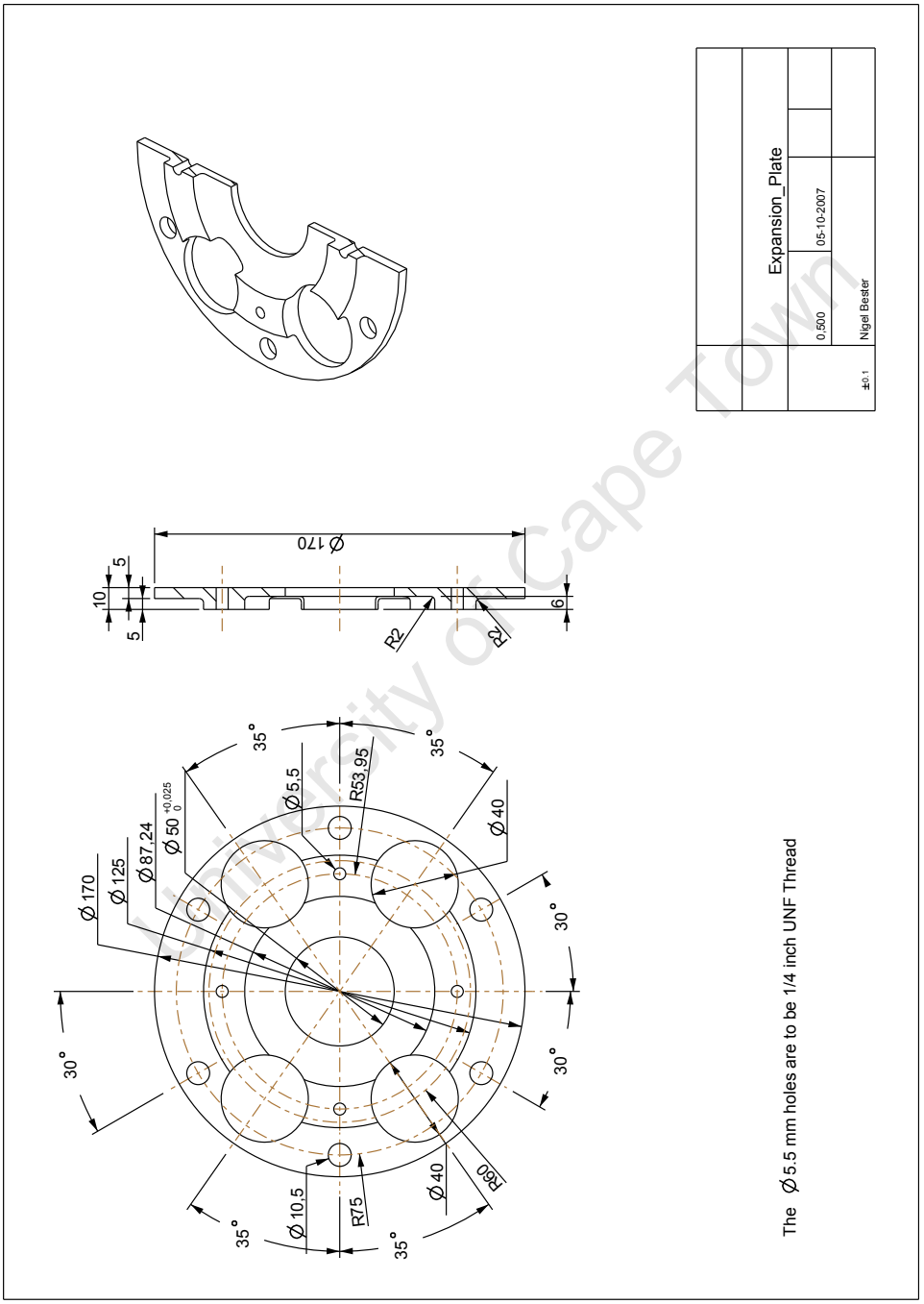

Figure F.10: Coupling–Engine adapter plate manufacturing drawing.